



Facoltà di Ingegneria Elettronica

Dottorato di Ricerca in Ingegneria dei Sistemi Sensoriali e di
Apprendimento

XXII Ciclo del Corso di Dottorato

Development of an atomistic/continuous simulation tool for nanoelectronic devices

Gabriele Penazzi

Anno Accademico 2009/2010

Tutor

Prof. Aldo Di Carlo

Coordinator

Prof. Corrado Di Natale

Marco Polo describe un ponte, pietra per pietra. “Ma qual è la pietra che sostiene il ponte?” chiede Kublai Khan. “Il ponte non è sostenuto da questa o quella pietra,” risponde Marco, “ma dalla linea dell’arco che esse formano”. Kublai Khan rimane silenzioso, riflettendo. Poi soggiunge: “Perchè mi parli delle pietre? È solo dell’arco che mi importa”. Polo risponde: “Senza pietre non c’è arco.”

Italo Calvino, *Le città invisibili*

Marco Polo describes a bridge, stone by stone. “But which is the stone that support the bridge?” Kublai Khan asks. “The bridge is not supported by one stone or another,” Marco answers, “ but by the line of the arch that they form.” Kublai Khan remains silent, reflecting. Eventually, he adds: “Why do you speak to me of the stones? It is only the arch that matters to me.” To which Marco Polo retorts: “Without stones there is no arch.”

Italo Calvino, *Invisible cities*

Acknowledgements

There's a lot of people I have to acknowledge for their contribution to this work. First of all I want to thank my supervisor, Prof. Aldo Di Carlo, for giving me the opportunity to join his worldwide recognized group as a PhD student. He has been a precious scientific guide, he allowed me to work in a challenging project and he gave me financial support to attend schools and international conferences. Working with him is a great satisfaction to me.

I want to thank Prof. Alessandro Pecchia, who has been a scientific tutor, a guide and a friend. I couldn't have done this work without his support, suggestions and contribution. I wish him the best. I thank Dr. Giuseppe Romano with whom I shared this walk, as a colleague and as a friend.

I thank Dr. Matthias Auf der Maur and Dr. Fabio Sacconi for their contribution and valuable scientific discussions, Dr. Alessio Gagliardi and Dr. Desiree Gentilini for great scientific and non-scientific discussions and for being the best officemate I could have. I want to thank also all the people of our group, they contributed to make my experience pleasant and we shared a lot of good time. In particular I would like to thank Luigi, Francesca (thanks for Betta!), Stefano Penna, Eleonora, Riccardo, Daniele D'Ercole, Giacomo, Mauro, Daniele Colonna, Mino, Andrea, Thomas, Stefano Bellocchio, Elisa, Monica and Giorgia. I really hope I didn't forget anyone. I would like also to thank Prof. Frauenheim and his group for allowing me to work with them in Bremen and for giving me the opportunity of a future challenging research experience.

Finally, I hope the reader will forgive me if I write some further acknowledgements in Italian.

Ringrazio i miei amici, specialmente quelli con cui ho avuto il piacere di condividere il palco. Ringrazio C. per avermi sopportato in più di un'occasione.

Ringrazio il Dr. Evangelisti per le stimolanti discussioni sulla teoria critica.

Ringrazio i ragazzi del Serpente, senza i quali avrei letto meno articoli.

Infine ringrazio fortemente la mia famiglia: i miei genitori, per avermi supportato in tutte le mie scelte, per avermi fornito gli strumenti che mi hanno permesso di raggiungere questo traguardo, per non avermi fatto mai mancare nulla e per avermi insegnato l'etica del lavoro non con le parole, ma con l'esempio. Ringrazio le mie sorelle per il preziosissimo affetto e auguro il meglio a loro, alle loro famiglie e specialmente alle loro bellissime bimbe.

Contents

List of Figures	ix
1 Abstract	1
2 Riassunto	3
3 Introduction	5
3.1 Motivation	5
3.1.1 What is nanotechnology?	5
3.1.2 The world at the nanoscale	6
3.2 Multiscale approach	7
3.3 TIBERCAD: a continuous/atomistic simulation tool	8
4 Continuum models	11
4.1 Continuum elasticity	11
4.1.1 Strain in heterostructures	13
4.1.2 Deformation effects	14
4.2 Drift Diffusion	15
4.2.1 Electron and hole transport	15
4.3 Continuum quantum mechanics	16
4.3.1 Envelope Function Approximation	17
4.3.2 Conduction and valence states	20
4.3.3 Quantum charge density	23
4.3.4 Optical matrix elements	24

CONTENTS

5	Atomistic models	25
5.1	Valence force field	25
5.1.1	The Keating VFF model	25
5.1.2	Keating model in zincblenda and wurtzite structures: limits and features	27
5.2	Tight Binding Method	31
5.2.1	Tight Binding Model: the atomistic approach	32
5.2.2	Empirical Tight Binding	34
5.2.2.1	Beyond bulk materials: strain, alloys and confined structures	38
5.2.3	Density Functional Tight Binding	41
6	Continuous/atomistic environment in TiberCAD	45
6.1	TIBERCAD structure	45
6.2	Mesh and atomistic structures	47
7	Applications	53
7.1	Strain in quantum dot structures: valence force field and continuum elasticity	53
7.2	Optical properties of a GaN quantum dot ambedded in a $\text{Al}_x\text{Ga}_{1-x}\text{N}$ nanocolumn	58
7.3	Self consistent tight binding/drift-diffusion simulation of a $\text{GaAs}/\text{Al}_x\text{Ga}_{1-x}\text{As}$ structure	64
8	Quantum Transport: NEGF theory and application	69
8.1	Equilibrium Green's function	69
8.1.1	Spectral function and density of states	72
8.1.2	Coherent transport	73
8.2	Non equilibrium Green's function	74
8.2.1	The correlation function $G^>$ and $G^<$	74
8.2.2	The kinetic equation	76
8.3	The iterative NEGF library	78
8.4	A ballistic molecular transistor	83
9	Conclusions	91

References	93
-------------------	-----------

CONTENTS

List of Figures

5.1	Zincblenda structure	29
5.2	Wurtzite structure	30
5.3	GaAs bandstructure	37
5.4	GaN bandstructure	38
5.5	GaN/ $\text{Al}_x\text{Ga}_{1-x}\text{N}$ well	40
6.1	TIBERCAD structure	46
6.2	Mesh geometry	48
6.3	Atomistic structure	50
7.1	InAs/ $\text{In}_x\text{Ga}_{1-x}\text{As}$ quantum dot	54
7.2	$\text{In}_x\text{Ga}_{1-x}\text{As}/\text{InAs}$ quantum dot strain.	55
7.3	GaAs/ InAs quantum dot structure and CE strain.	55
7.4	GaAs/ InAs quantum dot strain.	56
7.5	ε_{zz} profile in low aspect ratio quantum dot.	56
7.6	GaAs/ InAs quantum dot strain.	57
7.7	Nanocolumn	58
7.8	Piezoelectric polarization	59
7.9	Emission spectra and IV.	60
7.10	Electron and hole state	61
7.11	EFA states and spectrum.	62
7.12	Atomistic structure	63
7.13	ETB states	63
7.14	ETB spectra	63
7.15	GaAs/ AlGaAs nanocolumn.	65

LIST OF FIGURES

7.16	EFA energy band band profile and charge densities.	66
7.17	ETB energy band band profile and charge densities.	67
7.18	ETB spectra	67
8.1	Open boundary conditions	70
8.2	Block tridiagonal structure	79
8.3	Rectifying molecular device	83
8.4	IV characteristic	85
8.5	Local density of states	86
8.6	Three terminal molecular device	87
8.7	Three terminal device I-V	87
8.8	Three terminal device LDOS	88
8.9	Three terminal molecular device	89
8.10	Three terminal device I-V	89

Abstract

The simulation of novel optoelectronic devices is a great challenge for the engineering community. The enormous progress in device fabrication technology allowed such a massive downscaling that geometrical feature in the nanoscale play a crucial role. Furthermore we have a great effort in exploring alternative solutions respect to more traditional semiconductor devices. It involves molecular electronic, semiconductive polymers, self-assembled structures, quasi-one dimensional and two dimensional materials. In such scenario it's crucial to develop modular simulation tools able to connect different physical models on different length scales. Quantum effect play an important role and we need to take them into account, avoiding anyway an explosion of the computational complexity. Thus it's needed to go in the direction of a multiscale approach, which is already applied with success in mechanical science.

The goal of this work is to include atomistic description and atomistic models in TIBERCAD, a Technology CAD code for simulation of optoelectronic devices which can rely on excellent instruments for interfacing different models in a multiphysics/multiscale environment. Atomistic models for the calculation of strain, structure geometry and electronic states have been included. A novel technique for describing quantum transport with an efficient algorithm is also presented. These work wants to push TIBERCAD to be a reference tool for calculation of complex optoelectronic devices at the nanoscale.

1. ABSTRACT

2

Riassunto

La simulazione dei moderni dispositivi elettronici è una grande sfida per la comunità ingegneristica. L'enorme progresso nei processi di fabbricazione ha permesso una riduzione della dimensione dei dispositivi talmente spinta che fenomeni tipici della scala di lunghezza nanometrica giocano un ruolo cruciale. Inoltre stiamo assistendo a un grande sforzo teso ad esplorare soluzioni tecnologiche alternative ai tradizionali dispositivi a semiconduttore. Questo sforzo è rivolto verso la frontiera dell'elettronica molecolare, dei polimeri semiconduttori, delle strutture autoassemblanti, dei materiali quasi-unidimensionali e bidimensionali. In uno scenario simile è cruciale sviluppare strumenti di simulazione modulari, capaci di connettere modelli fisici differenti su scale geometriche differenti. Gli effetti quantistici giocano un ruolo fondamentale ed è necessario includere modelli che li descrivano, evitando per la tipica esplosione di complessità nell'implementazione di suddetti modelli. Per realizzare ciò è necessario andare verso un approccio multiscala, approccio già utilizzato con successo in meccanica statica.

Lo scopo di questo lavoro è includere descrizioni e modelli atomistici in TIBERCAD, un codice TCAD per la simulazione di dispositivi optoelettronici che può vantare eccellenti strumenti per interfacciare diversi modelli fisici in un ambiente multifisica/multiscala. I modelli atomistici inclusi sono utili al calcolo delle deformazioni elastiche, della geometria della struttura e degli stati elettronici. Infine, viene presentata anche una tecnica inedita per una descrizione quantistica efficiente del trasporto di carica. Questo lavoro vuole contribuire a rendere TIBERCAD uno strumento di riferimento per la simulazione di dispositivi optoelettronici su nanoscala.

2. RIASSUNTO

3

Introduction

3.1 Motivation

3.1.1 What is nanotechnology?

If the 20th century has been the century of semiconductor electronics, the 21st century will be probably the century of *nanotechnology*, or *nanotech*. What is nanotechnology? How electronics and optoelectronics are involved? Most of the scientific community identifies the birth of nanotech in a precise date: December 29, 1959. In that day Richard Feynman was giving a talk titled "*There's plenty of room at the bottom*" at an American Physical Society meeting at Caltech (25). Feynman proposed a top down approach to build what we would call a molecular factory, an instrument to assemble individual atoms in a controlled way. Feynman's idea was simple and brilliant: build robotic "hands" at one-fourth scale with respect to human size, then use these "hands" to manufacture other "hands" at the 1/16th size and so on.

Feynman was so enthusiastic that offered two prizes: one for miniaturizing written information down to an area 1/25000 smaller in linear scale, the other for building a rotating electric motor 1/64 inch cube small. Both the prizes have been won: the first in 1986, the latter in 1960.

What's our concept of nanotechnology in these days? There's not a unique definition, but we can say that nanotechnology is the science of manipulating and controlling matter features at nanometer scale (10^{-9} m). Looking at electronics technology, it started quite a long time ago. The first device that boosted scientific community on miniaturization issues was the MOSFET, the main component in integrated electronics. Since MOSFETs began to be integrated on one chip, the single transistor could be made smaller and smaller, halving its size every 18 months (51). The narrowest feature in a

3. INTRODUCTION

MOSFET is the oxide length (76). In the early 2000s the typical gate length was 180 nm while the oxide thickness was just 3 to 5 nm. In the early 1990s the typical gate length was 350 nm and the oxide thickness was less than 10 nm, a few atom layers (71). We were almost at nanometer scale features level.

Optoelectronics and nanotechnology has become to be deeply connected many years ago, in the 90s or earlier, thanks to the incredible progress in semiconductor manufacturing. Nowadays it's not only a matter of oxide thickness in transistors. We can control nanoscale features in three dimensions, we know different techniques to build nanowires, quantum dots, molecular devices, nanotubes, single layer graphene sheets. There's a lot of research on different materials and solution that falls under the nanotechnology umbrella. The future of optoelectronics is not clear, and it's not easy to determine which one is the best technology for controlling electrons and photons. Moreover, while in the past century research and industry focused exclusively on semiconductor devices, now there's an explosion of possible solutions for future device generation, ranging from strained semiconductors, heterostructures, carbon compounds (carbon nanotubes and graphene) polymeric conductors and single molecule devices. All of these solutions are promising in a sense or another, and probably their exploitation will be strictly application dependent.

3.1.2 The world at the nanoscale

Modelling devices at nanoscale is a really challenging topic. In his lecture (25) Feynman said:

As we go down in size, there are a number of interesting problems that arise. All things do not simply scale down in proportion. There is the problem that materials stick together by the molecular (Van der Waals) attractions. It would be like this: after you have made a part and you unscrew the nut from a bolt, it isn't going to fall down because the gravity isn't appreciable; it would be even hard to get it off the bolt. It would be like those old movies of a man with his hands full of molasses, trying to get rid of a glass of water. There will be several problems of this nature that we will have to be ready to design for.

Feynman's key point is the following: laws of physics don't scale linearly with length, and they don't scale down in the same way. When Feynman was talking, physicists were exploring the microscopic world much more deeply than molecular scale, but the point here is that controlling matter and engineering matter at nanoscale is a

completely new challenge. From an engineering point of view, our physics toolbox must be enriched, and the separation line with the physicist become fuzzy. Semiclassical models begin to be inadequate, quantum effects plays a key role in the study and design of devices. Different physical phenomena interact each other resulting in complex behaviours. Statistical variations, such as defects or doping distributions have to be taken exactly into account and quantum effects are more and more important.

At nanoscale, any single atom matter.

3.2 Multiscale approach

Historically, optoelectronics technology has been dominated by semiconductor lithography. It pushed scientific community for finding reliable models to describe the transport of electrons, heat and light at microscopic scale. Semiconductor modeling began in the nineteen-fifties after the formulation of *drift diffusion equations* (46). Drift diffusion provides a powerful semiclassical model which, despite of its inner limitations, can be still used in the description of many classes of device and it's still a must in the industry, thanks to robustness and reliability. However drift diffusion model doesn't take into account many of phenomena that occur at nanoscale. First of all, it lacks of any quantum mechanical effects, such as quantum confinement or tunneling. Moreover, when feature sizes are scaled down to nanometers, continuous media approximation can break down, and even continuous media quantum descriptions, such as effective mass an $\mathbf{k} \cdot \mathbf{p}$, can be no more reliable (22) and atomistic descriptions are needed.

However, atomistic models have some drawbacks: they are very computation-demanding, they cannot describe systems larger than millions of atoms and the physics behind scattering phenomena like light-matter interaction or heat dissipation is very difficult.

A modern device will have typically a nanometric active region, and this region will be coupled with an environment which involves phenomena on larger scale. It's clear that we'll have to use continuous or atomistic description where it's needed. This is what is called *Multiscale approach*: mixing physical models on different lenght scales. In computation material science it's already a well established approach (44; 67; 79). It's especially used to study crack propagation and structural properties, mixing models from continuous elasticity down to atomistic tight binding. However it's a few years that all the scientific community is moving to this new paradigma, pushed by the need to control physical phenoma at a very low scale. It's a fact that journals dedicated to this topic are borned (see *International Journal for Multiscale Computational Engineering*

3. INTRODUCTION

or *Journal of Multiscale Modeling*), testifying that the scientific community is moving in this direction.

However most of TCAD software used in optoelectronics do not fulfill the requirement of giving a flexible multiscale environment. There's plenty of software for simulation of most common optical and electronic device that are very reliable and popular, but none of them offer a flexible environment.

At the state of the art the most flexible solution for investigating multiphysics phenomena relies on COMSOL, a FEM environment which allows the user to add his own model in the form of differential equations. Although COMSOL represent a suitable solution for dealing with complex multiphysics continuum models, at the present time it lacks of any kind of atomistic description. It limits its usefulness in the study of nanometric devices.

On the other side we have very specific tools studied to describe one class of devices (ISE-TCAD or SILVACO for transistors, as an example), or scientific codes well suited for physics research but not suitable for the optoelectronics engineering community, because of the computational effort.

But for the exposed motivations, a modern TCAD tool must be capable to deal with a wide range of materials at very different length scale, offering a wide choice on implemented physical models and good flexibility to connect them in a multiphysics/multiscale approach.

3.3 TIBERCAD: a continuous/atomistic simulation tool

With this picture in mind, the optoelectronic group at the Electronic Engineering Department of *University of Rome Tor Vergata* started the TiberCAD project a few years ago (4; 6; 64) The aim of TIBERCAD is to provide a flexible environment for multiscale modelling of optoelectronic devices.

When we deal with condensed matter device physics we can distinguish two main categories: continuous media and atomistic (or corpuscular) approaches. In the first one matter is described as composed by effective media which properties can be expressed as continuous functions in the space. There's different techniques to implement a numerical calculation of a continuum model. The main ones are Finite Difference (32) and Finite Elements (8). In both approaches the real space is discretized in a three-dimensional grid of *nodes*, also called *mesh*, and constitutive equations, typically in the form of a partial differential equations, are solved on this mesh.

Instead in the atomistic models we deal with the corpuscular composition of matter, starting from the interaction of particles composing the matter itself. Then we'll have to

3.3 TIBERCAD: a continuous/atomistic simulation tool

deal with the atomic composition and typically the formulation of our problem will have the form of equations dependent on atomic positions. We can somehow interpret atoms similar to nodes in a discretized continuum model, but this vision is quite misleading. Although in the continuum model discretization is just a precision and convergency matter and it doesn't depend upon the total size of the system - it depends on the ratio between different feature size - in an atomistic model the number and the arrangement of atom depends upon the system dimensionality. However, from a mathematical point of view, we can take advantage from the fact that sometimes discretized continuum models and atomistic models have similar equations, and a smooth transition between them can be realized (67).

TIBERCAD environment supports both the description, and implement schemes to pass data from a model to another in a multiscale approach. Within some limits, it also allows models to get some physical models regardless they're calculated from an atomistic or a continuous media calculations.

In the following chapters a description of physical models used for a mixed continuous/atomistic description will be given. It follows an overview about TIBERCAD and the way the atomistic part is included. Then we'll show some applications where the technique introduced in this work can be useful.

3. INTRODUCTION

4

Continuum models

In this chapter some of the continuous media approximation physical models implemented in TiberCAD are described. They include a semiclassical particle transport model, a classical continuous elasticity model and a multiband $\mathbf{k} \cdot \mathbf{p}$ model. All the models are described by partial differential equations and discretised using the finite element method (FEM). Continuum model are not the main part of this work, but they are needed for understanding their coupling and comparison with atomistic models. For this reason further details about numerical implementation of these models are omitted and references are given instead. Furthermore, TiberCAD includes more models than the ones described below, but have not been coupled with atomistic models and they're not used in the applications shown here, so their description is beyond the scope of this work. ¹

4.1 Continuum elasticity

Elasticity is a particular branch of mechanics dealing with *elastic* bodies. A body is said to be elastic if it recovers its original shape when the forces causing deformation are removed (1). When the loading is not depending on time we are dealing with an *elastostatics* problem. The load can be either an external force or an internal force.

Why are we so interested in continuum elasticity while dealing with optoelectronics? The great progress in modern semiconductor growth techniques such as molecular beam epitaxy (MBE) and metal-organic chemical vapor deposition (MOCVD) made it possible to grow semiconductors of different atomic compositions on top of another

¹Strain module has been implemented by Dr. M. Povolotskyi. A much more detailed treatment of this topic is available in his PhD thesis. (63)

4. CONTINUUM MODELS

semiconductor substrate with monolayer precision (77). These are the so called heterostructure junctions, or heterojunctions.

In heterojunctions the starting materials will have different lattice constants, and the substrate will try to impose its own lattice constant to the material grown on top. This phenomena leads to an internal load, i.e. strain, that dramatically affects electronic and optical properties of devices and arises strong deviation from bulk material characteristics (16).

Using continuum elasticity theory we can evaluate the amount of strain in continuous media. Moreover we can calculate structure deformation under external forces or geometry of freestanding structure, a useful feature for the study of MEMS or NEMS devices. Although TIBERCAD implementation allows these kind of calculation, I'll focus on elasticity theory applied to heterostructures, as freestanding structures are beyond the scope of this work.

There are two levels of observation in mechanics of elastic solids: corpuscular or phenomenological. The latter is described by continuum theory, while the first operates at molecular or atomic scale. The main advantages in using continuum elasticity are the following:

- Mathematics models are well established and can be described using FEM techniques.
- Bodies with very different molecular structures can be described with a few parameters which describe their response to loads.
- Continuum model is not size-dependent. Within the theoretical limits for which the model is valid, structures of arbitrary dimension can be calculated.
- It allows the calculation of deformation under external load and freestanding structures with small effort.

On the other side, it suffers some drawbacks:

- It describes only continuous media, it cannot describe materials where local atomic composition matters, like random alloys.
- It has been demonstrated to fail when scaling down the dimensions of structures (65; 75).
- It cannot describe atomic features such as internal strain phenomena, which strongly affects electronic and optical properties of some class of devices. (80)

4.1.1 Strain in heterostructures

Under the action of external loads, any point belonging to the elastic body moves from the coordinates x, y, z to the coordinates x', y', z' , resulting in a displacement field \mathbf{u} , which is a vector field.

Then the relations

$$\mathbf{u} = \mathbf{r}' - \mathbf{r}, \quad \text{or} \quad u_i = x'_i - x_i \quad (4.1)$$

where $\mathbf{u}(\mathbf{r})$ is a point function, completely describe the deformation of the system. The distance between two adjacent points in the deformed system reads

$$dl'^2 = (d\mathbf{r} + d\mathbf{u})^2 \quad (4.2)$$

$d\mathbf{u}$ can be written as $du_i = (\partial u_i / \partial x_k) dx_k$. Then we can write dl'^2 as (Einstein sum convention is used here and in the following)

$$\begin{aligned} dl'^2 &= dl^2 + 2 \frac{\partial u_i}{\partial x_k} dx_i dx_k + \frac{\partial u_l}{\partial x_k} \frac{\partial u_l}{\partial x_i} dx_k dx_i \\ &= dl^2 + \left(\frac{\partial u_i}{\partial x_k} + \frac{\partial u_k}{\partial x_i} \right) dx_i dx_k + \frac{\partial u_l}{\partial x_k} \frac{\partial u_l}{\partial x_i} dx_i dx_k \end{aligned} \quad (4.3)$$

For small deformations we can neglect terms quadratic in $\partial u_i / \partial x_k$. and define the *strain tensor* as

$$\varepsilon_{ik} = \frac{1}{2} \left(\frac{\partial u_i}{\partial x_k} + \frac{\partial u_k}{\partial x_i} \right) \quad (4.4)$$

we can rewrite the equation (4.3) as

$$dl'^2 = dl^2 + 2\varepsilon_{ik} dx_i dx_k \quad (4.5)$$

Forces acting on an elastic body can be distributed over the volume (*body forces*) or over the surface (*surface forces*) (for further detail see (1), pag. 5). When a body is under the influence of any of these, internal forces are developed which balance the externally applied force.

Given a small volume dV , the i -th component of the force acting on it can be expressed as $\int_V F_i dV$. Using Gauss formula and defining a second-rank *stress tensor* σ_{ik} we rewrite the integral as follows:

$$\int_V F_i dV = \int_V \frac{\partial \sigma_{ik}}{\partial x_k} dV = \int_{\partial V} \sigma_{ik} ds_k \quad (4.6)$$

4. CONTINUUM MODELS

It follows that we can write forces as divergence of stress tensor. In equilibrium internal forces will compensate external ones such that

$$F_i = \frac{\partial \sigma_{ik}}{\partial x_k} = 0 \quad (4.7)$$

In a small deformation regime stress is related to strain through generalized Hooke's law:

$$\sigma_{ik} = C_{iklm} \varepsilon_{lm} \quad (4.8)$$

C_{iklm} is called *elasticity tensor*. The number of independent component is given by the symmetry of the crystal. We can finally write the system of equations to be solved to get deformation and strain in the structure:

$$\frac{\partial}{\partial x_k} (C_{iklm} \varepsilon_{lm}) = \frac{1}{2} \frac{\partial}{\partial x_k} \left[C_{iklm} \left(\frac{\partial u_l}{\partial x_m} + \frac{\partial u_m}{\partial x_l} \right) \right] = f_i \quad (4.9)$$

where f_i is an externally applied mechanical force.

To calculate the strain in a heterojunction one proceeds defining a reference lattice, i.e. the one of the substrate material. The material grown on the substrate will be forced to match this lattice constant, giving a body force. A lattice-matching strain ε_{ij}^0 can be defined, and it describes the deformation of the unit cells of the unstrained materials at the equilibrium.

The total strain is now given by

$$\varepsilon_{ij}(\mathbf{r}) = \tilde{\varepsilon}_{ij}(\mathbf{r}) + \varepsilon_{ij}^0(\mathbf{r}) \quad (4.10)$$

$\tilde{\varepsilon}_{ij}(\mathbf{r})$ is the strain according to eq. (4.4) due to the displacement $\mathbf{u}(\mathbf{r})$ with respect to the reference lattice.

4.1.2 Deformation effects

Strain has dramatic effects on semiconductor devices properties. It affects both the band structure of materials and the charge distribution inside the conventional cell. The first effect will be analyzed in the following chapters. In a piezoelectric material the electric displacement \mathbf{D} can be written as (53):

$$D_i = D_i^{(0)} + \kappa_{ik} E_k + e_{ikl} \varepsilon_{kl} \quad (4.11)$$

where κ_{ik} is the permittivity tensor, ε_{kl} is the strain tensor and e_{ikl} is the piezoelectric tensor. The term $D_i^{(0)}$ is the so called *pyroelectric polarization* and it represents

a spontaneous polarization that occurs when certain symmetry properties are present (53). We have pyroelectric polarization in semiconductors with wurtzite crystal structure, e.g. nitride based materials.

The second term of equation (4.11) is the electrostatic component depending on electric field.

The third term of the equation is the *piezoelectric polarization* \mathbf{P}^{pz} .

Deformation has also a strong effect on the electronic states, that will be discussed in sections 4.3.1 and 5.2.2

4.2 Drift Diffusion

The drift diffusion model represent a first order approximation to the Boltzmann transport equation (45; 73). Here we start from the constitutive equations for electrons and holes. A deeper description about the derivation of these equations and details about exciton transport can be found in ref. (5) and won't be discussed in this work.

4.2.1 Electron and hole transport

The drift diffusion equations, also referred as Van Roosbroeck equations, for electrons and holes are formed by continuity equations coupled together with the Poisson equation

$$\frac{\partial n}{\partial t} + \nabla \mathbf{j}_n = -R + G \quad (4.12a)$$

$$\frac{\partial p}{\partial t} + \nabla \mathbf{j}_p = -R + G \quad (4.12b)$$

$$\mathbf{j}_n = -D_n \nabla n + \mu_n n \nabla \varphi \quad (4.12c)$$

$$\mathbf{j}_p = -D_p \nabla p - \mu_p p \nabla \varphi \quad (4.12d)$$

$$-\nabla (\epsilon \nabla \varphi) = -e(n - p + C) \quad (4.12e)$$

The electrical current densities are given by $\mathbf{J}_n = -e\mathbf{j}_n$ and $\mathbf{J}_p = e\mathbf{j}_p$. We can express non-degenerate particle densities in local equilibrium in terms of electro-chemical potentials ϕ_n and ϕ_p (40)

$$n = N_c \exp \left(\frac{e\varphi - e\phi_n - E_c}{k_B T} \right) \quad (4.13a)$$

$$p = N_v \exp \left(\frac{E_v - e\varphi + e\phi_p}{k_B T} \right) \quad (4.13b)$$

4. CONTINUUM MODELS

where N_c and N_v are the electron and hole densities of states. In the effective mass approximation they can be calculated as follows:

$$N_c = 2 \left(\frac{k_B T m_n^*}{2\pi \hbar^2} \right)^{3/2} \quad \text{and} \quad N_v = 2 \left(\frac{k_B T m_p^*}{2\pi \hbar^2} \right)^{3/2} \quad (4.14)$$

where $m_{n,p}^*$ are the effective masses of electrons and holes. In the degenerate case equations (4.13) must be rewritten as (3)

$$n = N_c F_{1/2} \left(\frac{e\varphi - e\phi_n - E_c}{k_B T} \right) \quad (4.15a)$$

$$p = N_v F_{1/2} \left(\frac{E_v - e\varphi + e\phi_p}{k_B T} \right) \quad (4.15b)$$

where $F_{1/2}(x)$ is the Fermi integral of order 1/2

$$F_{1/2}(x) = \frac{1}{\pi^{1/2}} \int_0^\infty \frac{y^{1/2}}{1 + e^{y-x}} dy$$

If we assume the generalized Einstein relations

$$\mu_n = eD_n \frac{1}{n} \frac{\partial n}{\partial \varphi}, \quad \mu_p = -eD_p \frac{1}{p} \frac{\partial p}{\partial \varphi} \quad (4.16)$$

to hold locally we can rewrite the electron and hole flux in eq. (4.12) as a function of electron and hole quasi-fermi level

$$\mathbf{j}_n = \mu_n n \nabla \phi_n, \quad \mathbf{j}_p = -\mu_p p \nabla \phi_p \quad (4.17)$$

which actually is the description used inside TIBERCAD code. (5)

4.3 Continuum quantum mechanics

TIBERCAD includes a continuum quantum mechanical model based on Envelope Function Approximation (EFA) ¹. EFA is an effective mass method and is based on a single particle Shchroedinger picture. It allows calculation of electronical and optical properties of semiconductor heterostructures. Although some inner limitations will be clear in the description of the method, EFA has been demonstrated to be a reliable technique even for nanostructures (12) and take advantages of a complete literature about defining, testing and validating parameters.

¹EFA module has been coded by Dr. M. Povolotskyi. The author of this work contributed at the mantainment and extension.

4.3.1 Envelope Function Approximation

The starting point for calculating electronic eigenstates in heterostructures is the single-electron stationary Schrödinger equation:

$$\left[-\frac{\hbar^2}{2} \nabla_r \left(\frac{1}{m} \nabla_r \right) + V_{eff}(\mathbf{r}) \right] \psi(\mathbf{r}) = E \psi(\mathbf{r}) \quad (4.18)$$

The potential $V_{eff}\mathbf{r}$ is the sum of ionic contribution and external potential (including externally applied potential, Hartree potential of free carriers in a mean field scenario). Then the total Hamiltonian is the sum of three terms:

$$\begin{aligned} H &= H_1 + H_2 + H_3 = \\ &= -\frac{\hbar^2}{2} \nabla_r \left(\frac{1}{m} \nabla_r \right) + \sum_{\sigma, \mathbf{R}, \alpha} W_{\alpha}^{\sigma}(\mathbf{r}) v_{\alpha}^{\sigma}(\mathbf{r} - \mathbf{R} - \mathbf{d}_{\alpha}) + V_{ext}(\mathbf{r}) \end{aligned} \quad (4.19)$$

H_1 is the electron kinetic energy, H_2 is the ionic potential and H_3 is the external potential, possibly including Hartree contribution. σ is a material index, \mathbf{R} is the Bravais vector, α is the atomic basis index and \mathbf{d}_{α} the basis vector in the unit cell. v_{α}^{σ} is the local pseudopotential as seen by the α -th atom in the σ -th material. W_{α}^{σ} is a unit function that is zero only if the atom at position $\mathbf{R} + \mathbf{d}_{\alpha}$ does not belong to the σ material.

The contribution of ionic crystal is usually deduced in form of empiric potential through measurements on bulk band structure. Thus the atomic pseudopotential v_{α}^{σ} is unavailable. Instead we can use bulk periodic pseudopotential defined as follows:

$$V_{\alpha}^{\sigma} = \sum_{\mathbf{R}} v_{\alpha}^{\sigma}(\mathbf{r} - \mathbf{R}) \quad (4.20)$$

From a theoretical point choosing any complete set of basis functions the solution of equation (4.18) is exact (for definition of complete basis set see (69)). From a practical point of view it's convenient using uncomplete basis sets, and the choice of the right basis is strictly connected to the problem we're dealing with. A widely used choice is the so called *Envelope Function Approximation*.

If we expand the Schrödinger equation solution $\psi(\mathbf{r})$ using the Bloch functions (80) of one of the constituent materials - represented by index σ_0 - we still obtain the complete basis:

$$\psi(\mathbf{r}) = \sum_{n, \mathbf{k}} C_{n, \mathbf{k}} u_{n, \mathbf{k}}^{\sigma_0}(\mathbf{r}) e^{i \mathbf{k} \mathbf{r}} \quad (4.21)$$

4. CONTINUUM MODELS

We can consider only the bulk Bloch function $u_{n,\mathbf{k}}^{\sigma_0}$ at a certain $\mathbf{k} = \mathbf{k}_0$ without losing completeness. Defining the *envelope function set*

$$F_n(\mathbf{r}) = \sum_{\mathbf{k}} e^{i\mathbf{k}\mathbf{r}} C_{n,\mathbf{k}} \quad (4.22)$$

and $u_n(\mathbf{r}) = u_{n,\mathbf{k}_0}^{\sigma_0}$, the solution $\psi(\mathbf{r})$ is rewritten as

$$\psi(\mathbf{r}) = \sum_n F_n(\mathbf{r}) u_n(\mathbf{r}) \quad (4.23)$$

Substituting the expression (4.23) in equation (4.18) we obtain:

$$\begin{aligned} \sum_n \left(-\frac{\hbar^2}{2m} \nabla^2 + V \right) F_n(\mathbf{r}) u_n(\mathbf{r}) = \\ \sum_n \left[-\frac{\hbar^2}{2m} (\nabla^2 F_n(\mathbf{r})) u_n(\mathbf{r}) - \frac{\hbar^2}{m} \nabla F_n(\mathbf{r}) \nabla u_n(\mathbf{r}) - \frac{\hbar^2}{2m} (\nabla^2 u_n(\mathbf{r})) F_n(\mathbf{r}) + V F_n(\mathbf{r}) u_n(\mathbf{r}) \right] \\ = E \sum_n F_n(\mathbf{r}) u_n(\mathbf{r}) \quad (4.24) \end{aligned}$$

Following the approximation in ref. (12), the matrix elements of the different operators acting on u_n are:

(a)

$$\nabla u_n = \frac{i}{\hbar} \mathbf{p} u_n = \frac{i}{\hbar} \mathbf{p}_{n'n} u_{n'}, \quad \text{with} \quad \mathbf{p}_{n'n} = \frac{1}{\Omega_c} \int u_{n'}^* \mathbf{p} u_n \, dx$$

(b)

$$\nabla^2 u_n = -\frac{2m}{\hbar^2} T u_n = -\frac{2m}{\hbar^2} T_{n'n} u_{n'}, \quad \text{with} \quad T_{n'n} = \frac{1}{\Omega_c} \int u_{n'}^* T u_n \, dx$$

(c)

$$V u_n = V_{n'n} u_{n'}, \quad \text{with} \quad V_{n'n} = \frac{1}{\Omega_c} \int u_{n'}^* V u_n \, dx$$

where $\frac{1}{\Omega_c} \int u_{n'}^* u_n \, dx = \delta_{n'n}$.

Using the expressions above we get the final form of equation (4.24):

$$-\frac{\hbar^2}{2m} \nabla^2 F_n(\mathbf{r}) - i \frac{\hbar}{m} \sum_{n'} \mathbf{p}_{nn'} \nabla F_{n'}(\mathbf{r}) + \sum_{n'} H_{nn'}(\mathbf{r}) F_{n'}(\mathbf{r}) = E F_n(\mathbf{r}) \quad (4.25)$$

where $H_{nn'} = T_{nn'} V_{nn'}$.

Solving equation (4.25) still needs a huge numerical effort. Therefore we need some further simplification. In expansion (4.23) we distinguish between two separate band contributions, denoted by S and R . S bands are dominant while R represent remote bands which provides a small contribution. The envelope functions F_r can be expressed via the F_s function as

$$F_r \approx (E - H_{rr})^{-1} \sum_{s'} \left(-i \frac{\hbar}{m} \mathbf{p}_{rs'} \cdot \nabla F_{s'} + H_{rs'} F_{s'} \right) \quad (4.26)$$

Substituting eq. (4.26) in eq. (4.25) we get a constitutive equation for dominant bands

$$\begin{aligned} -\frac{\hbar^2}{2m} \sum_{s'} \nabla \cdot \left[\gamma_{ss'}^{(r)}(E, \mathbf{r}) \cdot \nabla F_{s'}(\mathbf{r}) \right] + \sum_{s'} \frac{-i\hbar}{m} \mathbf{p}_{ss'} \cdot \nabla F_{s'}(\mathbf{r}) + \\ \sum_{s'} H_{ss'}^{(2)}(E, \mathbf{r}) F_{s'}(\mathbf{r}) + \sum_{s', r} \frac{-i\hbar}{m} \mathbf{p}_{sr} \cdot \nabla \left[(E - H_{rr}(\mathbf{r}))^{-1} H_{rs'} \right] F_{s'}(\mathbf{r}) + \\ \sum_{s', r} \frac{-i\hbar}{m} \frac{\mathbf{p}_{sr} H_{rs'} + H_{sr} \mathbf{p}_{rs'}}{E - H_{rr}(\mathbf{r})} \cdot \nabla F_{s'}(\mathbf{r}) = E F_s(\mathbf{r}) \end{aligned} \quad (4.27)$$

where $\gamma_{ss'}^{(r)}$ is

$$\gamma_{ss'}^{(r)}(E, \mathbf{r}) = \mathbf{I} \delta_{ss'} + \frac{2}{m} \sum_r \frac{\mathbf{p}_{sr} \otimes \mathbf{p}_{rs'}}{E - H_{rr}(\mathbf{r})} \quad (4.28)$$

and $H_{ss'}^{(2)}$ is

$$H_{ss'}^{(2)}(E, \mathbf{r}) = H_{ss'}(\mathbf{r}) + \sum_r \frac{H_{sr}(\mathbf{r}) H_{rs'}(\mathbf{r})}{E - H_{rr}(\mathbf{r})} \quad (4.29)$$

The second rank tensor $\gamma_{ss'}^{(r)}$ express the rinormalization of the electron effective mass due to the contribution of remote bands. The term $H_{ss'}^{(2)}$ can be seen as a corrected band edge energy.

The equation (4.27) can be potentially simplified discarding small terms. Choosing different approximations we can derive different models, such as single band EMA equation or multiband Luttinger model.

In the next subsection we'll discuss how these model can be derived, in the case of zincblenda and wurtzite structures. The purpose is getting a starting point to show off the effect of spin-orbit interaction and the effect of strain on the calculation.

4. CONTINUUM MODELS

4.3.2 Conduction and valence states

In the simplest approximation only one band is considered as the dominant with all the rest as a small perturbation. This is typically the case of a semiconductor where the conduction band is far enough from valence bands, i.e. a large energy gap.

For a direct gap semiconductor eq. (4.27) reads

$$-\frac{\hbar^2}{2m}\nabla\left(\frac{1}{m_c(\mathbf{r})}\nabla F_c(\mathbf{r})\right) + E_c(\mathbf{r})F_c(\mathbf{r}) = EF_c(\mathbf{r}) \quad (4.30)$$

Note that we substituted the term $H_{cc}(E, \mathbf{r})$ defined in equation (4.29) (we are labelling the only dominant band s as c), as for large gaps we can remove energy dependences as $E - H_{rr}(\mathbf{r}) \approx E_g(\mathbf{r})$. Therefore also the effective mass energy dependence is removed. E_c and m_c are experimentally fitted parameters. Note two important facts: the first is that eq. (4.30) has no symmetry arguments, so it still holds in wurtzite crystals. The second is that when we're dealing with heterostructures, if the materials have the same Bravais lattice, $U_n((r))$ is the same anywhere, so the function $F_c(\mathbf{r})$ is a continuous function.

The single band approximation doesn't hold for the valence band, so we need to derive a different formulation for the valence band states. In a zincblende structure we have three dominant bands $|X\rangle$, $|Y\rangle$ and $|Z\rangle$ degenerate at the Brillouin zone center, with a p -type angular symmetry. Thus the eigenvalue problem reads

$$H_{vv}(\mathbf{r})\vec{F}_v(\mathbf{r}) = E\vec{F}_v(\mathbf{r}) \quad (4.31)$$

with $\vec{F}_v = \begin{pmatrix} F_X & F_Y & F_Z \end{pmatrix}^T$. We can write the Hamiltonian operator in the general form

$$H_{vv} = \begin{pmatrix} E_v + \frac{\hbar^2}{2m}k^2 & 0 & 0 \\ 0 & E_v + \frac{\hbar^2}{2m}k^2 & 0 \\ 0 & 0 & E_v + \frac{\hbar^2}{2m}k^2 \end{pmatrix} + \begin{pmatrix} k_x L_1 k_x + k_y M_1 k_y + k_z M_2 k_z & k_x C_1 k_y + k_y M_1 k_x & k_x C_2 k_z + k_z M_2 k_x \\ k_y C_1 k_x + k_x M_1 k_y & k_x M_1 k_x + k_y L_1 k_y + k_z M_2 k_z & k_y C_2 k_z + k_z M_2 k_y \\ k_z C_2 k_x + k_x M_2 k_z & k_z C_2 k_y + k_y M_2 k_z & k_x M_3 k_x + k_y M_3 k_y + k_z L_2 k_z \end{pmatrix} \quad (4.32)$$

In a zincblende structure $M_1 = M_2 = M_3$, $L_1 = L_2$ and $C_1 = C_2$ and x, y, z axis are chosen parallel to $[100]$, $[010]$ and $[001]$ orientations. For zincblende structures M, L, C are related to the widely used Luttinger parameters (63), while for wurtzite structure they're related to the A_i parameters in ref. (17; 31).

In the Hamiltonian (4.32) we don't consider any spin-orbit interaction. We can take into account adding a spin-orbit term in the Schrödinger equation:

$$H_{6 \times 6} = \begin{pmatrix} H_{vv} & 0 \\ 0 & H_{vv} \end{pmatrix} + H_{6 \times 6}^{s/o} \quad (4.33)$$

In the first order it's the same as adding an additional term $H_{6 \times 6}^{s/o}$:

$$H_{6 \times 6}^{s/o} = \frac{\Delta}{3} \begin{pmatrix} 0 & -i & 0 & 0 & 0 & 1 \\ i & 0 & 0 & 0 & 0 & -i \\ 0 & 0 & 0 & -1 & i & 0 \\ 0 & 0 & -1 & 0 & i & 0 \\ 0 & 0 & -i & -i & 0 & 0 \\ 1 & i & 0 & 0 & 0 & 0 \end{pmatrix} \quad (4.34)$$

where Δ is the spin orbit coupling energy, and it's a material-dependent parameter. Note that the so defined Hamiltonian is a 6×6 matrix, as we need to extend our basis in order to describe the spin states. Our new basis is given by $|X \uparrow\rangle$, $|Y \uparrow\rangle$, $|Z \uparrow\rangle$, $|X \downarrow\rangle$, $|Y \downarrow\rangle$ and $|Z \downarrow\rangle$, where \uparrow and \downarrow label spin-up and spin-down states. The spin-orbit term is needed as it breaks the degeneracy at Brillouin zone center and predict correctly the spin-off valence band splitting.

In wurtzite structures the anisotropy of the lattice in $[0001]$ direction leads to an additional term which contributes to energy splitting of valence bands. This is due to the pyropolarization, and it's called *crystal field* (16).

if E_v is the degenerate valence band edge without spinorbit effects, the crystal field Δ_{cf} split the levels as follows:

$$\begin{aligned} \langle X | H_0 | X \rangle &= E_v + \Delta_{cf} \\ \langle Y | H_0 | Y \rangle &= E_v + \Delta_{cf} \\ \langle Z | H_0 | Z \rangle &= E_v \end{aligned} \quad (4.35)$$

Another effect we need to take into account is strain. The strain has dramatic effects on electronic bandstructure and it's always present in heterostructures. The inclusion of strain effects in semiconductors has been first dealt by Pikus and Bir (10).

Given a strain tensor in the form of 4.4, we have an additional term (16; 31; 63)

$$H_c^\varepsilon = a_c \text{Tr}(\varepsilon) \quad (4.36)$$

4. CONTINUUM MODELS

for the conduction band and an additional term

$$H_{3 \times 3}^\varepsilon = \begin{pmatrix} l_1 \varepsilon_{xx} + m_1 \varepsilon_{yy} + m_2 \varepsilon_{zz} & n_1 \varepsilon_{xy} & n_2 \varepsilon_{xz} \\ n_1 \varepsilon_{xy} & m_1 \varepsilon_{xx} + l_1 \varepsilon_{yy} + m_2 \varepsilon_{zz} & n_2 \varepsilon_{yz} \\ n_2 \varepsilon_{xz} & n_2 \varepsilon_{yz} & m_3 \varepsilon_{xx} + m_3 \varepsilon_{yy} + l_2 \varepsilon_{zz} \end{pmatrix} \quad (4.37)$$

for the valence band. $a_c, l_1, l_2, n_1, n_2, m_1, m_2, m_3$ are the deformation potentials. In a zincblenda structure $l_1 = l_2 = l$, $n_1 = n_2 = n$ and $m_1 = m_2 = m_3 = m$. Note that this effect is not dependent on spin, then the total valence band hamiltonian is

$$H_{6 \times 6}^{tot} = \begin{pmatrix} H_{3 \times 3} + H_{3 \times 3}^\varepsilon & 0 \\ 0 & H_{3 \times 3} + H_{3 \times 3}^\varepsilon \end{pmatrix} + H_{6 \times 6}^{s/o} \quad (4.38)$$

In periodic systems we need also to remember that crystal deformation leads to a slight modification of reciprocal lattice vectors (24). If we define a deformation tensor ζ_{ij} such that $\varepsilon_{ij} = \frac{1}{2}(\zeta_{ij} + \zeta_{ji})$ is the deformation of the cell and $\delta_{ij} + \frac{1}{2}(\zeta_{ij} - \zeta_{ji})$ is the rotation of the cell, we need to apply the transformation

$$k'_i = (\delta_{ij} - \zeta_{ij})k_j \quad (4.39)$$

When the strain is removed $\mathbf{k}' = \mathbf{k}$.

What happens if we have to deal also with conduction-valence band mixing? In some materials the energy gap is too small to apply the approximation of independent conduction band, thus we need to include both the conduction and the top three valence bands as dominant. The basis include 8 envelope functions (4 without spin-orbit interaction): $|S \uparrow\rangle, |X \uparrow\rangle, |Y \uparrow\rangle, |Z \uparrow\rangle, |S \downarrow\rangle, |X \downarrow\rangle, |Y \downarrow\rangle, |Z \downarrow\rangle$. The total Hamiltonian is:

$$H_{8 \times 8}^{tot} = \begin{pmatrix} H_{4 \times 4}(\mathbf{k}') & 0 \\ 0 & H_{4 \times 4}(\mathbf{k}') \end{pmatrix} + \begin{pmatrix} H_{4 \times 4}^\varepsilon & 0 \\ 0 & H_{4 \times 4}^\varepsilon \end{pmatrix} + H_{8 \times 8}^{s/o} \quad (4.40)$$

The s states have not spin-orbit interaction, thus $H_{8 \times 8}^{s/o}$ from the (4.34) adding 0 rows and columns for the $|S\rangle$ states.

The strain hamiltonian is

$$H_{4 \times 4}^\varepsilon = \begin{pmatrix} H_c^\varepsilon & 0 \\ 0 & H_{3 \times 3}^\varepsilon \end{pmatrix} \quad (4.41)$$

and $H_{4 \times 4}(\mathbf{k}')$ is

$$H_{4 \times 4}(\mathbf{k}') = \begin{pmatrix} E_c + Ak'^2 & iP_0k'_x & iP_0k'_y & iP_0k'_z \\ -iP_0k'_x & \ddots & & \\ -iP_0k'_y & & H_{vv}(\mathbf{k}') & \\ -iP_0k'_z & & & \ddots \end{pmatrix} \quad (4.42)$$

$H_{3 \times 3}(\mathbf{k}')$ is the one defined in eq. (4.32), but the parameters are slightly different as conduction band is no more a remote band. Expression for the modified parameters can be found in ref. (16; 63). A and P_0 are material parameters.

Once that the Hamiltonian is built, Schrödinger equation can be solved to calculate the electronic states. This information can be used to find quantum charge densities and optical matrix elements, as described in the following subsection. The numerical solution is performed in TIBERCAD using Galerkin finite element method. Further informations can be found in ref. (5; 63).

4.3.3 Quantum charge density

Once that eigenfunctions and eigenenergies are known, they can be used to calculate electron and hole density. First of all we need to define an electro-chemical potential to calculate occupation of states.

In equilibrium, the electrochemical potential $\phi(\mathbf{r})$ is well defined, depending on material properties.

Out of equilibrium we assume that the local electro-chemical potentials defined in eq. (4.13) are slowly varying in the regions where quantum states are confined. Then we can define a mean electro-chemical potential defined as follows

$$\bar{\phi}_{n/p,s} = \langle F_s | \phi | F_s \rangle = \int_{\Omega} \phi_{n/p}(\mathbf{r}) |F_s(\mathbf{r})|^2 d\mathbf{r} \quad (4.43)$$

and apply the equilibrium definition for electrons

$$n_Q(\mathbf{r}) = \sum_s \frac{1}{(2\pi)^d} \int_{BZ_{\parallel}} |F_s(\mathbf{r}, \mathbf{k}_{\parallel})|^2 f \left(\frac{E_s(\mathbf{k}_{\parallel}) + e\bar{\phi}_{n,s}}{k_B T} \right) d\mathbf{k}_{\parallel} \quad (4.44)$$

and holes

$$p_Q(\mathbf{r}) = \sum_s \frac{1}{(2\pi)^d} \int_{BZ_{\parallel}} |F_s(\mathbf{r}, \mathbf{k}_{\parallel})|^2 f \left(-\frac{E_s(\mathbf{k}_{\parallel}) + e\bar{\phi}_{p,s}}{k_B T} \right) d\mathbf{k}_{\parallel} \quad (4.45)$$

where f is the Fermi distribution.

4. CONTINUUM MODELS

4.3.4 Optical matrix elements

Consider an electric field, expressed as a vector potential A defined in the Coulomb gauge

$$\mathbf{A}(\mathbf{r}, t) = \frac{ecF_0}{2\omega} \left(e^{i(\omega t - \mathbf{q}\mathbf{r})} + e^{-i(\omega t - \mathbf{q}\mathbf{r})} \right) \quad (4.46)$$

where \mathbf{e} is the polarization vector, \mathbf{q} the wave vector, ω the angular frequency, c the speed of light in the medium and F_0 the field intensity. In the approximation of classical electromagnetic field, thus avoiding second quantization formalism, the Hamiltonian for an electron including the electromagnetic field is

$$H = \frac{\mathbf{p}^2}{2m} + V^s(\mathbf{r}) + \frac{e}{mc} (\mathbf{p} \cdot \mathbf{A}) + \frac{e^2 \mathbf{A}^2}{2m} \quad (4.47)$$

If we consider low intensity fields we can neglect the quadratic term. Treating the linear term as a perturbation and using the *dipole approximation* $\mathbf{q} = 0$ the probability of optical transitions is given by the Fermi golden rule(16; 80):

$$P = \frac{2\pi}{\hbar} |\langle \Psi_i | \tilde{V} | \Psi_f \rangle|^2 \delta(E_f - E_i \pm \hbar\omega) \quad (4.48)$$

where $\tilde{V} = e/mc(\mathbf{p} \cdot \mathbf{A})$ and we choose between $+$ and $-$ whether the photon is emitted or absorbed.

It follows that the device optical properties are determined by the matrix elements

$$M_{if} = \langle \Psi_i | \mathbf{p} | \Psi_f \rangle \quad (4.49)$$

These are the so called *optical matrix elements*. In the EFA model they can be obtained from the derivative of the EFA Hamiltonian over \mathbf{k} (24):

$$M_{if} = \langle \Psi_i | \nabla_{\mathbf{k}} | \Psi \rangle \quad (4.50)$$

Usually it's more convenient to make reference to a derived quantity, the oscillator strength of the dipole transition, which expresses the probabilities of transitions between different levels with a dimensionless quantity:

$$F_{if} = \frac{2|\mathbf{e}M_{if}|^2}{m\hbar\omega} \quad (4.51)$$

5

Atomistic models

In this chapter physical models implemented in TIBERCAD which rely on an atomistic description will be presented. They include a valence force field method, an empirical and a semi-empirical tight binding technique. The atomistic modelling, together with its implementation in a multiscale environment, is the main contribution of this work.

5.1 Valence force field

As described in 4.1, elastic deformation occurs in semiconductor heterostructures, having dramatic effects on the electrostatic and electronic states of a device. We've already described the drawbacks of continuum elastostatic model. An atomistic approach has the purpose to overcome the continuum model limitations.

In molecular mechanics we refer to force field as the functional form and the set of parameters used to describe the potential energy of a system of particles.

There's a lot of force field methods, both empirical or *ab initio*. In this work we'll focus on the so called *valence force field method* (VFF), which offers the best compromise between accuracy and computational effort in the study of semiconductor nanostructures.

5.1.1 The Keating VFF model

The VFF method is an empirical approach to solve the problem of geometry relaxation in crystal structures.

The first model used to describe covalent and ionic crystals is based on the work of Born and von Karman (see a summary in ref (40)). In a notable article Keating

5. ATOMISTIC MODELS

explains the failures of Born Von Karman model and proposes a novel technique to calculate strain energy in diamond structures (36).

The starting point in Keating work is finding a functional form that fulfill the requirement of having a suitable invariant form. Infact the strain energy in a crystal is subjected to two classes of conditions: general physical conditions, such as rotational and translational invariance, and specific conditions imposed by crystal simmetry.

Consider a generic crystal. The first requirement is that the energy V must be invariant under rigid translation of the lattice. Thus V must depend only on the difference between nuclear positions.

$$V = V(\mathbf{r}_k - \mathbf{r}_l) = V(\mathbf{r}_{kl}) \quad (5.1)$$

where \mathbf{r}_k is the position of k th nucleus after deformation. The above expression is not invariant under crystal rotations. The only invariant that can be built with the difference of nuclei positions includes scalar products between them and functions of such products. We have to define

$$\lambda_{klmn} = (\mathbf{r}_{kl} \cdot \mathbf{r}_{nm} - \mathbf{R}_{kl} \cdot \mathbf{R}_{nm}) / 2a \quad (5.2)$$

where a is a lattice constant needed to ensure that λ_{klmn} goes to zero when we have no deformation. Then the enrgy is a function $V(\lambda_{klmn})$. In small deformation regime we can use the terms λ_{klmn} as a basis for a series expansion of V . The linear terms must vanish so that the change in potential energy under any infinitesimal uniform strain from equilibrium is zero. The constant term is not important, so V can be expressed as a summation of quadratic terms plus higher order terms.

$$V = \frac{1}{2} B_{klmn}^{pqrs} \lambda_{klmn} \lambda_{pqrs} + \mathcal{O}(\lambda^3) \quad (5.3)$$

It's important to notice that higher order terms represent anharmonic effects, and that we're completely ignoring them, thus the model is only valid in small linear deformation regime.

The equation (5.3) has still a large amount of redundancy. Infact $3N - 6$ invariants are sufficient to describe an arrangement of N points in a three-dimensional space, while the number of coefficients λ_{klmn} in eq. (5.3) is much larger. The main contribution of Keating is overcoming the difficulty to reduce the set of λ to $3N - 6$ parameters.

The procedure followed by Keating (36) is quite general and in way of principle can be applied to any zincblende crystal, and to wurtzite crystal with some slight modifications. The final expression for the strain potential energy in a diamond structure is

$$V = \frac{1}{2} \sum_l \left[\frac{\alpha}{4a^2} \sum_{i=1}^4 (|\mathbf{x}_{0i}|^2(l) - 3a^2)^2 + \frac{\beta}{2a^2} \sum_{i,j>i}^4 (\mathbf{x}_{0i}(l) \cdot \mathbf{x}_{0j}(l) + a^2)^2 \right] \quad (5.4)$$

where l is a primitive cell, 0 is the index of one atom in the primitive cell, $i = 1, 2, 3, 4$ its nearest neighbours, a the lattice constant. α is the bond stretching force constant, as it rules potential variation under bond length variation, and β is the angle bending force constant, as it rules potential variation under bond angle variation. These parameters are related to elasticity tensor components. From symmetry considerations, the elasticity tensor of a diamond structure is completely described by three components. The relation between them and Keating parameters are

$$\begin{aligned} C_{11} &= (\alpha + 3\beta) / 4a \\ C_{12} &= (\alpha - \beta) / 4a \\ C_{44} &= \frac{\alpha\beta}{a(\alpha + \beta)} \end{aligned} \quad (5.5)$$

From the point of view of Keating model, the three components are not linearly independent and a predicted relation between the elastic constant exists. From a practical point of view usually α and β are derived from c_{11} and c_{12} , which are experimentally measured, and the obtained c_{44} differs from the measured one by less than one percent in diamond. However it's important to remember that this model is not directly applicable to generic fcc structures, as the model is derived for homopolar diamond structures. When we're dealing with a structure with a ionic crystal or a covalent crystal with different ionic species, a point-ion Coulombic force must be added.

5.1.2 Keating model in zincblende and wurtzite structures: limits and features

It follows from eq. (5.5) that according to Keating model we derive the following relation

$$\kappa = \frac{2C_{44}(C_{11} + C_{12})}{(C_{11} - C_{12})(C_{11} + 3C_{12})} = 1 \quad (5.6)$$

This relation is fulfilled for silicon, but it presents deviation up to 20% for non homopolar compounds (75).

Furthermore the Keating model as is doesn't take into account internal strain phenomena, as it doesn't include any Coulomb contribution. This limitation has been

5. ATOMISTIC MODELS

	Si	Ge	GaAs	InAs	InP
κ	0.99	1.07	1.13	1.22	1.20

Table 5.1: - Ratio κ for some zinblenda semiconductors according to eq. (5.6)

workarounded by Martin (47), who proposes a scheme to derive elastic constants and the internal strain parameter (80) in non homopolar zinblenda structures, starting from α , β , a Coulomb term and a dynamic effective charge term derived by the optic mode splitting. As an example, for InAs Martin's approach reduces the error in C_{44} calculation from 22% down to 10%.

Nonetheless Keating model can still achieve reasonable description of elasticity of most semiconductor materials, and it's used in its original formulation in the study of complex nanostructures such as quantum dots (65).

Another approximation in Keating model is neglecting anharmonic effects due to higher order perturbations (see eq. (5.3)). As pointed out by Klimeck et al. (ref. (41)), when we deal with structures with a large lattice mismatch, like InAs/GaAs quantum dots where strain can reach 7%, it introduces an overstimation of hydrostatic strain that leads to an error up to 100 meV in the electron band offset. We should then consider that applying a simple Keating model in heterostructures with high lattice mismatch can lead to an overstimation of the diagonal strain components.

Currently TIBERCAD implements Keating model with the following formulation:

$$\begin{aligned}
 U &= \sum_i U_{i\alpha} + U_{i\beta} \\
 U_{i\alpha} &= \sum_j \frac{3\alpha_{ij}}{16r_{0ij}^2} \left(|\mathbf{r}_{ij}|^2 - r_{0ij} \right)^2 \\
 U_{i\beta} &= \sum_j \sum_{k \neq j} \frac{3\beta_{ijk}}{8r_{0ij}r_{0ik}} (\mathbf{r}_{ij} \cdot \mathbf{r}_{ik} - r_{0ij}r_{0ik} \cos \theta_{0ijk})^2
 \end{aligned} \tag{5.7}$$

Where r_{0ij} is the reference distance between atoms i and j , θ_{0ijk} is the reference angle between atoms i, j, k .

Summation i is over all atoms. When i, j and k belong to different materials, β is geometrically averaged:

$$\beta_{ijk} = \sqrt{\beta_{ij}\beta_{ik}} \tag{5.8}$$

This relation allows us to apply Keating model to interfaces between different materials and to random alloy. Consider as an example a ternary alloy, in the form $A_x B_{1-x} C$,

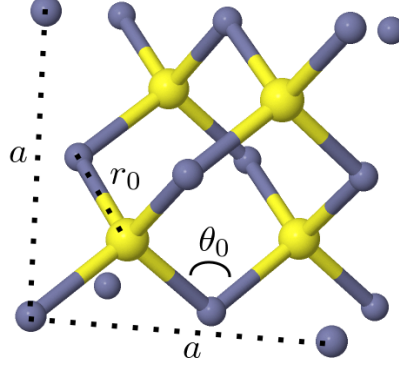


Figure 5.1: A generic zincblenda structure and its characteristic parameters

where AC and BC are two generic $III - V$ semiconductors. In the growth process x represent the percentual of anion A in the alloy, where the exact arrangement of atoms is unknown. We've two way to model a ternary alloy: studying an ensamble of stocastic realizations of structures where we substitute the anion according to the probability x , or defining an effective material, i.e. the virtual crystal approximation. In the latter, we consider the alloy as a fictitious material whose properties are a weighted average of AC and BC properties, according to the molar fraction x . For example, for the elastic constants in eq. (5.5), we would have:

$$C_{ij}^{alloy} = xC_{ij}^{AB} + (1 - x)C_{ij}^{BC} \quad (5.9)$$

Also the lattice constant follows this relation, and it's called *Vegard's law* (20). Not all the properties can be calculated from a linear relation, for example the energy gap has a more complicated expression, including higher order corrections. As the elastic constants can be calculated according to eq. (5.9), α and β can still be calculated with eq. (5.5) and we can define a VFF model on virtual crystals. Otherwise, as α is dependent an anion-cation couple, and β can be averaged for different anion-cation couples as stated in (5.8), we can choose to use a random alloy description and still apply the VFF model.

In wurtzite structures there's an additional complication. While anharmonic and long range Coulomb effects are the same as in zincblende structures, there's an additional issue due to internal strain.

An ideal wurtzite structure (see fig. 5.2) has equal bond lenghts and angle . This is only true when $c = \sqrt{8/3}$ and $u = 3/8$.

Moreover wurtzite are a different point group respect to zincblenda, and the elastic

5. ATOMISTIC MODELS

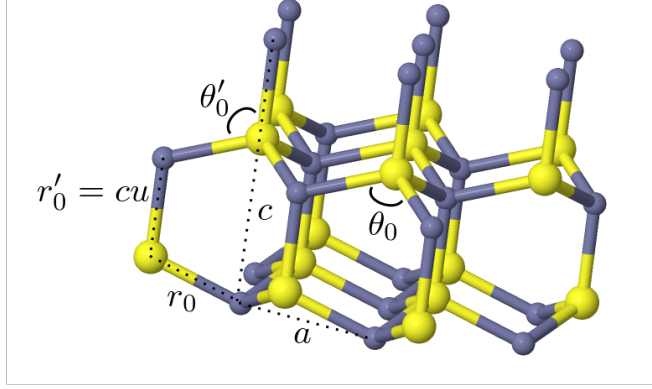


Figure 5.2: A generic wurtzite structure and its characteristic parameters

constant tensor has 6 non zero values (13). A first work by Martin (48) establish the relation between α , β and elastic constants in an ideal wurtzite crystal. But when we're dealing with a non ideal wurtzite, the internal displacement u is important, as it has effect on phonon dispersion, piezoelectric effect and electronic structure. That's why some authors worked on a generalization of Keating VFF model to non ideal structures (13; 29). A nice formulation has been proposed by Niquet (13), and it's the one we apply in TIBERCAD as it can go smoothly from an ideal wurtzite formulation to an ideal one. Referring to lattice parameters in figure 5.2, the VFF potential is generalized as follows

$$\begin{aligned}
 U &= \sum_i U_{i\alpha} + U_{i\beta} \\
 U_{i\alpha} &= \sum_{j=1}^3 \frac{3\alpha_{ij}}{16r_{0ij}^2} (r_{ij}^2 - r_{0ij}^2)^2 + \frac{3\alpha_{i4}}{16r_{0i4}'^2} (r_{i4}^2 - r_{0i4}'^2)^2 \\
 U_{i\beta} &= \sum_{j=1}^3 \sum_{k \neq j} \frac{3\beta}{8r_{0ij}r_{0ik}} (r_{ij}r_{ik} - r_{0ij}r_{0ik} \cos \theta_{0ijk})^2 + \\
 &\quad + \sum_{k \neq 4} \frac{3\beta}{8r_{0i4}'r_{0ik}'} (r_{i4}'r_{ik}' - r_{0i4}'r_{0ik}' \cos \theta_{0i4k}')^2
 \end{aligned} \tag{5.10}$$

For an ideal wurtzite $\alpha = \alpha'$ and $\beta = \beta'$.

Once a potential U is defined, the structure geometry is that one which minimizes the potential. The minimization of the functional can be performed with different techniques. The method used in TIBERCAD is a non linear conjugate gradient method (26). This is an iterative method based on a generalization of conjugate gradient

algorithm. The informations needed for finding a minimum of $U(\mathbf{r})$ are an initial guess array \mathbf{r}_0 and the gradient $\nabla_{\mathbf{r}}U(\mathbf{r})$. In general not all the atom are free to move, but we'll have a function $U(\mathbf{r}, \mathbf{r}_{fixed})$, where the \mathbf{r}_{fixed} can be considered as fixed parameters.

In a nonperiodical structure fixed atoms represent our boundary conditions (BC). If all the atoms are free to move we say we're applying *freestanding* BC. If we want to implement *substrate* BC, equivalent to imposing a lattice mismatch strain as in (4.10), we simply consider the first atomic layer of the substrate material as fixed.

Once we've defined we need to evaluate $\nabla_{\mathbf{r}}U(\mathbf{r})$. The gradient can be calculated numerically through Finite Difference or analitically. The latter method reduces drastically the computational effort and the memory consumption. The expression of gradient for the Keating model in eq. (5.7) is:

$$\begin{aligned}
\frac{\partial U}{\partial x_n} &= \frac{\partial U_{i=n}}{\partial x_n} + \frac{\partial U_{j=n}}{\partial x_n} + \frac{\partial U_{k=n}}{\partial x_n} \\
\frac{\partial U_{i=n}}{\partial x_n} &= \sum_i \sum_{j \neq n} \frac{3\alpha_{ij}}{4r_{0ij}^2} (\mathbf{r}_{ij}\mathbf{r}_{ij} - r_{0ij}^2) (x_i - x_j) + \\
&\quad + \sum_i \sum_j \sum_{k \neq j} \frac{3\beta_{ijk}}{4r_{0ij}r_{0ik}} (\mathbf{r}_{ij}\mathbf{r}_{ik} - r_{0ij}r_{0ik} \cos \theta_{0ijk}) [(x_i - x_k) + (x_i - x_j)] \\
\frac{\partial U_{j=n}}{\partial x_n} &= -\frac{3\alpha_{ij}}{4r_{0ij}^2} (\mathbf{r}_{ij}\mathbf{r}_{ij} - r_{0ij}^2) (x_i - x_j) + \\
&\quad - \sum_{k \neq j} \frac{3\beta_{ijk}}{4r_{0ij}r_{0ik}} (\mathbf{r}_{ij}\mathbf{r}_{ik} - r_{0ij}r_{0ik} \cos \theta_{0ijk}) (x_i - x_k) \\
\frac{\partial U_{k=n}}{\partial x_n} &= -\frac{3\beta_{ijk}}{4r_{0ij}r_{0ik}} (\mathbf{r}_{ij}\mathbf{r}_{ik} - r_{0ij}r_{0ik} \cos \theta_{0ijk}) (x_i - x_j)
\end{aligned} \tag{5.11}$$

There are different libraries aimed to solve optimization problems that can be used to solve nonlinear conjugate gradient problems. TIBERCAD includes TAO (9), a generic optimization C++ code based on PETSc library (7).

5.2 Tight Binding Method

The Tight binding method (TB) is a technique to describe the electronic and optical properties of a material through an atomistic description. A corpuscular approach is needed in devices with nanometric features, where a detailed description of electronic and optical properties cannot be reached with an effective description.

5. ATOMISTIC MODELS

The followig sections will give a brief description of general features of Tight Binding Model. Then we'll focus on two different techniques implemented in TIBERCAD: empirical tight binding (ETB) and density functional tight binding (DFTB).

5.2.1 Tight Binding Model: the atomistic approach

The TB model has been introduces by Slater and Koster in a notable publication in 1954 (74). The starting point is the LCAO (*linear combination of atomic orbitals* representation). If we assume that the electronic states Ψ in the system under observation are perturbations of the atomic states, it's convenient to use the LCAO basis:

$$|\Psi\rangle = \sum_{\alpha \mathbf{R}} C_{\alpha \mathbf{R}} |\alpha, \mathbf{R}\rangle \quad (5.12)$$

Where \mathbf{R} is the atom position and α a quantum number to distinguish between different orbitals. We can then write the time independent Schrödinger equation:

Using the (5.12) in the Schrödinger equation, we get, for every i, α , the expression:

$$\sum_{\alpha' \mathbf{R}'} C_{\alpha' \mathbf{R}'} [H_{\alpha' \mathbf{R}' \alpha \mathbf{R}} - E S_{\alpha' \mathbf{R}' \alpha \mathbf{R}}] = 0 \quad (5.13)$$

where $H_{\alpha' \mathbf{R}' \alpha \mathbf{R}}$ and $S_{\alpha' \mathbf{R}' \alpha \mathbf{R}}$ are the hamiltonian matrix element and the overlap matrix, and are given by:

$$H_{n' \alpha', n \alpha} = \langle n' \alpha' | H | n \alpha \rangle \quad (5.14a)$$

$$S_{n' \alpha', n \alpha} = \langle n' \alpha' | n \alpha \rangle \quad (5.14b)$$

The Hamiltonian can eventually include an external potential V_{ext} term, including externally applied potential and mean field corrections. The overlap matrix is the identity when the basis is orthogonal. This is not the case as in general atomic orbitals have non zero overlap. In general the basis set can be orthogonalized using a Löwdin orthogonalization (43). However resulting wavefunctions have longer range, and it trades in a worst numerical formulation than using a non orthogonal basis. The overlap matrix S can be calculated from the basis function, but in order to solve the generalized eigenvalue problem of equation (5.14) the matrix elements of the Hamiltonian need to be evaluated. The method used to obtain these matrix elements classifies the different TB implementation. Let us assume the effective one-particle Hamiltonian H to be of the form

$$H = \frac{\mathbf{p}^2}{2m} + \sum_n V_n(\mathbf{r} - \mathbf{R}_n) \quad (5.15)$$

where each V_n is the (spherically symmetric) potential produced by the atom at position \mathbf{R}_n . With this, the Hamiltonian matrix elements can be written as

$$H_{n'\alpha',n\alpha} = \int \psi_{\alpha'}^*(\mathbf{r} - \mathbf{R}_{n'}) \left[\frac{\mathbf{p}^2}{2m} + \sum_{n''} V_{n''}(\mathbf{r} - \mathbf{R}_{n''}) \right] \psi_{\alpha}(\mathbf{r} - \mathbf{R}_n) d\mathbf{r} \quad (5.16)$$

The Hamiltonian matrix elements can be classified in four categories (22):

On-site when the atomic wavefunctions and the potential are centered on the same site, i.e. $n = n' = n''$.

Two-centre when wavefunction and potential are on the same site and the other wavefunctions are on different sites, i.e. $n \neq n' = n''$ or $n' \neq n = n''$.

Three-centre when the wavefunctions and the potential are all on different sites, i.e. $n \neq n' \neq n''$.

Local environment correction when the two wavefunctions are on the same site and the potential is on a different site, i. e. $n = n' \neq n''$. This category was ignored by Slater and Koster (74) and is described by Mercer and Chou (50) and shares features with both the two-center and three-center integrals.

Neglecting three-centre and the latter matrix elements is a reasonable tradeoff between computational effort and accuracy. As it's the approach used in TIBERCAD, in the following we'll consider only on-site and two-centre contributions.

Periodical systems can be described using a Block waves representation:

$$|n, \mathbf{k}_{\parallel}\rangle = \sum_{\alpha, \mathbf{R}_{\perp}} C_{\alpha, \mathbf{R}_{\perp}}(n, \mathbf{k}) |\alpha, \mathbf{R}_{\perp}, \mathbf{k}_{\parallel}\rangle \quad (5.17)$$

with

$$|\alpha, \mathbf{R}_{\perp}, \mathbf{k}_{\parallel}\rangle = \frac{1}{\sqrt{N}} \sum_{\mathbf{R}_{\parallel}} e^{i\mathbf{k}_{\parallel}\mathbf{R}_{\parallel}} |\alpha, \mathbf{R}\rangle \quad (5.18)$$

\mathbf{k} is the wave vector in the periodic directions, i.e. the parallel space, N is the number of units cell in the parallel space, \mathbf{R}_{\perp} is the Bravais vector along confined directions and α refers to the basis atom and to the atomic orbital.

In the Bloch sum expansion the Schrödinger equation (5.19) can be written as

$$\sum_{\alpha' \mathbf{R}'_{\perp}} C_{\alpha' \mathbf{R}'_{\perp}} \left[H_{\alpha' \mathbf{R}'_{\perp} \alpha \mathbf{R}_{\perp}} - E S_{\alpha' \mathbf{R}'_{\perp} \alpha \mathbf{R}_{\perp}} \right] = 0 \quad (5.19)$$

5. ATOMISTIC MODELS

It follows that in a bulk crystal, where the system is periodical in all the directions, we have no confined direction, thus no R_\perp can be defined. If we label as ν the atom in the periodical basis and α labels now the orbital of atom ν , the Bloch representation becomes:

$$|n, \mathbf{k}\rangle = \sum_{\alpha, \nu} C_{\alpha\nu} (n, \mathbf{k}) \left[\sum_{\mathbf{R}} e^{i\mathbf{k}\mathbf{R}_\nu} |\alpha, \mathbf{R}_\nu\rangle \right] \quad (5.20)$$

where $\mathbf{R}_\nu = \mathbf{R} + \mathbf{d}_{nu}$ with \mathbf{R} is the lattice vector and d is the basis atom displacement.

Then the Schrödinger equation become:

$$\sum_{\alpha'\nu'} C_{\alpha'\nu'} [H_{\alpha'\nu'\alpha\nu} - ES_{\alpha'\nu'\alpha\nu}] = 0 \quad (5.21)$$

The bulk crystal properties calculation is at the basis of the so called *empirical tight binding*.

5.2.2 Empirical Tight Binding

As seen in previous section, the type of matrix element included in a TB representation is one of the discriminants between one model and another. The other characteristics which differentiate different TB models are the number of interacting neighbours (usually nearest neighbours or second nearest neighbours), the orthogonality of the basis set and the method used to calculate the matrix elements. Focusing on the last point, there's three main techniques to evaluate these parameters: empirical, semi-empirical and ab initio methods.

In empirical tight binding (ETB), matrix elements are calculated as fitting parameters of characteristic bulk quantities, such as effective mass, energy gap and split-off energy.

Referring to eq. (5.14), it's clear that in order to solve the Shrödinger equation and find the set of coefficients $C_{\alpha\nu}$ of equation (5.21), we need to evaluate to different kinds of matrix element: *on-site* matrix elements and *hopping* matrix elements. The on-site matrix elements are defined as follows

$$\varepsilon_{\alpha\nu} = \langle \alpha \mathbf{R}_\nu | H | \alpha \mathbf{R}_\nu \rangle \quad (5.22)$$

while the hopping matrix elements are expressed as

$$t_{\alpha\alpha'}(\mathbf{R}'_\nu - \mathbf{R}_\nu) = \langle \alpha' \mathbf{R}'_\nu | H | \alpha \mathbf{R}_\nu \rangle \quad (5.23)$$

Then the bulk hamiltonian can be defined as

$$H = \sum_{\alpha, \mathbf{R}_\nu} |\alpha \mathbf{R}_\nu\rangle \varepsilon_{\alpha\nu} \langle \alpha \mathbf{R}_\nu| + \sum_{\alpha, \alpha', \mathbf{R}_\nu \neq \mathbf{R}'_\nu} |\alpha' \mathbf{R}'_\nu\rangle t_{\alpha\alpha'}(\mathbf{R}'_\nu - \mathbf{R}_\nu) \langle \alpha \mathbf{R}_\nu| \quad (5.24)$$

Our problem is now reduced to finding on-site and hopping matrix elements. The empirical tight binding technique consists in finding these quantities by fitting the bulk properties of semiconductors, assuming an orthogonal basis, i.e. $S = I$ with I the identity matrix.

The physical meaning of the on-site term is straight: it's the eigenenergy of the corresponding orbital. The hopping energy can be written in different notation. In the original work of Slater and Koster (74), hopping elements are given by linear combinations of atomic orbitals in a two centre approximation. Note that Slater and Koster is based on a Lowdin orthogonalized basis, leading to zero overlap between orbitals. This is a crucial point in ETB technique, as it allow to solve an eigenvalue problem instead of a generalized eigenvalue problem, with a much lower computational effort, and it's the key for the efficiency of ETB respect to ab initio techniques.

It means that any interatomic parameter is labeled as $V_{\alpha\beta\mu}$, where $\alpha, \beta = (s, p, d)$ are the atomic orbitals involved and μ is the component of angular momentum around the bond axis, i.e. $\mu = \sigma$, $\mu = (\sigma, \pi)$, $\mu = (\sigma, \pi, \delta)$ respectively for ss , sp , sd , pp , dd and dd bonds. This is the so called *molecular orbital notation*. The relationship between these quantities and hopping matrix elements (Koster notation) is shown in Slater and Koster work.

The chemistry of localized states in covalent semiconductors needs at least an eight band parametrization (one s and three p orbitals with spin degeneracy) (78). Historically, the first approach to empirical tight binding has been using these sp^3 basis, expanding often the interaction to second nearest neighbours. Infact first-neighbour sp^3 models fail in many points: it's proofed that they cannot reproduce an indirect gap in diamond and zincblende materials and they cannot fit even the lowest conduction bands of semiconductors as Ge, Si, AlAs and GaP (15). However a second-neighbour basis is not desirable as it cannot be used to describe random alloys and heterointerfaces in a straight way, while first neighbour parametrizations are used under the assumption that parameters are portable when we're not dealing with bulk structures, and locally the neighbours interact as in the corresponding bulk material.

Vogl (78) overcame this deficiencies by including an excited s state, i.e. the s^* state, on each atom. With this approach it's possible to get a ten band nearest neighbour

5. ATOMISTIC MODELS

sp^3s^* parametrization which describe with a good degree of accuracy bulk IV group semiconductors, zincblenda and wurtzite III-V materials and ternary alloys.

If we consider a binary compound this parametrization leads to six on-site parameters and seven hopping terms ($s - s^*$ interactions are neglected). In the notation used by Vogl (derived from Slater notation, see (78)), they're so defined:

$$\begin{aligned}
 V_{sa,sa} &= 4t_{ss}(\mathbf{R}_a - \mathbf{R}_c) & V_{xa,yc} &= 4t_{p_x p_y}(\mathbf{R}_a - \mathbf{R}_c) & V_{pa,sc} &= 4t_{p_x s}(\mathbf{R}_a - \mathbf{R}_c) \\
 V_{pa,s^*c} &= 4t_{p_x s^*}(\mathbf{R}_a - \mathbf{R}_c) & V_{xa,xc} &= 4t_{p_x p_x}(\mathbf{R}_a - \mathbf{R}_c) & V_{sa,pc} &= 4t_{s p_x}(\mathbf{R}_a - \mathbf{R}_c) \\
 V_{s^*a,pc} &= 4t_{s^* p_x}(\mathbf{R}_a - \mathbf{R}_c)
 \end{aligned} \tag{5.25}$$

Similarly to EFA approach (see 4.33), Chadi (14) has introduced a spin orbit correction on p orbitals in the TB framework. Using the states $|p_{x\nu}, \uparrow\rangle$, $|p_{y\nu}, \uparrow\rangle$, $|p_{z\nu}, \uparrow\rangle$, $|p_{x\nu}, \downarrow\rangle$, $|p_{y\nu}, \downarrow\rangle$, $|p_{z\nu}, \downarrow\rangle$ as a basis, where ν stands for the anion or the cation, we have

	$ p_{x\nu}, \uparrow\rangle$	$ p_{y\nu}, \uparrow\rangle$	$ p_{z\nu}, \uparrow\rangle$	$ p_{x\nu}, \downarrow\rangle$	$ p_{y\nu}, \downarrow\rangle$	$ p_{z\nu}, \downarrow\rangle$
$ p_{x\nu}, \uparrow\rangle$	0	$-i\Delta_{\nu}^{s/o}$	0	0	0	$\Delta_{\nu}^{s/o}$
$ p_{y\nu}, \uparrow\rangle$	$\Delta_{\nu}^{s/o}$	0	0	0	0	$\Delta_{\nu}^{s/o}$
$ p_{z\nu}, \uparrow\rangle$	0	0	0	$-\Delta_{\nu}^{s/o}$	$i\Delta_{\nu}^{s/o}$	0
$ p_{x\nu}, \downarrow\rangle$	0	0	$-\Delta_{\nu}^{s/o}$	0	$i\Delta_{\nu}^{s/o}$	0
$ p_{y\nu}, \downarrow\rangle$	0	0	$-i\Delta_{\nu}^{s/o}$	$-i\Delta_{\nu}^{s/o}$	0	0
$ p_{z\nu}, \downarrow\rangle$	$\Delta_{\nu}^{s/o}$	$i\Delta_{\nu}^{s/o}$	0	0	0	0

where $\Delta_{\nu}^{s/o}$ is a fitting parameter.

sp^3s^* has been used for years and it's still routinely applied. However, it still suffers some inner limitations. It cannot fit the X valley transverse mass (11), making its application critical in cases where X valley contribution are important, as highly confined structures or materials with a band minimum in X like Silicon. There are two ways to overcome these limitation: increasing the number of neighbours or increasing the number of parameters.

For the reasons previously explained, we find more convenient not to abandon the nearest neighbour approach. Luckily we can rely on modern parametrizations that include d orbitals, leading to a 30 bands description. The parametrization by Jancu *et al* (34; 35), gives a very accurate description of C, Si, Ge, AlP, InP, GaAs, AlAs, InAs, GaSb, AlSb, InSb, GaN, AlN and InN. This parametrization introduces seven additional hopping matrix elements, but at the cost of an increased computational cost, it offers a very accurate description of nanostructures. Figure 5.3 and 5.4 shows two bandstructures calculated with Jancu parameters within TIBERCAD

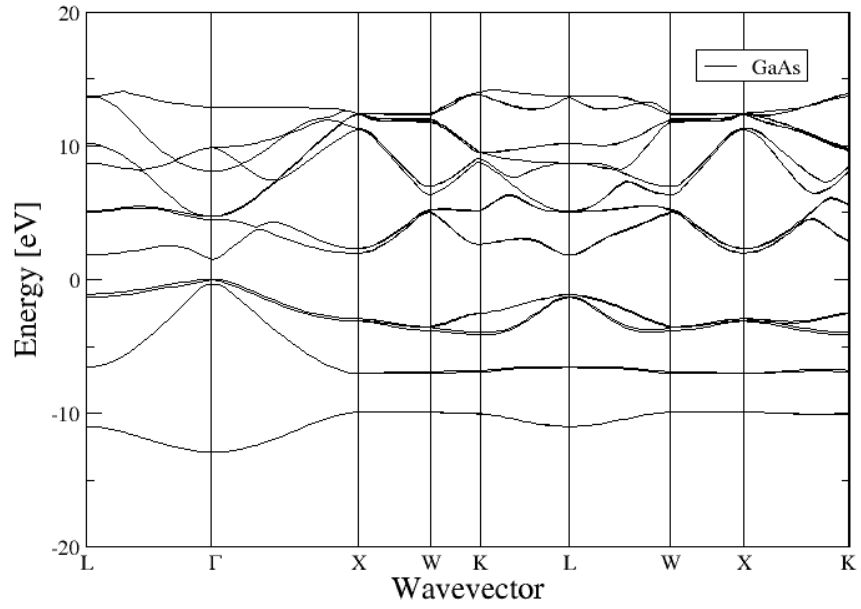


Figure 5.3: bandstructure of Gallium Arsenide calculated with Jancu $sp^3d^5s^*$ parametrization

5. ATOMISTIC MODELS

For wurtzite structures, it includes a crystal field term, similar to what explained in sec. 4.32.

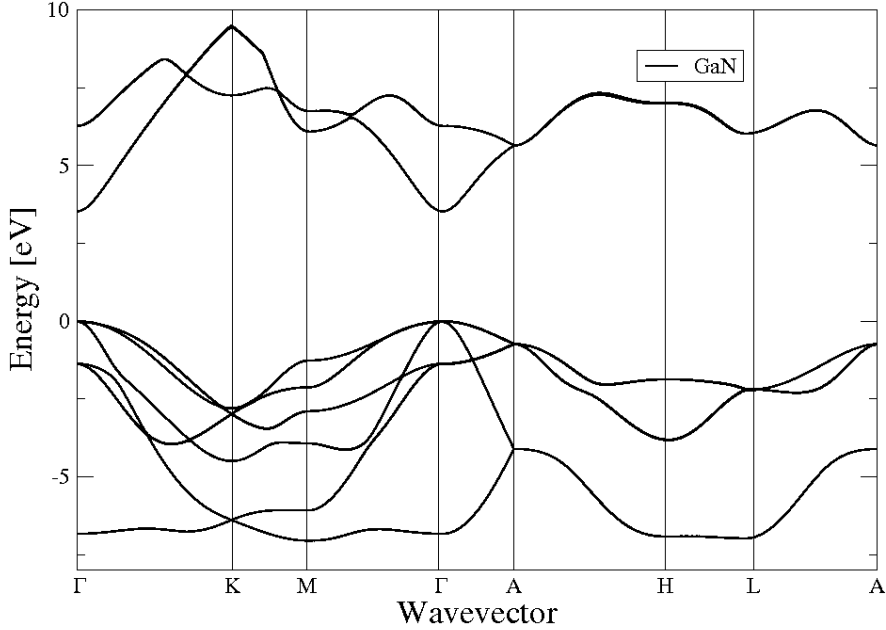


Figure 5.4: bandstructure of Gallium Nitride calculated with Jancu $sp^3d^5s^*$ parametrization

5.2.2.1 Beyond bulk materials: strain, alloys and confined structures

Thanks to its features, empirical tight binding is an ideal technique to model semiconductor optoelectronic devices. Parameters are portable, and in the two centre nearest neighbour picture we can easily deal with interfaces and random alloys.

An important issue in tight binding calculations is the effect of the strain. As seen in sec. 4.3.1, the strain has dramatic effects on the electronic states. Strain has three effects on an atomistic description: it modifies the reciprocal lattice vector in a periodic structure, similarly of what happens in \mathbf{k} theory as described in sec. 4.3.1, it modifies the two centre matrix elements and it affects the crystal field.

The first effect is the most trivial, and it's taken into account defining the Bloch functions according to the new reciprocal lattice. The second effect is due to the change in bond length respect to the reference bulk lattice used to fit the ETB parameters. It has been first investigated by Harrison (27), and then refined by many authors (22). The so called *Harrison scaling law* states that ETB parameters scale approximately linearly with d^{-2} , where d is the bond length. In its modern formulation, the scaling

law is defined by

$$H'_{ll'm} = H_{ll'm} \left(\frac{d_0}{d'} \right)^{\eta_{ll'm}} \quad (5.26)$$

where d_0 and d' are respectively the distances between the two atoms without and with strain. $\eta_{ll'm}$ is a constant dependent on the kind of matrix element in molecular orbital notation.

The last of the three effects is the most complicated. Note that after a deformation, in materials that have no polarization fields in their bulk configuration, i.e. zincblende, the anisotropy of the crystal can be broken, leading to polarization fields that shift bond energies.

For example, uniaxial [001] strain introduces a tetragonal crystal field which lifts the degeneracy of the xy, xz and yz atomic levels (34). Jancu proposes an *ad hoc* relation between d states matrix elements and uniaxial strain tensor. However, being it valid only in uniaxial strain approximation, it's a valid solution only in quantum well growth along [001] direction.

In general this is still an hot topic, and there's a lot of different solution proposed in literature. Boykint *et al* introduce position-dependent orbital energies in the $sp^3d^5s^*$ Hamiltonian. Niquet *et al* introduce corrections on the onsite matrix elements between s, p and d orbitals. However, neglecting this latter effect and adjusting matrix elements with the Harrison scaling law is a reasonable approximation for practical applications. and this is the approximation assumed in TIBERCAD.

Harrison scaling is also used to represent alloys. Using the virtual crystal approximation (VCA), we define a fictitious material which characteristics are determined by constituent bulk materials. Bond distances scale following Vegard's rule. As an example, for a ternary alloy $A_xB_{1-x}C$ we have

$$d(A_xB_{1-x}C) = xd(A_xB_{1-x}C) + (1-x)d(A_xB_{1-x}C) \quad (5.27)$$

Matrix elements are then scaled according to Harrison's rule. In fig. 5.5 the energy gap in a GaN/Al_xGa_{1-x}N quantum well is shown as the molar fraction x varies.

Another problem that we encounter when we are not dealing anymore with bulk structures is defining boundary conditions. Depending on the physical problem investigated, several boundary conditions (BC) can be used: periodic, cluster and open.

When we deal with a confined region usually we assume that the wavefunction needs to vanish going far from that region. Take as an example a structure confine in one direction: a quantum well. We assembly the Hamiltonian considering the structure

5. ATOMISTIC MODELS

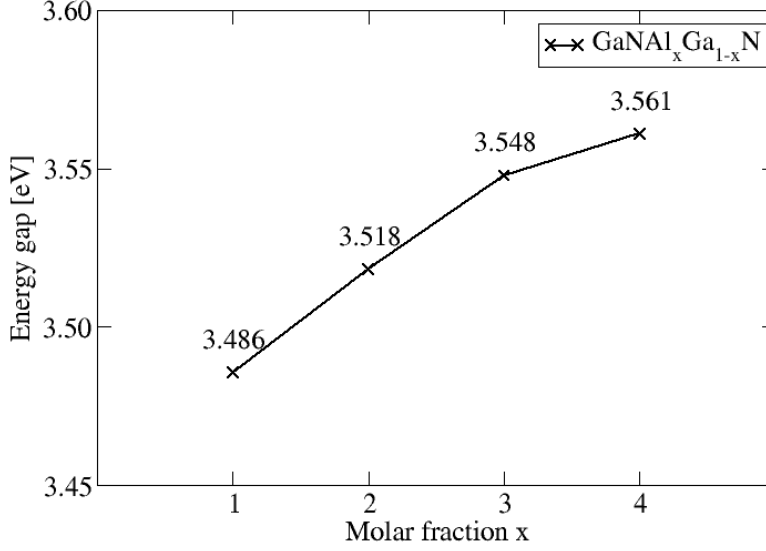


Figure 5.5: Distance between first valence and conduction state in 6 nm $GaN/Al_xGa_{1-x}N$ quantum well.

periodic in y, z directions and confined in x direction, i.e. we have no k_x components in the wvector. At the edge atoms we'll have dangling bonds, which introduce spurious surface states. Moreover these states can fall in the band gap, leading to unphysical predictions.

To avoid this effect we need to saturate dangling bonds. This operation is usually called *passivation*, and there's different solution proposed in literature (42; 61). In TIBERCAD we saturate the bond with fictitious hydrogen atoms. Matrix elements are supposed to be the same of the missing element in the bond, increased by a scaling factor, i.e. $V_{\alpha h} = V_{\alpha\beta}s_h$ where $V_{\alpha\beta}$ is any matrix element between anion and cation and s_h is a constant with a typical value of 100. On-site element is considered to be a huge energy ($\varepsilon \sim -200eV$), to avoid hydrogen states population.

The effect of this numerical trick is that it shots dangling states to energies not in our region of interest. Also passivation technique in ref. (42) has been implemented but it still has not been fully verified in our code and our parametrizations, so no results obtained with this technique are presented in this work.

We can also impose open boundary conditions, i.e. electronic states are free to propagate in semi-infint contacts, generating a current flow in the device. There are

different techniques to impose open BC (22). Previously a transmission matrix formalism has been used in TIBERCAD (5). In this work the Green's function technique will be discussed. See chapter 8 for further details.

Once that the Hamiltonian has been set up including strain, passivation and eventually external potential, we solve the associated eigenvalue problem and we get the quantum states.

Similarly to EFA, we can use these informations to calculate many quantities: quantum charge can be calculated populating the states Ψ_i with the electrochemical potential $\langle \Psi_i | \phi | \Psi_i \rangle$. The atomic charge can be easily written as (52)

$$q_\nu = \frac{1}{2} \sum_{\text{occupied states}} \sum_{\alpha} (C_{\alpha\nu}^{k*})^2 \quad (5.28)$$

Optical matrix elements are obtained from the derivative of the EFA Hamiltonian over \mathbf{k} , plus a correction due to intra-atomic contributions (58).

Summarizing, ETB is a powerful technique when we need to deal with semiconductors. The empirical parametrization ensure that all the characteristic quantities are describe with a very high degree of accuracy. Moreover it uses an orthogonal basis, reducing computational effort and allowing to use smart algorithms. Nevertheless, we cannot rely only on ETB. Empirical tight binding has no informations about repulsive ion-ion potential, so it's not appliable for structure relaxations, and it's intrinsically a technique for studying crystal structure, making it almost unuseful in molecular electronics.

5.2.3 Density Functional Tight Binding

For the previously explained reasons, we cannot rely only with an ETB description of atomistic quantum mechanics. TIBERCAD includes a Density Functional Tight Binding (DFTB) module developed by the Bremen Center for Computational Material Science (21). DFTB is a semiempirical method based on the work on Frauenheim, Seifert and Porezag (62; 72). In this method the atomic-like wavefunctions used in the LCAO expansion (5.12) are obtained by solving an *ab initio* DFT atomic problem in the local density approximation (LDA).

The main result of DFT theory is that we can reduce a system of interacting particles to a system of non interacting particles experiencing an effective potential that generate the same charge ditribution at equilibrium. The system is described by the *Kohn-Sham* equations:

5. ATOMISTIC MODELS

$$\left(\frac{\hbar^2}{2m} \nabla^2 + V_{eff}(\mathbf{r}) \right) \chi_n(\mathbf{r}) = \varepsilon_n \chi_n(\mathbf{r}) \quad (5.29)$$

$$n(\mathbf{r}) = \sum_{n=1}^N |\chi_n(\mathbf{r})|^2 \quad (5.30)$$

where V_{eff} is the *Kohn-Sham* potential, and it includes external and hartree potential and a exchange-correlation term which take into account the effects of quantum interference.

$$V_{eff}(\mathbf{r}) = V(\mathbf{r}) + \int \frac{n(\mathbf{r}')}{|\mathbf{r} - \mathbf{r}'|} d\mathbf{r}' + \frac{\delta E_{xc}(n)}{\delta n} \quad (5.31)$$

where the second term is the Hartree potential. In the DFTB model the atomic wavefunctions are calculated using:

$$V_{eff}(\mathbf{r}) = V_{nucleus}(\mathbf{r}) + V_{Hartree}[n(\mathbf{r})] + V_{xc}^{LDA}[n(\mathbf{r})] + \left(\frac{r}{r_0} \right)^N \quad (5.32)$$

The last term is introduced to ensure that the wavefunction vanishes far away from the nucleus (in the original work $N=2$ for any element). This approximation is really crucial as it allows to use the calculated wavefunctions to build a two centre representation. The term V_{LDA} represent the exchange-correlation term of eq. (5.31) (see ref. (60)) in a local density approximation.

The states used in eq. (5.29) are the so called *Kohn-Sham orbitals*. In DFTB we represent them in Tight Binding basis, as a sum of pseudoatomic wavefunctions ψ_ν . Thus, solving the eigenvalue problem

$$[\hat{T} + V_{eff}(\mathbf{r})] \psi_\nu(\mathbf{r}) = \varepsilon_\nu \psi_\nu(\mathbf{r}) \quad (5.33)$$

where \hat{T} is the kinetic part of the Hamiltonian, we get the wavefunctions ψ_ν that we'll use as LCAO basis. These are (s, p, d) -like orbitals. In this way we solve the atomic DFT problem and find the (s, p, d) -like basis to be used in LCAO representation. Within a minimal basis description, only valence orbital are considered. Then we write the one electron potential of the many-body DFT solution as:

$$V_{eff}(\mathbf{r}) = \sum_k V_0^k(|\mathbf{r} - \mathbf{R}_k|) \quad (5.34)$$

where V_0 is the Kohn-Sham potential of a neutral pseudoatom due to its compressed electron density. Thus the matrix element is

$$H_{\mu\nu} = \begin{cases} \varepsilon_{\mu}^{freeatom} & if \mu = \nu \\ \langle \psi_{\mu}^A | \hat{T} + V_0^A + V_0^B | \psi_{\nu}^B \rangle & if A \neq B \\ 0 & otherwise \end{cases}$$

The resulting Hamiltonian matrix elements can be used to describe the electronic band structure (BS) of a system using a twocentre LCAO representation, but it doesn't contain any information about the repulsive atom-atom interaction, thus it cannot be used to relax the geometry.

The repulsive potential naturally arises from the exchange-correlation part of DFT, as it's due to Pauli exclusion principle. In general, it can be expressed as

$$V_{rep}(r) = E_{LDA}^{xc}(r) - E_{BS}(r) \quad (5.35)$$

Where V_{rep} is spherically symmetric. This quantity is extracted from the DFT calculation on different sets of couple of atoms. Then a potential that can fit well the different cases is chosen and taken as an additional set of atom parameters. Finally our set is described by these parameters and the atomic-like wavefunctions.

It arises naturally that the main advantages of DFTB approach are the following:

- i The inclusion of repulsive LDA part allows to perform geometry relaxation and to take into account exchange-correlation effects.
- ii Once that the parametrization for the atom is calculated, it's portable to a wide range of systems, including molecules.
- iii Being a two-centre representation, we can take advantage from the fact that the basis is still a local basis.
- iiii Its computational cost is much lower than DFT techniques

By the other side, the atomic-like wavefunctions are not an orthogonal basis, thus they overlap and $S \neq I$ where S is the overlap matrix and I is the identity matrix. For this reason its computational cost is typically higher than ETB, making it a good method for structure up to a few thousands atoms.

DFTB has been extended to take calculate self-consistent charge-field solutions. This extension, call SCC-DFTB, has been developed by Elnster *et al* (23), and it's based on a second-order expansion of Kohn-Sham energy functional respect to charge fluctuations.

In SCC-DFTB the matrix element reads

5. ATOMISTIC MODELS

$$H_{\mu\nu} = \langle \psi_\nu | \hat{H}_0 | \psi_\nu \rangle + \frac{1}{2} S_{\mu\nu} \sum_{i=1}^N (\gamma_{\alpha i} + \gamma_{\beta i}) \Delta q_i = H_{\mu\nu}^0 + H_{\mu\nu}^1 \quad (5.36)$$

where $S_{\mu\nu} = \langle \psi_\mu | \psi_\nu \rangle$ is the overlap matrix, Δq_i is the variation of Mulliken charge of atom i :

$$q_i = \frac{1}{2} \sum_{\text{occupied states}} n_k \sum_{\alpha \in i} \sum_{\mu, j} (c_{k, \mu j}^* c_{k, \alpha i} s_{\mu j, \alpha i} + c_{k, \alpha i}^* c_{k, \mu j} s_{\alpha i, \mu j}) \quad (5.37)$$

γ_α is a functional that can be approximated with (23) $\gamma_{\alpha\alpha} = U_\alpha$, where U_α is the Hubbard parameter of atom α .

For the off-site elements the γ functional has the general form

$$\gamma_{ij} = \int \int \frac{F_{00}^i(r') F_{00}^j(r)}{|r - r'|} dr dr' \quad (5.38)$$

where $F_{00}^i(r)$ are spherical densities centered around the atoms. The term H^1 in eq. (5.36) must be calculated in a self-consistent way, as total charge and Kohn-Sham potential have a reciprocal dependency. The effect is more visible in systems with a big charge transfer, which is the case of organic molecules, binary semiconductors and in general systems with highly electronegative elements.

The boundary conditions can be treated in a way similar to empirical tight binding. However, cluster can be passivated through real functionalizations (like H or OH), or a self consistent treatment of surface dangling states can be performed through SCC-DFTB. We can also impose open boundary conditions. Green formalism is an optimal technique as it can be integrated in the self-consistent mechanism, as it will be discussed in next chapter.

6

Continuous/atomistic environment in TiberCAD

After having explained many physical models involved in continuous/atomistic calculations in TIBERCAD, in this chapter we'll see the structure of the simulator itself, how these different models are arranged in a unique environment and how it deals with information at atomistic level.

6.1 TIBERCAD structure

TIBERCAD (64) is simulation software born from the long experience of optolab group (30) in optoelectronic devices modelling and simulation.

The aim of TIBERCAD is to give a flexible environment for the calculation of electronic and optical properties of devices ranging from micrometric to nanometric dimensions. This project has been also presented in other works (5), the novel contents presented here are focused on the integration with atomistic models.

TIBERCAD can be divided into different components, as schematically shown in figure 6.1.

Input : the input section is composed by three elements. The first is a *mesh* file which contains a geometrical description of the device and the discretization mesh for FEM calculation. TIBERCAD has not an internal modeler, but it supports two external graphical tools: DEVISE (33) and GMSH (28). Providing a mesh geometry is mandatory. The second element can be an atomistic structure in *xyz* or *gen* format. TIBERCAD supports also its own format (*tgn*) which is derived by *gen* format and contains additional informations useful in its environment.

6. CONTINUOUS/ATOMISTIC ENVIRONMENT IN TIBERCAD

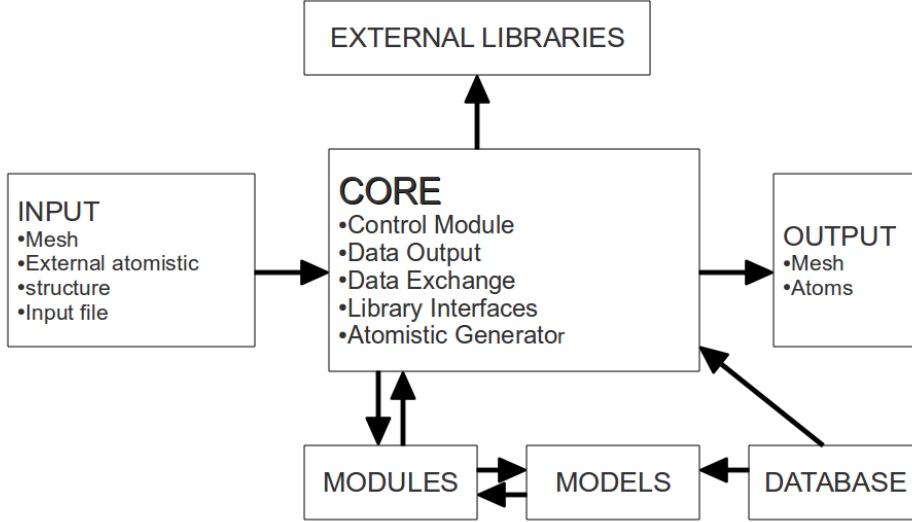


Figure 6.1: schematic representation of TIBERCAD software

Providing an atomistic structure from file is not mandatory, as for some classes of materials it can be built internally, according to mesh geometry. Then an input file is needed, where informations about the materials and the simulations are provided.

Core : the core is the main TIBERCAD infrastructure. It's written in C++, as an object-oriented language allows to manage complex data structures and to handle simulation models in a flexible way, taking advantage of class polymorphism. It includes a *control module* that take care of managing the execution of different modules. Methods for data exchange allow multiphysics and multiscale calculations on both continuous and atomistic representations. Generic methods for data output allow to reduce code redundancy. The core includes also wrappers for external libraries, in order to ensure that the communication between modules and external codes is painless and that internally the developer can handle a smaller subset of data structures. The core includes also an input parser that handles the input file, making the entries easily accessible for the developers. I'll focus on the following on the atomistic generator.

Modules and models : these are the units which pratically perform the matrix assembly and solve the problem of interest. As *model* we mean classes that can manage any physical parameter that depends on material (or on more complex

quantities) which do not affect discretization or matrix assembly (for example a mobility model for drift-diffusion). By *modules* we mean we mean larger classes which handle the simulation themselves (for example the drift-diffusion module), handle the mesh or the atomistic structure and assembly the matrix, possibly using values provided by models.

Database : it contains parameters for a wide range of materials, ranging from semi-conductors to insulators to organic materials. It can be accessed by modules and models.

Output : methods implemented in the core are used to produce output values on mesh nodes (VTK, GMV) or atomistic structure (JMOL).

External libraries : TIBERCAD relies on a wide range of external open source libraries, written in C++ and Fortran 90: Libmesh (39), PETSc (7), SLEPc, TAO (9) and homemade libraries.

6.2 Mesh and atomistic structures

TIBERCAD is mainly based on a geometrical description of the device at a continuous level. This description is based on a finite element discretization, i.e. a *mesh* file. The mesh can be defined in one, two or three dimensions and it contains a list of the elements, and boundary elements used for the description of boundary conditions. The elements are grouped into non-overlapping *regions*. In the input file the regions are reassembled into *physical regions* or *clusters*. The physical regions are made of a single material characterized by a set of constant parameters (doping, crystal orientation, molar fraction). Clusters are groups of physical regions, regardless of their material or parameter. An example of mesh geometry is shown in figure 6.2

If we need also an atomistic description for the whole device, or even only for some regions (or clusters). One solution is providing the structure from file. However this is an annoying task, especially if we have to deal with lot of different structures. Moreover not all scientific communities are used to manage atomistic descriptions, in particular people involved in optoelectronic device simulation as almost all technology-CAD codes used are based on a continuous media description.

To overcome these problems I included a tool for automatic generation of crystal structure for any complex geometry. Let's suppose that we are dealing with the structure in figure 6.2 and that we want to perform an empirical tight binding calculation or a VFF geometry relaxation on regions 2, 3, 4.

6. CONTINUOUS/ATOMISTIC ENVIRONMENT IN TIBERCAD

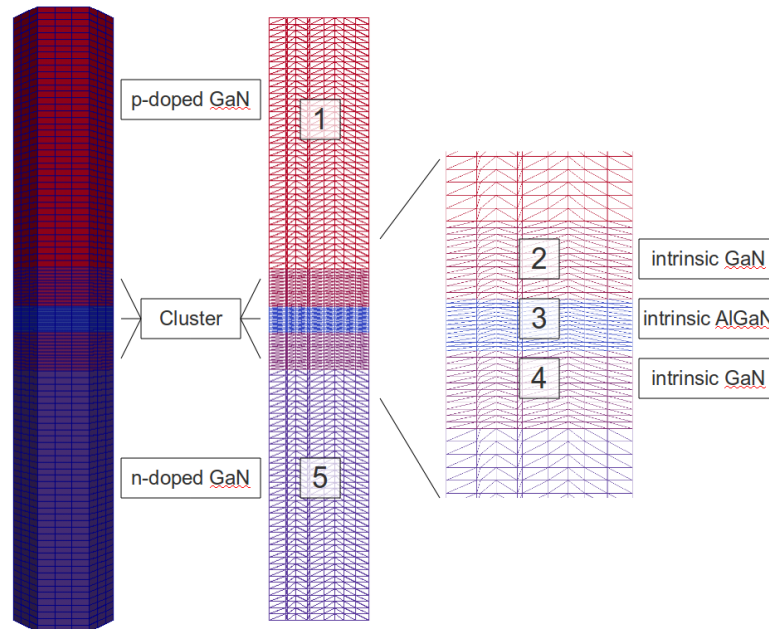


Figure 6.2: example of mesh geometry of a p-i-n GaN/AlGaN nanocolumn structure

In the input file we can describe these regions in a **Device** section as follows ¹:

```
$Device
{
    Options
    {
        meshfile = example.msh
        structure = wz
        x-growth-direction = (-1,0,1,0)
        y-growth-direction = (1,-2,1,0)
        z-growth-direction = (0,0,0,1)
    }

    Region buffer1
    {
        reg_numb = 1
        mat = GaN
    }

    Region qdisk
```

¹for more exhaustive input file examples and tutorials see www.tibercad.org


```

{
  reg_numb = 2
  mat = AlGaN
  x = 0.3 #molar fraction
}

Region buffer2
{
  reg_numb = 3
  mat = GaN
}

Cluster quantum
{
  mesh_regions = (buffer1, qdisk, buffer2)
}

Atomistic example
{
  physical_regions = quantum
  reference_region = buffer1
  print = (gen, xyz, xyb, tgn)
  passivation = yes
}
}

```

The **Option** section contains information common to all regions. In this example, we are specifying the mesh file and fixing the crystallographic orientation and the crystal phase (wurtzite). The **Region** sections contain specific information for any physical regions (regions 1 and 5 are omitted for sake of brevity). **Cluster**, as stated before, group different regions together to avoid redundancy.

The **Atomistic** tells that we want an atomistic description of some physical regions. We can charge an external structure with the keyword `load = external_structure.xyz` or we can take advantage of the internal generator, as in this example. The result is the structure in figure 6.3.

This is the meaning of the different entries:

- **physical_region** tells which regions we want to cover with a crystal structure.
- **reference_region** the region specified here states which material and param-

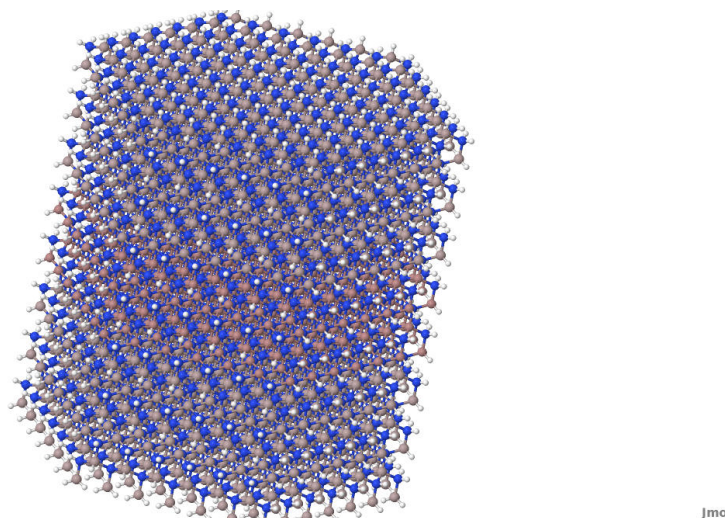


Figure 6.3: structure associated with regions 2, 3, 4 of figure 6.2.

eters (growth direction, molar fraction, crystal phase) we will use to build the crystal. Note that we assume a pseudomorphic growth, i.e. all the structure has the same lattice constants and only the atomic specie is changed according to materials different from that one specified in **reference_region**. The structure will be eventually relaxed with the continuum elasticity or VFF or DFTB model.

- **print** it specifies that we want an output file containing the structure in different formats. *xyb* is a modified *xyz* format with additional columns containing the bond map. *tdn* is an internal TIBERCAD format which combines informations on the mesh and the atoms.
- **passivation** it states that we want to add an hydrogen passivation to the structure. Hydrogen atoms are put at a distance of 1 Å, in the same direction of the original crystal bond.

The internal atomistic generator has the following features:

- It supports any crystal structure with fcc, bcc, cubic and hexagonal Bravais lattice. Informations about basis and primitive vectors is taken from the database, and new materials can be added without changing the code.
- It performs hydrogen passivation for any crystal structure supported, with a reasonable choice in hydrogen position that minimize relaxation efforts, whether a physical relaxation of hydrogens is needed.

- It includes an $\mathcal{O}(N)$ algorithm to calculate the bond map of any structure.
- It can be used to generate commensurable interfaces.

Once that our device has been described defining continuous and atomistic regions, we can feed with these informations the modules that implement the physical models previously described. As we'll see in the application examples, output can be provided both on the mesh or on the atoms, depending on the particular simulation.

6. CONTINUOUS/ATOMISTIC ENVIRONMENT IN TIBERCAD

7

Applications

In this chapter some applications that allows to take advantage of a mixed continuous/atomistic simulation environment are shown. The reader will notice that they cover a wide range of classes of optoelectronic devices, some of them nearer to an engineering application side, some other more interesting from a theoretical point of view. This is the key point: showing the flexibility allowed by TIBERCAD code to experiment novel combinations between physical models with different complexity.

7.1 Strain in quantum dot structures: valence force field and continuum elasticity

Continuum elasticity model has been already predicted to give slightly different results respect to VFF in nanostructured heterointerface (65; 75). The discrepancy is not easy to evaluate, as it depends on the materials and on the geometry of the structures.

We present a comparison between the two models in quantum dot InAs/ $\text{In}_x\text{Ga}_{1-x}\text{As}$ structures. We first consider a spherical quantum dot with a diameter of 1nm , embedded in a cubic box with a side length of 16nm . We fix a *substrate* boundary condition, i.e. the structure is grown along z axis on a $\text{In}_x\text{Ga}_{1-x}\text{As}$ substrate. The structure is shown in figure 7.1

For all the calculations we used parameter from ref. (75). The elastic costants are calculated within a virtual crystal approximation, the lattice parameters is calculated with Vegard's law (20).

In figure ?? the strain components along an axis parallel to z crossing the middle of the dot. An InAs/ $\text{In}_{0.6}\text{Ga}_{0.4}\text{As}$ stucture is considered. The strain obtained with VFF is interpolated with a cubic function, as we can get the exact strain only on anion (or

7. APPLICATIONS

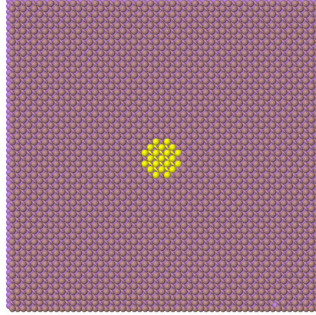


Figure 7.1: spherical quantum dot structure used for the calculations

cation) sites. We can first notice that there's a relevant difference at the interfaces for the ε_{xx} and ε_{zz} ($\varepsilon_{xx} = \varepsilon_{yy}$ as $C_{11} = C_{22}$). The VFF calculation does not allow an abrupt discontinuity as the strain is somehow averaged on the displacements of the unit cell. However, even in the middle of the structure there's a quantitative difference between VFF and CE, that is about 15% in the centre of the dot.

It's interesting to underline what happens to the shear strain component ε_{xy} . For symmetry reason, in an ideal spherical dot we should not see any shear strain component, and it's exactly what we get in continuum elasticity model (see Fig. ??). On the contrary we can see that with the VFF calculation we obtain a non-zero value. This is probably due to the fact that in the atomistic model we cannot have a structure with exact spherical symmetry and the dot is squared according to the crystal structure.

The high difference in the two calculations can be due to the size of the structure, which is so small that differences between the two models at the interfaces can affect the whole dot. We propose some calculations on more realistic structure, i.e. GaAs/InAs quantum dots with truncated pyramid shape. These structures are realized via Stranski-Krastanov growth and the strain is actually the driving force for the creation of self-organized quantum dots (54), with the possibility to control the shape of the self-assembled structures (68).

We considered the structure in figure 7.3, which is a truncated square pyramid quantum dot with a high aspect ratio. The InAs dot has a base of 9 nm and a height of 2 nm, and it's grown on a 0.5 nm wetting layer. The dot is embedded in a GaAs box, which act as a substrate.

A comparison between x and z diagonal components of the strain tensor is shown in figure ???. In the middle of the dot we have a difference of about 4.7% for the ε_{xx} component and 14% for the ε_{zz} component. A little mismatch of the interfaces in the z direction is due to the fact that the continuous mesh and the atomistic structure are

7.1 Strain in quantum dot structures: valence force field and continuum elasticity

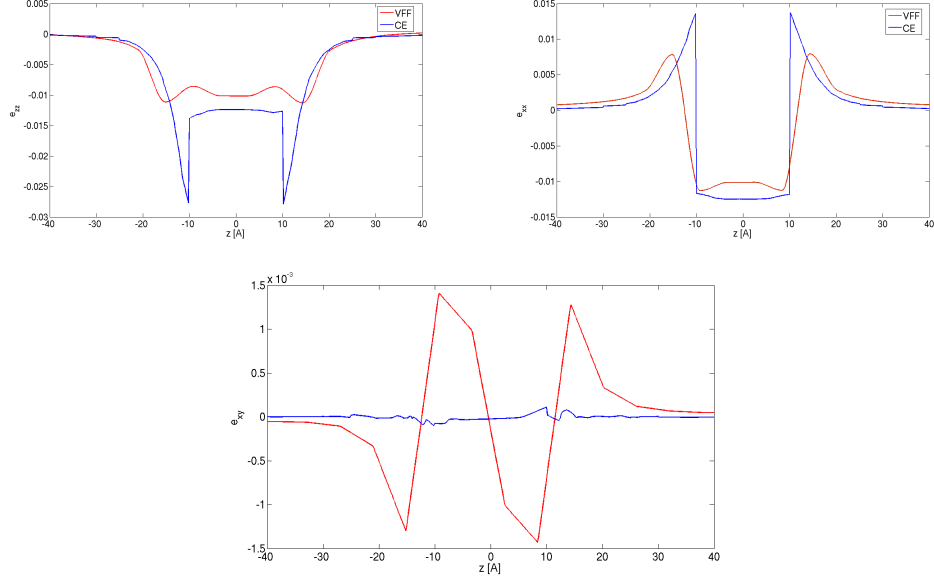


Figure 7.2: VFF and CE strain profile in the $\text{In}_x\text{Ga}_{1-x}\text{As}/\text{InAs}$ quantum dot of figure 7.1. The plot is considered to be along a line parallel to z direction and passing through the centre of the dot.

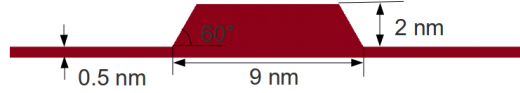


Figure 7.3: GaAs quantum dot device with wetting layer (left) and ε_{zz} calculated with CE model.

aligned within an atomic layer.

The difference between the ε_{zz} component is higher than the one found in literature (65; 75). However the previous work are based on pyramidal structures. Moreover, Bimberg (75) compares a continuum elasticity model with a VFF with anharmonic corrections. Although it's physically more reasonable, as the strain in these kind of heterointerfaces can go up to 5%, a comparison between Keating VFF and continuum elasticity is meaningful as we are comparing two different harmonic models.

It can be seen that if we consider a truncated pyramid with a lower aspect ratio, i.e. a height of 5 nm, the strain components inside the dot calculated with VFF and CE are in good agreement. The difference between the two calculation is about 2% inside

7. APPLICATIONS

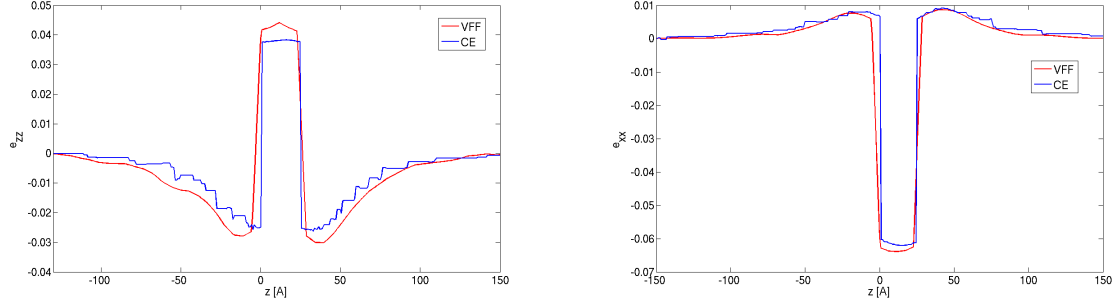


Figure 7.4: VFF and CE strain profile in the GaAs/InAs quantum dot of figure 7.3. The plot is considered to be along a line parallel to z direction and passing through the centre of the dot.

the dot and the bigger difference is at the interfaces.

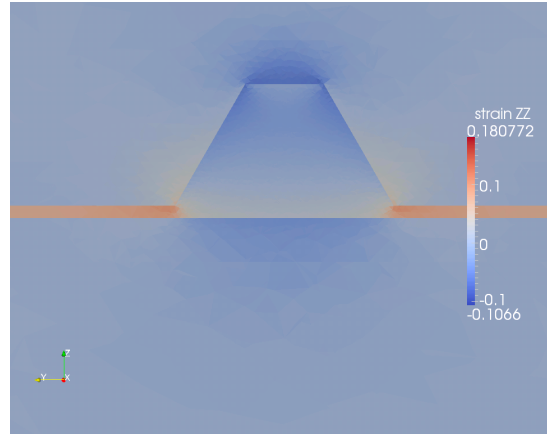


Figure 7.5: ε_{zz} profile calculated with CE in a GaAs/InAs quantum dot with lower aspect ratio.

7.1 Strain in quantum dot structures: valence force field and continuum elasticity

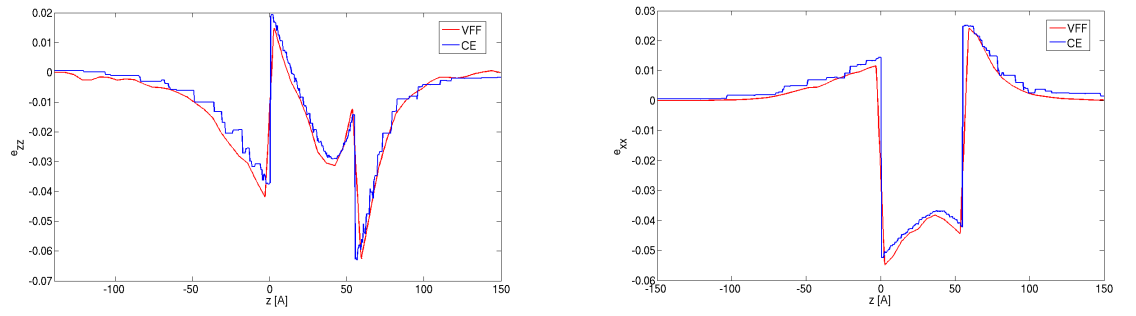


Figure 7.6: VFF and CE strain profile in the GaAs/InAs quantum dot of figure 7.3. The plot is considered to be along a line parallel to z direction and passing through the centre of the dot.

7. APPLICATIONS

7.2 Optical properties of a GaN quantum dot embedded in a $\text{Al}_x\text{Ga}_{1-x}\text{N}$ nanocolumn

We present an application of TIBERCAD to calculate study the spontaneous emission of a nanostructured LED under biased conditions. Novel optoelectronic devices based on III-V alloys and nanostructured geometries, such as nanocolumns, has been already proposed in literature (38; 66). Advantages of such structures are in their high crystalline quality, self-organized growth process, compatibility with Si(111) substrates and promising optical properties. Also conical quantum dots grown in similar structures has been recently studied (70), in the direction of realizing optical devices with complex nanostructured geometries.

The device under study is shown in figure 7.7.

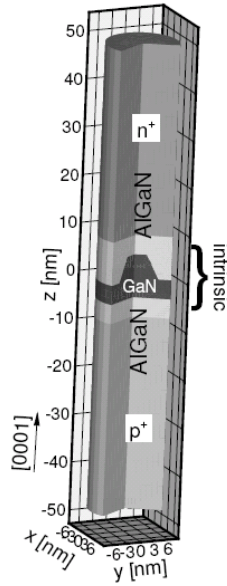


Figure 7.7: structure of the nanocolumn with the embedded quantum dot

This is a 15 nm diameter $\text{Al}_{0.3}\text{Ga}_{0.7}\text{N}$ nanocolumn of 100nm height with a conical GaN quantum dot with a diameter of 10 nm at the bottom and 6 nm on the top, grown on a thin wetting layer. The device is doped with a $p^+ - i - n^+$ profile. Dopant density is 10^{19}cm^{-3} for both donors and acceptors. Acceptors are supposed to have an activation energy of 170 meV. Donors activation energy is typically lower, and it has been set to 25 meV, leading to a much higher electron density at room temperature. Undoped regions have been modeled with a 10^{15}cm^{-3} donor residual concentration.

The following models have been used: continuous media strain, drift-diffusion, en-

7.2 Optical properties of a GaN quantum dot ambedded in a $\text{Al}_x\text{Ga}_{1-x}\text{N}$ nanocolumn

velope function approximation multiband $\mathbf{k}\cdot\mathbf{p}$ and empirical tight binding. First the strain tensor is calculated through continuum elasticity, in order to get the piezoelectric polarization, and relative displacement in any mesh point.

Transport of hole and electrons is calculated through drift-diffusion model. Spontaneous and piezoelectric polarization are included, the latter coming from previous strain calculations. Semiconductor parameters (energy gap and mobility) are calculated with bulk $\mathbf{k}\cdot\mathbf{p}$ models, taking into account local strain.

Both an EFA and ETB quantum calculation are performed to calculate the electronic states and the emission spectra. The result of Drift-diffusion is seen as a potential correction that, together with the inclusion of strain in the Hamiltonian (?), provide external corrections to quantum calculation. the atomistic structure is generated within TIBERCAD and the atoms are moved according to displacement calculated by the CE module.

We characterize the device by comparing the electronic and optical properties in devices with (0001) and (000 $\bar{1}$) growth directions along z axis. The aim is to evaluate the role of macroscopic polarization on the emission spectra, as inverting the growth direction we're inverting the piezopolarization, as shown in fig. 7.8.

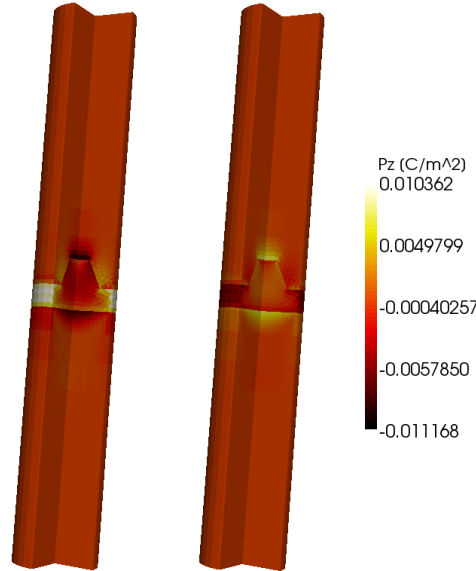


Figure 7.8: Z component of piezoelectric polarization for (0001) (left) and (000 $\bar{1}$) (right) device.

In figure ?? a calculation of the spontaneous emission with an EFA model is shown, both including or not the strain Hamiltonian. We can observe the blue shift due to

7. APPLICATIONS

compressive strain acting on the active layer. This effect is shown for both (0001) and (000 $\bar{1}$) directions. By inverting the growth direction, the piezoelectric field direction is inverted, whereas strain is left unchanged. Therefore, there is no difference in the shifts between the opposite directions, but we have different spectrum shapes due to, as we'll see, electrostatic effects included in the Hamiltonian. Both current profile and emission spectrum are affected by changing growth direction. From an engineering point of view we are interested in finding the direction that optimize both electrical and optical efficiency.

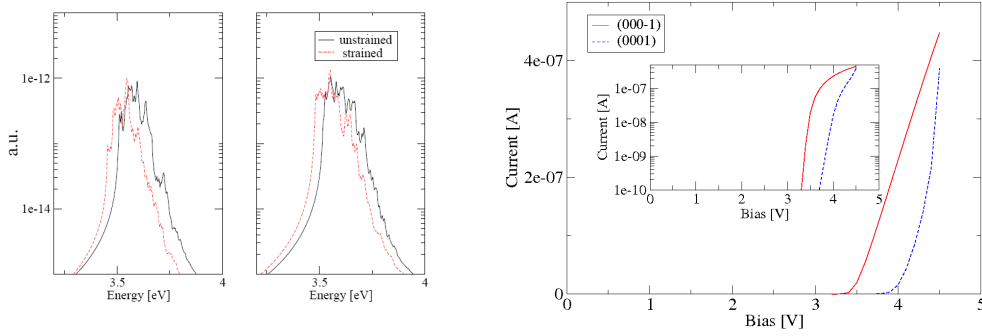


Figure 7.9: Emission spectra for (0001) device (left), (000 $\bar{1}$) device (middle) with and without strain corrections. IV characteristics (right).

We can easily calculate the ratio between quantum efficiencies obtained with the different devices. Fixing a current point, chosen to be $0.3\mu A$, it's simply given by:

$$\frac{\eta_{000\bar{1}}}{\eta_{0001}} = \frac{P_{000\bar{1}}^{opt}}{P_{0001}^{opt}}$$

where P_{opt} is just obtained integrating the emission spectra. As arbitrary units are coherent between the two calculations, we neglect any error due to power units. The result is that the (000 $\bar{1}$) device has a quantum efficiency increase of 16%.

This difference is not only due to the difference in the electric characteristic, but it's also due to the effect of macroscopic polarization on the arrangement of states. The injected charge in the intrinsic region cannot completely screen the piezoelectric field, which is strong enough to swap electron and hole states position, as shown in figure 7.10.

This increases the overlap between states for the (000 $\bar{1}$) device, as the hole state is confined by the geometry, and the electron state is confined by the transverse piezoelec-

7.2 Optical properties of a GaN quantum dot embedded in a $\text{Al}_x\text{Ga}_{1-x}\text{N}$ nanocolumn

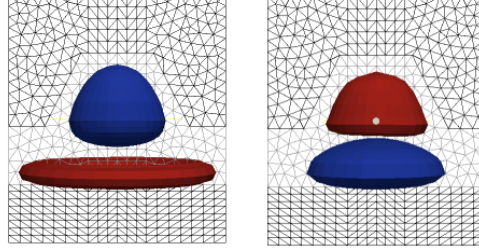


Figure 7.10: ground state of electron (blue - upper) and hole (red - lower) for (0001) (left) and ground state of electron (blue - lower) and hole (red - upper) for (000 $\bar{1}$) (right) device.

tric field, while in the (0001) device the hole ground states is confined in the wetting layer rather than in the dot. This can be seen also in figure ??, where the first peak is lowered for the (0001) direction. Such phenomena are reduced if we consider a wetting layer scaled down from 4 to 1 nm. As shown in figure ??, the effect of the piezoelectric field is still the same, leading to states swapping, but the hole state is no more confined in the wetting layer, and we obtain a good states overlap even for the (0001) direction. This implies that, as can be seen in the emission spectra in figure ??, the first emission peak has the same intensity for both the directions, while a notable difference can be seen in figure ?? for the previous structure. The result is that, for (000 $\bar{1}$) device, efficiency increase is only 4% respect to (0001) growth direction.

EFA has been demonstrated to be a suitable theoretical instrument also for the study of nanostructured devices, despite its inner physical limitations (12). We can compare the results obtained with the EFA model with an empirical tight binding. The same corrections are applied: macroscopic potential are included in the Hamiltonian as an additional term on Hartree potential, i.e. it's projected on the on-site element of the Hamiltonian. The geometry is relaxed with CE calculation. In figure ?? the atomic structure for the thin wetting layer device is shown, overlapped to the mesh and the electric potential profile.

Note that the effect of macroscopic polarization is crucial. When piezoelectric and bias contributions are projected on to the Hamiltonian, a band bending is induced and the salateX skip page me state arrangement as in the EFA calculations is observed 7.13.

We can also calculate the emission spectrum using the ETB states (occupancy level is considered respect to drift-diffusion quasi-fermi level). The results are in a good qualitative agreement, we've the same trend changing growht direction 7.14. However

7. APPLICATIONS

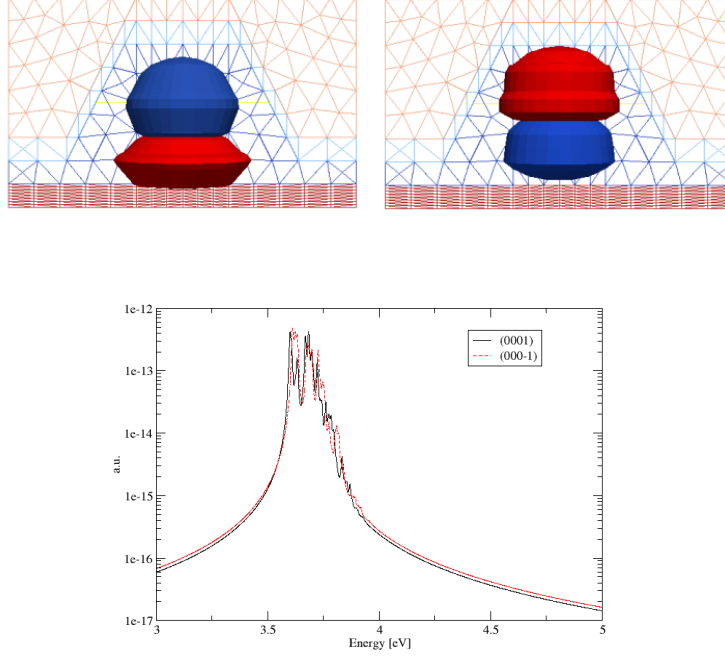


Figure 7.11: EFA ground states for (0001) device (upper left) and (000 $\bar{1}$) device (upper right) for electron (blue) and hole (red). Spontaneous emission spectra (lower).

there's a not negligible quantitative difference in the emission energy. With EFA model we get the first emission at 3.560 eV for the (0001) device and 3.9707 eV for the (000 $\bar{1}$) device. With ETB model we get the first emission at 3.6072 eV for the (0001) device and 3.9057 eV for the (000 $\bar{1}$) device. We see that a difference of tens of electronvolt.

7.2 Optical properties of a GaN quantum dot embedded in a $\text{Al}_x\text{Ga}_{1-x}\text{N}$ nanocolumn

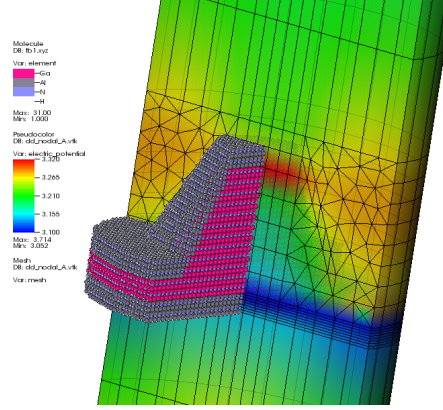


Figure 7.12: Atomistic structure, mesh and electric potential profile.

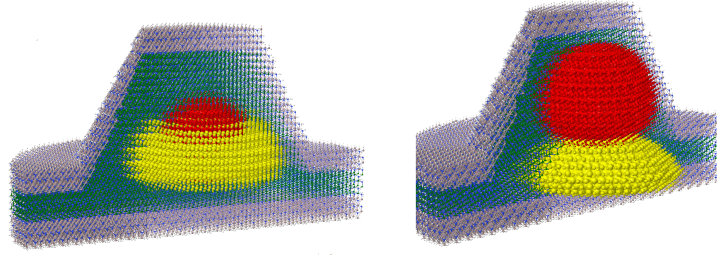


Figure 7.13: First valence (yellow) and conduction (red) states without projected potential (left) and with projected potential (right).

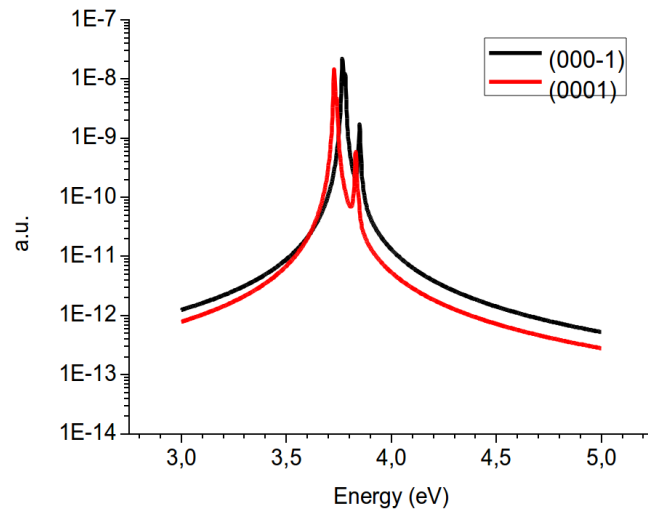


Figure 7.14: emission spectra calculate with ETB for (0001) and (000 $\bar{1}$) growth direction

7.3 Self consistent tight binding/drift-diffusion simulation of a GaAs/Al_xGa_{1-x}As structure

In this application we present an example of self consistent Schrödinger/drift-diffusion calculation. In the previous example we could see that it's necessary to evaluate the Schrödinger equation, whether by ETB or EFA, adding corrections due to external polarization and strain. At a first glance, we used the results from a 'pure' macroscopic drift-diffusion, i.e. the density of states is the density of states of the bulk material in the whole device. This is one strong approximation we make. In this application we propose a corrected scheme that couples a DOS derived with quantum calculation in the confined region with a drift-diffusion extended on the whole device. Note that we're still assuming that the quantum region is almost at equilibrium, and that states are confined such that we can apply close bounday conditions. The only way to overcome this approximation is switching to a NEGF calculation, but we have at least two drawbacks: we cannot calculate the whole device with NEGF because of a huge computational effort and drift-diffusion allows to take macroscopic effects into account more easily out of the active region.

The selfconsistent loop is implemented using a simple predictor-corrector scheme which assumes that the quantum density n_Q varies with the potentials as the classical density n_{cl} . Under this assumption the predictor for the electron density to enter the drift-diffusion model during the $(k + 1)^{th}$ selfconsistent iteration reads

$$n_Q(\phi^{(k)} + \delta\phi) \approx \frac{n_Q(\phi^{(k)})}{n_{cl}(\phi^{(k)})} n_{cl}(\phi^{(k)} + \delta\phi) ,$$

where $\phi^{(k)}$ is the potential after the k^{th} iteration, and $\delta\phi$ is the correction to the potential that has to be calculated.

As the electron and hole states in the system are calculated applying closed boundary conditions, the quantum densities near the interface between quantum mechanical and classical simulation domains suffer from artifical behaviour. To obtain a continuous transition from purely classical to purely quantum mechanical densities we define an embracing region with an extension of a few nanometers where we use a linear combination of the two.

As an example we present a simulation of a rectangular AlGaAs/GaAs nanocolumn in p-i-n configuration. The GaAs quantum disk is embedded in the center of the intrinsic zone. The device structure is shown in Fig. ???. All quantum mechanical calculations are restricted to the intrinsic part of the device, and correspondingly the

7.3 Self consistent tight binding/drift-diffusion simulation of a GaAs/Al_xGa_{1-x}As structure

atomistic structure is created only in this region. The resulting atomistic structure contains 50'945 atoms, including the hydrogen passivation atoms (see Fig. ??).

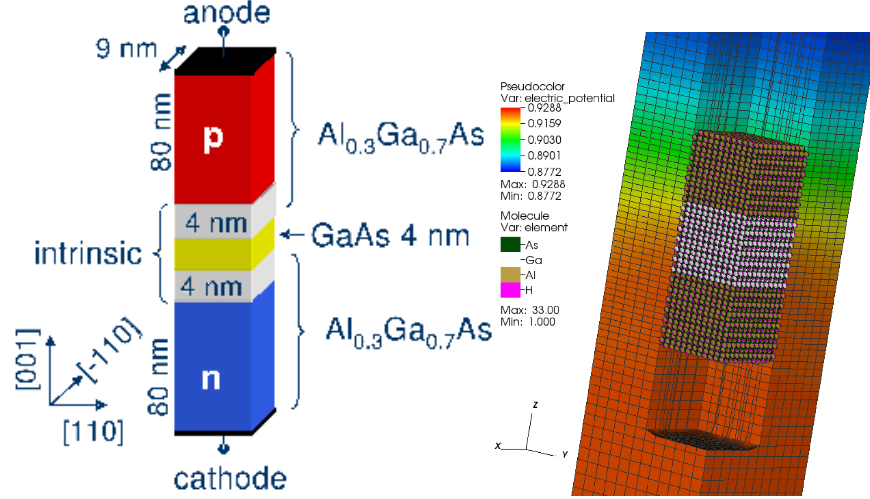


Figure 7.15: Geometrical structure of device under investigation (left) and atomistic structure and mesh (right).

We first use the drift-diffusion model without considering quantum mechanical particle densities to obtain the IV curve of the device. Then we chose a bias voltage for which the device is in nearly flat band condition and we restart the simulation for this voltage (1.875 V), considering in a selfconsistent loop the quantum mechanical particle densities resulting from the confinement in the GaAs quantum disk (using EFA). The selfconsistent band edges and electrochemical potentials in comparison with the classical results and the selfconsistent electron and hole densities are reported in Fig. 7.16. As the quantum mechanical carrier densities spread into the AlGaAs barriers, a higher density compared with the classical case is observed, leading to a flattening of the electrochemical potentials. Therefore a lower gradient of the electrochemical potential is needed to maintain a nearly constant particle flux across the barrier. Fig. 7.16 reports the selfconsistent particle densities in the intrinsic part of the column.

We can take advantage from the TIBERCAD environment running the same simulation with an atomistic ETB model. Note that substituting an EFA model with an ETB model is quite painless and the possibility to run such a wide set of quantum models is a unique TIBERCAD feature. In the following we present a selfconsistent calculation using ETB only for the electron states.

Due to the fact that for the considered structure there are many dense hole states in

7. APPLICATIONS

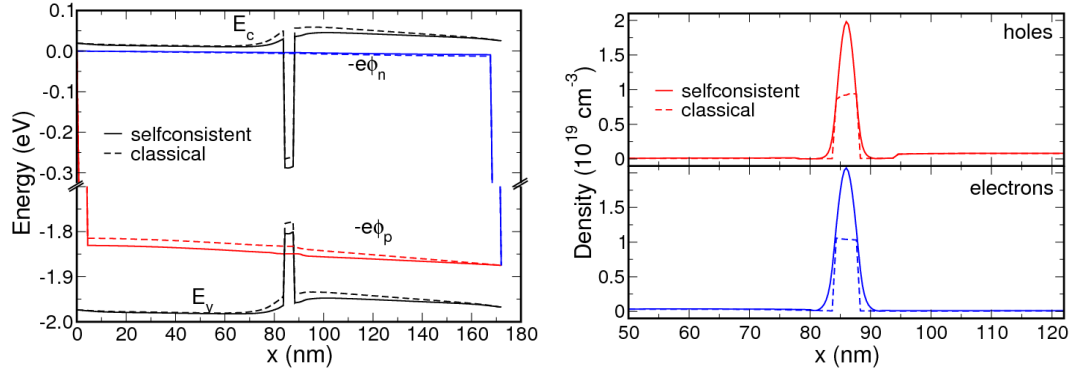


Figure 7.16: Band profile and electrochemical potentials along the z-axis for selfconsistent and classical solutions (left), selfconsistent and classical particle densities along the same line (right). The quantum mechanical model is EFA.

the GaAs quantum disk, it is computationally unfeasible to use ETB for the hole states. Using an $sp^3d^5s^*$ parametrization including spin-orbit interaction, the Hamiltonian of the system has dimension in the order of 900'000 and the solution of a single hole state requires on a standard PC about 3–4 hours. On the contrary, there is only one confined electron state. For this reason we use ETB for the electrons only, calculating two states (due to spin degeneracy), and EFA for the holes such that we can include enough hole states to obtain an approximately convergent hole density. Fig. ?? presents the selfconsistent band profile and the particle densities for this simulation along the z-axis compared with the classical result. We observe a slightly smaller electron density due to the fact that the states calculated by ETB are less localized compared to those calculated by EFA.

The band structure and the charge density for this calculation are shown in figure 7.17.

Finally we compute the ETB emission spectra, including the first electron and the first three hole states.

The values of the energy levels are reported in the table 7.1, compared with the corresponding EFA results.

We see that the hole states are in a quite good agreement, making meaningful our choice to calculate valence states with EFA and conduction states with ETB. As we expect, the second heavy hole states differs slightly more, as EFA model is less accurate for the higher states.

7.3 Self consistent tight binding/drift-diffusion simulation of a GaAs/Al_xGa_{1-x}As structure

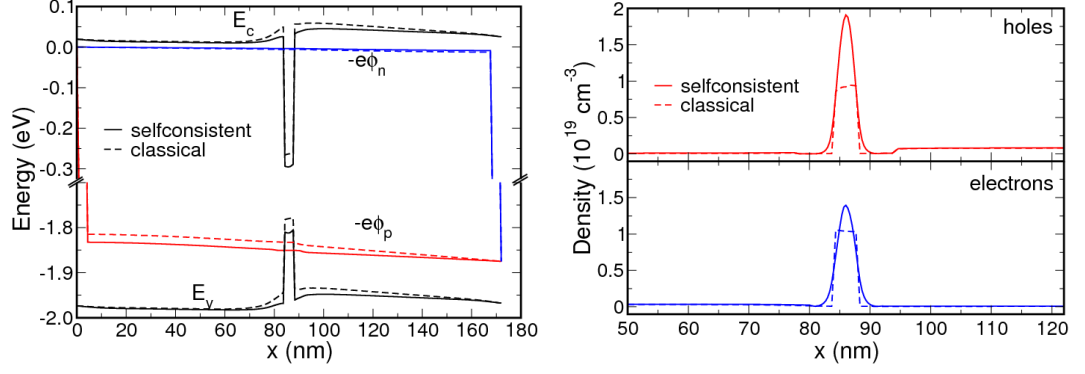


Figure 7.17: Band profile and electrochemical potentials along the z-axis for selfconsistent and classical solutions (left), selfconsistent and classical particle densities along the same line (right). The quantum mechanical model is ETB.

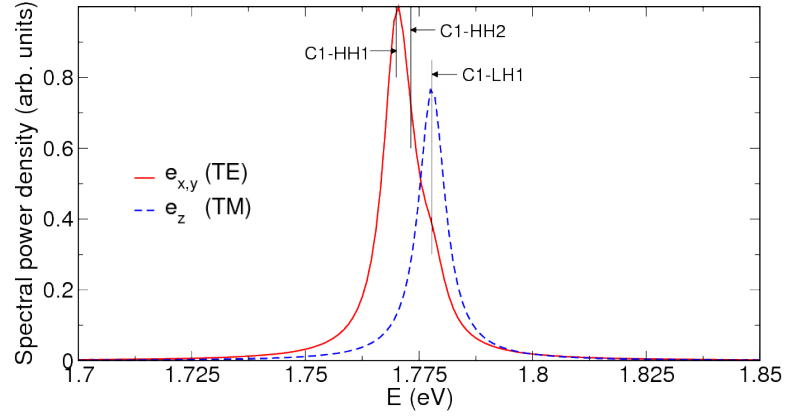


Figure 7.18: spontaneous emission spectra for different polarizations.

Table 7.1: Energy levels of ETB iand EFA states

band	eigenenergy (eV)	
	ETB	EFA
C1	-0.11	-0.0464
HH1	-1.8809	-1.8858
HH2	-1.8839	-1.8912
LH1	-1.889	-1.8936

7. APPLICATIONS

Quantum Transport: NEGF theory and application

In this chapter a powerful tool for describing open boundary conditions in quantum systems is described. EFA, ETB and DFTB are the techniques used in TIBERCAD to describe the Hamiltonian of the system. Even if they are based on a description on a different level, they share one fundamental characteristic: they are representations on a local basis, i.e. the interactions in the Hamiltonian have a finite extension. We can take advantage of this property if we implement a technique general enough to deal with all these descriptions.

There's different technique used to describe open BC. In this work we apply the *Non Equilibrium Green's Function* (NEGF) formalism in an efficient iterative formulation. This section has been kept separated as NEGF library has been used within the gDFTB code, a quantum transport extension to DFTB (?) developed by our group, with a strong contribution of the author of this work. The application of NEGF library within TIBERCAD is still a work in progress.

8.1 Equilibrium Green's function

Let's consider an open system, as in figure 8.1

A device is connected with the environment with two semi-infinite contacts. The total Hamiltonian can be partitioned as follows

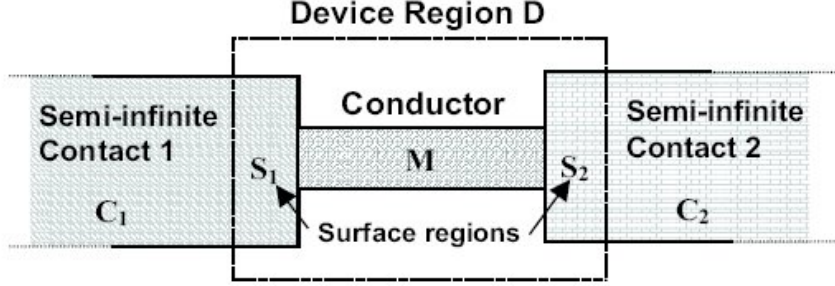


Figure 8.1: scheme of a device with open boundary conditions

$$H = \begin{pmatrix} \ddots & & & & \\ & H_{c_1} & -\tau_{c_1 d} & 0 & \\ & -\tau_{c_1 d}^\dagger & H_d & -\tau_{c_2 d} & \\ & 0 & -\tau_{c_2 d}^\dagger & H_{c_2} & \\ & & & & \ddots \end{pmatrix} \quad (8.1)$$

where H_d is the Hamiltonian of the isolated device, H_{c_1} and H_{c_2} the Hamiltonian of the isolated contacts and τ_c the interactions between molecule and contacts. Note that if we're dealing with a local basis, we can always define a region S in the contact where the interaction is non-zero, while it is zero elsewhere. We also suppose that the contact is periodical where S is the principal layer.

As the contacts are semi-infinite, H_{c_1} and H_{c_2} are infinite matrices and cannot be explicitly evaluated. To overcome this problem the Green's function formalism is used (19; 56; 59).

Let's consider a quantum system with a constant perturbation $|v\rangle$:

$$H|\psi\rangle = E|\psi\rangle + |v\rangle \quad (8.2)$$

The Green's function is defined as the response of the system to this perturbation:

$$|\psi\rangle = -(E - H)^{-1}|\psi\rangle = -G(E)|v\rangle \quad (8.3)$$

Using Green's function formalism we can consider the wavefunctions in the close system contacts ψ_1 and ψ_2 as a perturbation to the contacts ψ_1 and ψ_2 . Taking into account one contact, for example c_1 , we get:

$$\begin{aligned} H_1|\psi_1\rangle - \tau_1\psi_d &= E|\psi\rangle \rightarrow \\ |\psi_1\rangle &= -g_1(E)\tau_1\psi_m \end{aligned} \quad (8.4)$$

where g_1 is the Green's function of the isolated contact 1. It's important to note that this formalism allows us to establish a relation between the isolated device and the contact.

In general two kind of Green's functions can be defined: the retarded Green's function G^R and the advanced Green's function G^A , corresponding to outgoing and incoming waves in the contacts. Formally the retarded and advanced Green's Function can be defined as follows (for further detail about the analytical derivation and their meaning see (19; 59))

$$G^{R,A} = [(E \pm i\delta)I - H]^{-1} \quad (8.5)$$

where δ is an infinitesimal quantity that adds poles to $G(E)$ in the upper (Advanced) or lower (Retarded) complex half-plane. The following relation sussists

$$G^R = G^{A\dagger} \quad (8.6)$$

The reason for using Green's functions is that they can provide a description for the semi-infinte contact. Let's consider the system in figure 8.1, limiting to one contact. The Hamiltonian is

$$H = \begin{pmatrix} H_c & -\tau \\ -\tau^\dagger & H_d \end{pmatrix} \quad (8.7)$$

The Green's function (retarded) can be defined as

$$\begin{pmatrix} G_c & G_{cd} \\ G_{dc} & G_d \end{pmatrix} = \begin{pmatrix} (E + i\delta)I - H_c & +\tau \\ +\tau^\dagger & (E + i\delta)I - H_d \end{pmatrix}^{-1} \quad (8.8)$$

As we are interested in describing the device region, we try to calculate G_d . If we define the retarded Green's function for the contact as

$$g_c^R = [(E + i\delta)I - H_c]^{-1} \quad (8.9)$$

and the *self energy* of the contact as

$$\Sigma_c^R = \tau^\dagger g_c^R \tau \quad (8.10)$$

8. QUANTUM TRANSPORT: NEGF THEORY AND APPLICATION

then the Green's function of the device is

$$G_d = [(E + i\delta)I - H_d - \Sigma_d^R]^{-1} \quad (8.11)$$

If we have more contacts, we can generalize the (8.11) substituting Σ_d^R with

$$\Sigma_c^R = \tau^\dagger g_c^R \tau \quad (8.12)$$

Despite the fact that the contacts are semi-infinite, under the assumption that they're a repetition of principal layer, the surface Green's function g_n can be calculated through the *decimation algorithm* (18; 81). Note that thanks to the equation (8.12), the effect of contacts is non-zero only in the region where the device and the contact interact. We have then reduced our problem to the dimensionality of the device, where the open boundary conditions are defined using an effective Hamiltonian $H_{eff} = H_d + \Sigma$.

From the imaginary part of the self energy we define

$$\Gamma = i [\Sigma - \Sigma^\dagger] \quad (8.13)$$

This quantity represents the broadening of energy states in the device after the coupling with the contact, and it's a crucial quantity as it express how strong is the coupling between contact and device.

The Green's function can be used to calculate properties of the device such as the density of states, the density matrix or transmission coefficients. It follows a brief description of these quantities and how there are derived.

8.1.1 Spectral function and density of states

The spectral function is an important quantity derived from the Green's function as

$$A = i (G^R - G^A) \quad (8.14)$$

Using the (8.11) and remembering that the Hamiltonian of the close device is hermitian, we can demonstrate that

$$G^A - G^R = A = iG^R \Gamma G^A \quad (8.15)$$

The trace of the spectral function represent the *density of states* of the sistem:

$$N(E) = \frac{1}{2\pi} \text{Tr} [A(E)] \quad (8.16)$$

The spectral function is useful for the calculation of the *density matrix*. This is defined as

$$\rho = \sum_k f(k, \mu) |\psi_k\rangle \langle \psi_k| \quad (8.17)$$

where the sum runs over all states and $f(k, \mu)$ is the occupation of state k under an electrochemical potential μ . Using an orthonormal basis, the trace of the density matrix is the charge density (see (19)). The density matrix can be calculated from the spectral function in this way:

$$\rho = \frac{1}{2\pi} \int_{-\infty}^{+\infty} F_0(E - \mu) [A(E)] dE \quad (8.18)$$

where F_0 is a diagonal matrix containig the Fermi distributions $(F_0(\varepsilon_1 - \mu), F_0(\varepsilon_2 - \mu), \dots, F_0(\varepsilon_k - \mu))$

8.1.2 Coherent transport

Let's consider a device as in figure 8.1, where a potential is applied such that the contacts are locally in equilibrium with electrochemical potential μ_1, μ_2 . Let's also assume that the contacts are reflectionless. The total density of states in the conducting device can be expressed as

$$D(E) = D_{1 \rightarrow 2}(E) + D_{2 \rightarrow 1}(E) \quad (8.19)$$

where $D_{1 \rightarrow 2}(E)$ are the states injected from contact 1 to contact 2 and viceversa. The density matrix can be rewritten as

$$\rho^{NE} = \int_{-\infty}^{+\infty} [F_1(E) D_{1 \rightarrow 2}(E) + F_2(E) D_{2 \rightarrow 1}(E)] dE \quad (8.20)$$

Using eq. (8.15) we can separate the contributes of states injected by any single contact as:

$$D_{m \rightarrow n}(E) = \frac{1}{2\pi} G^R \Gamma_m G^A = \frac{i}{2\pi} G^R (\Sigma_m^R - \Sigma_m^A) G^A \quad (8.21)$$

where $D_{m \rightarrow n}(E)$ is the density of states injected from contact m to all other contacts n . Then the density matrix can be written as

$$\rho = \int_{-\infty}^{+\infty} \left[\sum_{m \neq n} F_m(E) G^R \Gamma_m G^A \right] dE \quad (8.22)$$

8. QUANTUM TRANSPORT: NEGF THEORY AND APPLICATION

To calculate the current that flows in the device we can take advantage of the relation (19; 55; 56)

$$T_{1,2}(E) = \text{Tr} [\Gamma_1 G^R \Gamma_2 G^A] \quad (8.23)$$

where $T_{1,2}$ is the transmission coefficient from contact 1 to contact 2. Through this relation we can derive the Landauer formula in terms of Green's functions

$$I_{1,2} = \frac{e}{\pi \hbar} \int_{-\infty}^{+\infty} (f(E, \mu_1) - f(E, \mu_2)) \text{Tr} [G^R \Gamma_2 G^A \Gamma_1] dE \quad (8.24)$$

8.2 Non equilibrium Green's function

In the previous chapter we've seen that it's possible to calculate the current flow in a quantum system with open boundaries. However there's still something missing, especially if we want to deal with realistic devices. In the equilibrium formalism we can only describe ballistic conduction, i.e. we cannot take into account any scattering mechanism. Moreover, we are under the assumption that the system is in a state of quasi-equilibrium, as the density matrix depend only on the self energies and the equilibrium Green's functions. It means that polarization doesn't affect the charge distribution.

To overcome these problems and get a more realistic picture, the Non Equilibrium Green's Function (NEGF) technique is used. NEGF has been introduced by Keldysh (37) in 1964, and it's a powerful technique that extend the use of Green's function in many body problem to system out of thermodynamic equilibrium.

We will explain NEGF formalism using Datta's intuitive approach (19), in order to avoid the complex mathematical formalism behind that.

8.2.1 The correlation function $G^>$ and $G^<$

We can interpretate the density matrix $\rho(i, i')$ as a generalized distribution function $f(i)$ which take into account quantum interference effects between states i and i' . We can include the time coordinate defining a time-varying density matrix $\rho(i, i', t)$, but to have a general treatment we need a two-time correlation function that tells us the correlation between state i at time t and state i' at time t' .¹

$$f(i; t) = G^n(i, i'; t, t') \quad (8.25)$$

¹The reader can find a good explanation of this concept in reference (49)

In steady state G^n depends only on the difference $\tau = t - t'$, and we can calculate the Fourier transform in order to get a correlation function $G^n(i, i'; E)$, where E is the energy.

$$G^n(i, i'; E) = \int \frac{1}{\hbar} G^n(i, i'; \tau) e^{-iE\tau/\hbar} d\tau \quad (8.26)$$

The density matrix $\rho(i, i'; t)$ can be calculated through the limit of eq. (8.26) for $\tau \rightarrow 0$, that is:

$$\rho(i, i'; t) = \left[G^n(i, i'; t, t') \right]_{t=t'} = \int \frac{1}{2\pi} G^n(i, i'; E) dE \quad (8.27)$$

We can calculate the number of electrons occupying a state i as

$$f(i) = \rho(i, i; t) = \int \frac{1}{2\pi} G^n(i, i; E) dE \quad (8.28)$$

Note that i labels any quantum number, thus it can be a \mathbf{k} vector or a real space representation. Suppose that we're in a real space basis, we can write the spatial electron charge as

$$n(\mathbf{r}) = \int n(\mathbf{r}; E) dE = \int \frac{1}{2\pi} G^n(\mathbf{r}, \mathbf{r}; E) dE \quad (8.29)$$

It's clear that the correlation function is a quantistic generalization such that $G^n(\mathbf{r}, \mathbf{r}; E)$ takes trace of occupied electron states.

The advantage is that, as scattering states transfer energy from a state to another, we can calculate the quantum evolution of the system at only as a final step perform the integration, in order to maintain a description of scattering at a quantum level.

An analogous correlation function G^p can be written for the hole states (or unoccupied electron states, if we want) (19). Usually in literature a slightly different notation is used, with the following correspondence:

$$G^n = iG^< \quad (8.30)$$

$$G^p = iG^> \quad (8.31)$$

With a similar procedure we can redefine the outscattering and inscattering functions $\Sigma^{in}(i, i'; t, t')$ and $\Sigma^{out}(i, i'; t, t')$, related in the same way as Green's function to the more popular notation $\Sigma^<, \Sigma^>$. In generale the non equilibrium self energies can contain any kind of scattering source. In literature techniques for electron-phonon and electron-photons are described and used (19; 56). Since the NEGF module integrated

8. QUANTUM TRANSPORT: NEGF THEORY AND APPLICATION

in TIBERCAD still doesn't include scattering, I won't get into this topic. However the important point to remark is that it allows scattering to be included, and that is just a question of expanding the existent implementation.

In the previous chapter we saw that the spectral function represents a generalized density of states. As the non equilibrium Green's function are related the the occupied and unoccupied we can expect, and it's demonstrated to be true, that

$$G^n + G^p = -i [G^< + G^>] = i [G^R - G^A] = A \quad (8.32)$$

Similar relation to hold between self-energies and scattering functions, even if it's less intuitive (for a nice intuitive picture see (19)).

$$\Sigma^{in} + \Sigma^{out} = -i [\Sigma^< + \Sigma^>] = i [\Sigma^R - \Sigma^A] = \Gamma \quad (8.33)$$

8.2.2 The kinetic equation

The central result of NEGF formalism is the kinetic equation which relates correlation and scattering functions. We can write the identity $[EI - H - \Sigma^R]G^R = I$ in spatial representation:

$$[E - H]G^R(\mathbf{r}, \mathbf{r}') - \int \Sigma(\mathbf{r}, \mathbf{r}_1)G^R(\mathbf{r}_1, \mathbf{r}')d\mathbf{r}_1 = \delta(\mathbf{r} - \mathbf{r}') \quad (8.34)$$

Confronting the equation (8.3), the wavefunction due to an excitation source $S(\mathbf{r})$ is

$$[E - H]\Psi(\mathbf{r}) - \int_{-\infty}^{+\infty} \Sigma^R(\mathbf{r}, \mathbf{r}_1)\Psi(\mathbf{r}_1)d\mathbf{r}_1 = S(\mathbf{r}) \quad (8.35)$$

Ψ can be expressed as

$$\Psi(\mathbf{r}) = \int_{-\infty}^{+\infty} G^R(\mathbf{r}, \mathbf{r}_1)S(\mathbf{r}_1)d\mathbf{r}_1 \quad (8.36)$$

Multiplying by the complex conjugate we have

$$\Psi(\mathbf{r})\Psi(\mathbf{r}')^* = \iint_{-\infty}^{+\infty} G^R(\mathbf{r}, \mathbf{r}_1)G^R(\mathbf{r}', \mathbf{r}_1)^*S(\mathbf{r}_1)S(\mathbf{r}_1')^*d\mathbf{r}_1d\mathbf{r}_1' \quad (8.37)$$

As it's also true that $G^n(\mathbf{r}, \mathbf{r}') \sim \Psi(\mathbf{r})\Psi(\mathbf{r}')^*$ and $\Sigma^{in}(\mathbf{r}, \mathbf{r}') \sim S(\mathbf{r})S(\mathbf{r}')^*$ we can write

$$\begin{aligned}
G^n(\mathbf{r}, \mathbf{r}_1) &= \iint_{-\infty}^{+\infty} G^R(\mathbf{r}, \mathbf{r}_1) \Sigma^{in}(\mathbf{r}_1, \mathbf{r}'_1) G^R(\mathbf{r}', \mathbf{r}'_1)^* d\mathbf{r}_1 d\mathbf{r}'_1 = \\
&= \iint_{-\infty}^{+\infty} G^R(\mathbf{r}, \mathbf{r}_1) \Sigma^{in}(\mathbf{r}_1, \mathbf{r}'_1) G^A(\mathbf{r}', \mathbf{r}'_1) d\mathbf{r}_1 d\mathbf{r}'_1
\end{aligned} \tag{8.38}$$

Similarly a relation for G^p can be derived. In matrix notation this can be written as

$$G^n = G^R \Sigma^{in} G^A \tag{8.39}$$

$$G^p = G^R \Sigma^{out} G^A \tag{8.40}$$

using the $<, >$ notation:

$$G^< = G^R \Sigma^< G^A \tag{8.41}$$

$$G^> = G^R \Sigma^> G^A \tag{8.42}$$

These are the *kinetic equations*, and they are the fulcrum of Keldysh theory.

If we are dealing with a ballistic conduction problem, the scattering functions can be expressed in term of equilibrium quantities as:

$$\Sigma_\alpha^< = f(E - \mu_\alpha) \Gamma_\alpha \tag{8.43}$$

$$\Sigma_\alpha^> = (1 - f(E - \mu_\alpha)) \Gamma_\alpha = f(-E + \mu_\alpha) \Gamma_\alpha \tag{8.44}$$

Then we can use the kinetic energy to express the $G^<$ as

$$G^< = \sum_{\alpha} f_{\alpha} G^R \Gamma_{\alpha} G^A \tag{8.45}$$

With some algebra it can be demonstrated (59) that

$$\begin{aligned}
G^< &= f_c \left(\sum_{\alpha} G^R \Gamma_{\alpha} G^A \right) + \sum_{\alpha \neq c} (f_{\alpha} - f_c) G^R \Gamma_{\alpha} G^A = \\
&= f_c G^R \Gamma G^A + \sum_{\alpha \neq c} (f_{\alpha} - f_c) G^R \Gamma_{\alpha} G^A = \\
&= f_c A + \sum_{\alpha \neq c} (f_{\alpha} - f_c) G^R \Gamma_{\alpha} G^A
\end{aligned} \tag{8.46}$$

8. QUANTUM TRANSPORT: NEGF THEORY AND APPLICATION

where c is a reference contact (collector) with the lowest potential and α all the others.

This form is more convenient as it allows to calculate the charge density

$$\rho = \frac{1}{2\pi i} \int_{-\infty}^{+\infty} G^<(E) dE \quad (8.47)$$

using a smart integration path in the complex plane. This technique has been already discussed in previous works and references can be found in (56; 59).

The current contribution of contact α is given by (56):

$$I_\alpha(E) = \frac{2e}{h} \text{Tr} [\Sigma_\alpha^< G^>(E) - \Sigma_\alpha(E) G^<(E)] \quad (8.48)$$

If we are in ballistic conduction we can still use the equation (8.24).

8.3 The iterative NEGF library

Note that in the description of NEGF technique we haven't made any assumption about the representation used for the quantum states. Infact in way of principle the formalism doesn't depend on the choice of the basis. However calculating the Green's function $G^{R,A}$ and $G^{<,>}$ involve always the inversion $(ES - H)^{-1}$. This operation requires a huge computational effort, as it scales as N^3 where N the number of basis functions. For this reason there's a big effort in finding efficient algorithms to calculate Green's functions.

The method that offers the best performance without any lack of generality is the iterative Green's function method (also referred as recursive Green's function method) (2; 57; 59).

The only assumption in the iterative Green's function is that the atoms (or the nodes for EFA scheme) can be arranged in principal layer (PL) such that H and S take a tridiagonal form as in figure 8.2. Such a partitioning can be always done if the Hamiltonina is built in a local basis. Clearly, the most the structure is quasi-one-dimensional, the most the algorithm will be efficient.

Our implementation (for the genesis of this work cfr. (59)) has two improvements respect to codes at the state of the art: it's a general formulation for N contacts and it supports a non-orthogonal basis, i.e. the S matrix is not the identity matrix.

This point is crucial as it allow us to use our library with any local basis, from EFA, ETB and DFTB in TIBERCAD, but for examples it could be used also with an LCCB

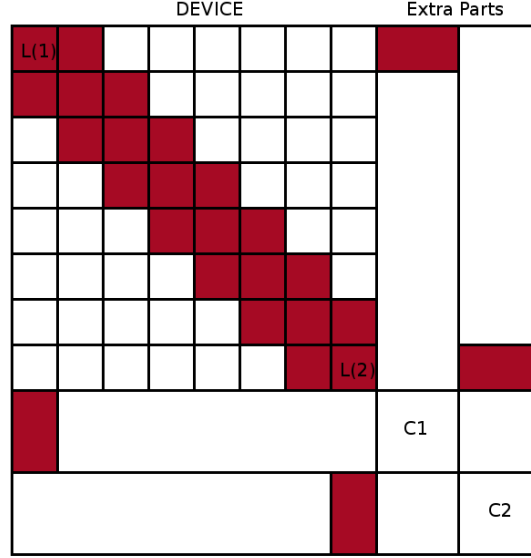


Figure 8.2: block structure of H and S for a system with two contacts assumed to interact with the first and the last PL

(Linear Combination of Bulk Bands) basis. Moreover, while the calculation of $G^{R,A}$ is similar, the derivation of $G^{<,>}$ is not that trivial.

Let's now see how the iterative algorithm works. We can write the equation (8.5) in the block tridiagonal form

$$\sum_k (ES_{i,k} - H_{i,k}) G_{k,j} = \delta_{i,j}, \quad (8.49)$$

It's convenient to define the off-diagonal terms as

$$T_{L,L+1} = ES_{L,L+1} - H_{L,L+1}. \quad (8.50)$$

In a non orthogonal basis the charge can be calculated from the density matrix as

$$q_i = \sum_{\mu \in i} \sum_{\nu} \Re [\rho_{\mu\nu} S_{\nu\mu}], \quad (8.51)$$

where i can label an atom in ETB or DFTB or a spatial node in EFA, consequently only the Green's function sub-blocks where S is non-vanishing are needed.

8. QUANTUM TRANSPORT: NEGF THEORY AND APPLICATION

In the following we assume to have partitioned a device in N layers, interacting with two contacts at layer 1 and N , and eventually with other contacts interactin with inner layers.

The self energies are first computed as

$$\Sigma_\alpha = T_{L(\alpha),\alpha} g_{\alpha,\alpha} T_{\alpha,L(\alpha)}, \quad (8.52)$$

where $L(\alpha)$ is the layer of the device interacting with contact α and $g_{\alpha,\alpha}$ is the surface Green's function of contact α . The self-energies are added to the corresponding diagonal blocks of the Hamiltonian, $H_{L(\alpha),L(\alpha)}$.

Then we define the left partial Green's functions, $g_{L,L}^L$, as the exact surface Green's functions of a system cutted at layer L and interacting only to the left part of the system. Similarly a right partial Green's function $g_{L,L}^R$ is defined. These Green's functions obey the following recursive relations,

$$g_{L,L}^R = \left[ES_{L,L} - H_{L,L} - T_{L,L+1} g_{L+1,L+1}^R T_{L+1,L} \right]^{-1} \quad (8.53)$$

and

$$g_{L,L}^L = \left[ES_{L,L} - H_{L,L} - T_{L,L-1} g_{L-1,L-1}^L T_{L-1,L} \right]^{-1}. \quad (8.54)$$

In our implementation we compute first the partial Green's functions, $g_{L,L}^R$, then we can start computing the complete Green's functions iterating *downward*, starting from layer 1,

$$G_{1,1} = \left[ES_{1,1} - H_{1,1} - \Sigma_{1,1} - T_{1,2} g_{2,2}^R T_{2,1} \right]^{-1}, \quad (8.55)$$

and then all subsequent layers down to N , using

$$G_{L,L} = g_{L,L}^R + g_{L,L}^R T_{L,L-1} G_{L-1,L-1} T_{L-1,L} g_{L,L}^R. \quad (8.56)$$

The off-diagonal blocks can be obtained from the expressions

$$G_{L-1,L} = -G_{L-1,L-1} T_{L-1,L} g_{L,L}^R, \quad (8.57)$$

and

$$G_{L,L-1} = -g_{L,L}^R T_{L,L-1} G_{L-1,L-1}. \quad (8.58)$$

These expressions are sufficient to calculate the spectral function and then the density matrix in equilibrium. To achieve the expressions for the non-equilibrium Green's functions we need to evaluate the product (8.45).

Again we only need the tridiagonal blocks of the matrices $G^{<,\alpha} = G^r \Gamma_\alpha G^a$, which can be written

$$G_{L,L}^{<,\alpha} = G_{L,L(\alpha)}^r \Gamma_\alpha G_{L(\alpha),L}^a = G_{L,L(\alpha)}^r \Gamma_\alpha G_{L,L(\alpha)}^{r\dagger} \quad (8.59)$$

$$G_{L-1,L}^{<,\alpha} = G_{L-1,L(\alpha)}^r \Gamma_\alpha G_{L(\alpha),L}^a = G_{L-1,L(\alpha)}^r \Gamma_\alpha G_{L,L(\alpha)}^{r\dagger} \quad (8.60)$$

$$G_{L,L-1}^{<,\alpha} = G_{L,L(\alpha)}^r \Gamma_\alpha G_{L(\alpha),L-1}^a = G_{L,L(\alpha)}^r \Gamma_\alpha G_{L-1,L(\alpha)}^{r\dagger} \quad (8.61)$$

This set of equations shows that the computation of $G_{L,L}^{<,\alpha}$ requires the computation of the column-blocks $G_{L,L(\alpha)}^r$, corresponding to the layer $L(\alpha)$. Referring to equation 8.46, we observe that for a system of N contacts, the computation of $N - 1$ columns are needed. These column-blocks can be obtained as follows

$$G_{j,L(\alpha)} = -g_{j,j}^{\mathcal{R}} T_{j,j-1} G_{j-1,L(\alpha)}, \quad (8.62)$$

valid for $j > L(\alpha)$, and

$$G_{j-1,L(\alpha)} = -g_{j-1,j-1}^{\mathcal{L}} T_{j-1,j} G_{j,L(\alpha)}, \quad (8.63)$$

valid for $j < L(\alpha)$.

A further complication is in the computation of the Mulliken charges, because of the non-zero overlap between device and contact atoms. As a consequence to equation (8.51), the density matrix needs to be computed on extra blocks outside the device, corresponding to the overlap between device and contacts, as shown in Figure ???. Concerning G^r , the calculation of these blocks is simple and can be derived in analogy to equation (8.57) as

$$G_{L(\alpha),\alpha}^r = -G_{L(\alpha),L(\alpha)}^r T_{L(\alpha),\alpha} g_{\alpha,\alpha}^r. \quad (8.64)$$

Things are a little more complicated for the corresponding blocks of $G^{<,\alpha}$. With lengthy algebra, it is possible to obtain the general expressions

$$\begin{aligned} G_{L(\alpha),\alpha}^{<,\alpha} = & -i G_{L(\alpha),L(\alpha)}^r T_{L(\alpha),\alpha} (g_\alpha^r - g_\alpha^a) + \\ & -G_{L(\alpha),L(\alpha)}^r \Gamma_\alpha G_{L(\alpha),L(\alpha)}^a T_{L(\alpha),\alpha} g_\alpha^a, \end{aligned} \quad (8.65)$$

and

$$G_{L(\beta),\beta}^{<,\alpha} = -G_{L(\beta),L(\alpha)}^r \Gamma_\alpha G_{L(\alpha),L(\beta)}^a T_{L(\beta),\beta} g_{\beta}^a, \quad (8.66)$$

valid only for $\beta \neq \alpha$.

This method allows a much more efficient calculation (for some profiling, see (57; 59)) and it's general enough to be applied to different representations. It can be possibly coupled to a Poisson equation in order to solve a self-consistent problem. Results and details on coupled SCC-DFTB/NEGF where also Poisson equation is solved and

8. QUANTUM TRANSPORT: NEGF THEORY AND APPLICATION

coupled has been published by the author of this work (57) *et al.* An application is described in the next section, where SCC-DFTB/NEGF simulation of a molecular device is shown.

8.4 A ballistic molecular transistor

In this section we present an application for quantum transport calculations with NEGF techniques. The approaches shown in previous calculation cannot be applied when quantum phenomena are relevant in the whole device. This what typically happens when the quantum states are not well confined and they're coupled with the contacts. In this section we'll consider a molecular device. At first a rectifying donor-acceptor molecule is considered. The structure is shown in figure 8.3

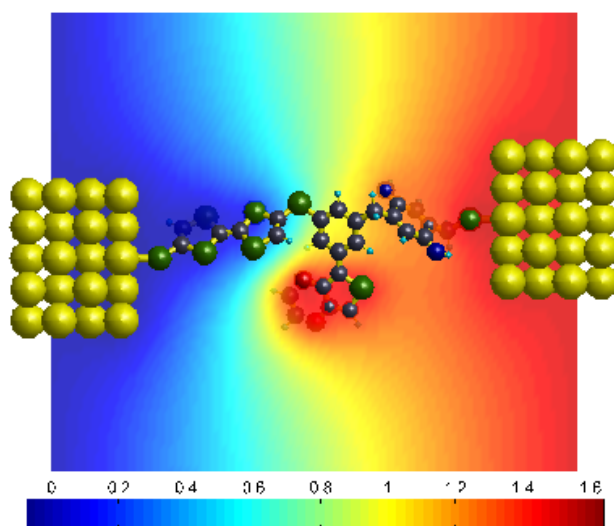


Figure 8.3: rectifying TTF-BQD molecule and the electrostatic potential at bias $V=1.5$ V. The potential is drawn on a plane cutting the molecule and is referenced with respect to $V=0$. Black atoms correspond to C, green atoms to S, blue atoms to N, yellow atoms to Au

The device comprises a Tetrathiafulvalene (TTF) unit and benzo-quinone-diimine (BQD) unit separated by a phenyl ring. An ethyl-dioxy-thiophene (EDT) group has been attached to the central benzene ring for a following three terminal study. Both the geometry relaxation and the calculation of electronic properties are done within the DFTB technique. The molecule is first relaxed in a free standing configuration, with S atoms saturated with H. Subsequently the terminating Hydrogens have been removed and two Au contacts leads have been placed at a distance of 2.5 \AA from the S atoms, which is known to be the equilibrium A distance from previous relaxations of thiols on Au surfaces. The Au leads are taken as Au(110) nanowires. The rectifying effect is due to the alignment of the HOMO level in TTF with the LUMO level of the

8. QUANTUM TRANSPORT: NEGF THEORY AND APPLICATION

BQD. The benzene ring in between acts as an insulating bridge that separates the two molecular islands, because of its larger energy gap. In order to increase localisation of the states on the two dots we have introduced a CH₂ group between the phenyl ring and the BQD.

The whole calculation stands on a self-consistent Poisson/Schrödinger scheme, where the Poisson provides the Hartree potential needed for the self-consistent iteration of the Kohn-Sham equations in a SCC-DFTB scheme. Thus the Hamiltonian includes open boundary conditions within NEGF technique, while the potential act as a Dirichlet boundary condition for the Poisson. The calculations are coupled in the following way:

The Poisson equation for the mean field electrostatic potential should be written

$$\begin{cases} \nabla^2 V = 4\pi \sum_i [n_i^0(r) + F_{00}^i(r)\Delta q_i] \\ + \text{boundary conditions.} \end{cases} \quad (8.67)$$

where $n_i^0(r)$ are the atomic reference densities, $F_{00}^i(r)$ are spherical s-like radial functions and Δq_i are the Mulliken charges. The self-consistent potential is related to the electronic density fluctuations, whereas the effective potential, V^0 , corresponding to the reference charge density, $n^0(r)$, is included in H^0 . Hence, by linearity, we split the Poisson equation (8.67) into two equations, one for the reference density and the other for the self-consistent correction,

$$\nabla^2 V_{el}^{(1)} = 4\pi \sum_i F_{00}^i(r)\Delta q_i. \quad (8.68)$$

When solved with the usual boundary conditions (potential vanishing at infinity), equation (8.68) gives the usual Hartree potential,

$$V_{el}^{(1)}(r) = \sum_i \Delta q_i \int \frac{F_{00}^i(r')}{\|r - r'\|} dr'. \quad (8.69)$$

This potential can be projected on the atom centers, using

$$V_j = \int V_{el}^{(1)}(r) F_{00}^j(r) dr, \quad (8.70)$$

This potential can be projected on the atom centers, using

$$V_j = \int V_{el}^{(1)}(r) F_{00}^j(r) dr, \quad (8.71)$$

which can be used to recover the gamma functional in the SCC-DFTB scheme (see eq. (8.13)). The equation (8.68) is solved with the boundary conditions imposed by the contact potentials. These conditions arise from the natural requirement that deep

inside the contacts the effective potential for the Kohn-Sham equations must correspond to the bulk electrochemical potentials. Therefore, at the boundaries between the *device* region and the contacts, the potential must match the intrinsic effective bulk potential (which originates from any equilibrium charge density) shifted by the applied bias. At the device-contacts interfaces, C_α/S_α , the potential must satisfy

$$V_{S_\alpha}^{(1)}(r)|_{C_\alpha/S_\alpha} = V_{C_\alpha,bulk}^{(1)}(r)|_{C_\alpha/S_\alpha} + \Delta V_\alpha, \quad (8.72)$$

where ΔV_α is the applied external potential to the α -contact (57).

Once that self-consistency is reached, we can evaluate the charge transport. We're neglecting any scattering source, so we're calculating the tunneling current. An IV characteristic is shown in figure 8.4, where we consider the TTF group grounded and we apply a forward bias to the contact at the BQD side.

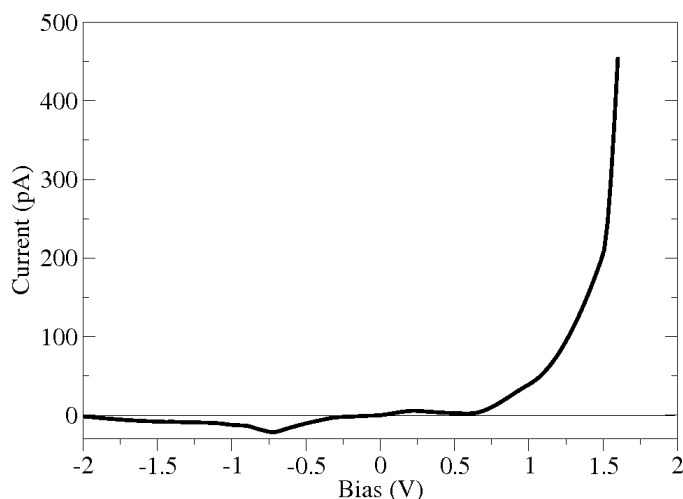


Figure 8.4: I-V characteristics of the TTF-BQD rectifier.

In order to understand how the rectifying behaviour is obtained, the most useful information is the local density of states in the different molecular units. In forward bias the HOMO level at the TTF side is brought into resonance with the LUMO level of the BQD side, leading to a state of high conduction of the molecular bridge, as shown in Figure 8.5. In reverse bias the same levels are moved far apart, giving a low tunneling current.

Once that we proofed a rectifying behaviour, we can go further and demonstrate a multiterminal application. These results have been also published (see ref. (57)), as

8. QUANTUM TRANSPORT: NEGF THEORY AND APPLICATION

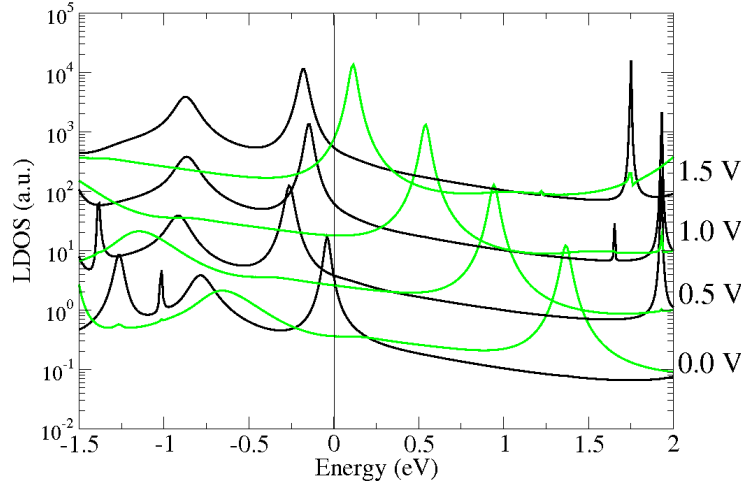


Figure 8.5: LDOS projected on the TTF (black) and the BQNA (green) islands for the molecular rectifier. The curves referring to different biases are shifted by one order of magnitude for clarity.

the first application of a non-equilibrium calculation in a three terminal configuration with a selfconsistent potential. The TTF-EDT-BQD molecule has been arranged in a three-terminal configuration, as represented in Figure 8.6. A sulphur atom has been added to the EDT group to bind to a third Au-wire. The molecule is finally relaxed in the three terminal configuration, keeping fixed the Au atoms.

The TTF-BQD acts as source-drain channel and the contact attached to the EDT group plays the role of a gate that modulates the conductance. The gate field modulates the HOMO-LUMO energy alignment of the central benzene ring with respect to the FFT and BQD levels, increasing or decreasing the tunneling current. By applying a negative potential to the gate, the HOMO level of the benzene ring is moved upwards, getting closer to the HOMO-LUMO levels of the TTF-BQD and favouring the tunneling current. The drain bias is applied to the BQD side of the molecule. The I-V characteristic of the device is shown in figure

We observe a certain degree of modulation induced by the gate field, however, for drain biases larger than 0.2 V, the drain current starts to decrease considerably, and the modulation effect is considerably reduced for drain voltages larger than 1.0 V. This result can be understood in terms of the so called “drain-induced barrier lowering” known in semiconductor device physics. In practice the gate field is not able to pin

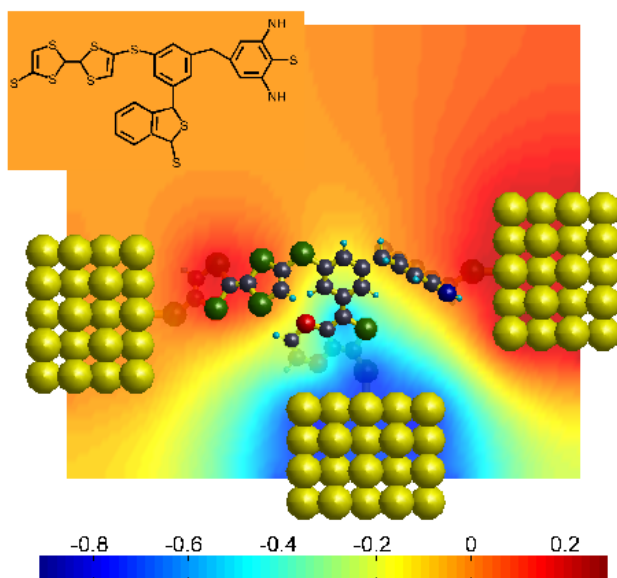


Figure 8.6: representation of the three terminal TTF-EDT-BQD molecule and electrostatic potential for $V_G = -0.7V$ and $V_D = 0.2V$

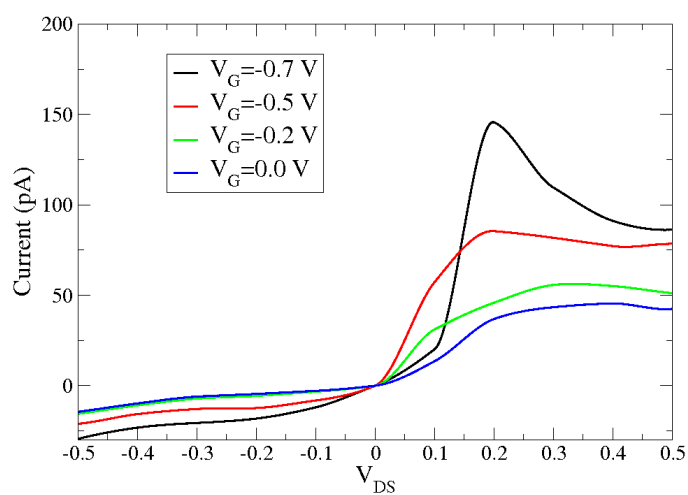


Figure 8.7: I-V characteristic of the three terminal device in fig. 8.6 for different gate voltages.

8. QUANTUM TRANSPORT: NEGF THEORY AND APPLICATION

the potential of the benzene ring, which is strongly affected by the drain voltage. The effect can be clearly seen in Figure ??, where the peak corresponding to the benzene ring is strongly shifted downwards by the drain potential rather than being pinned by the gate.

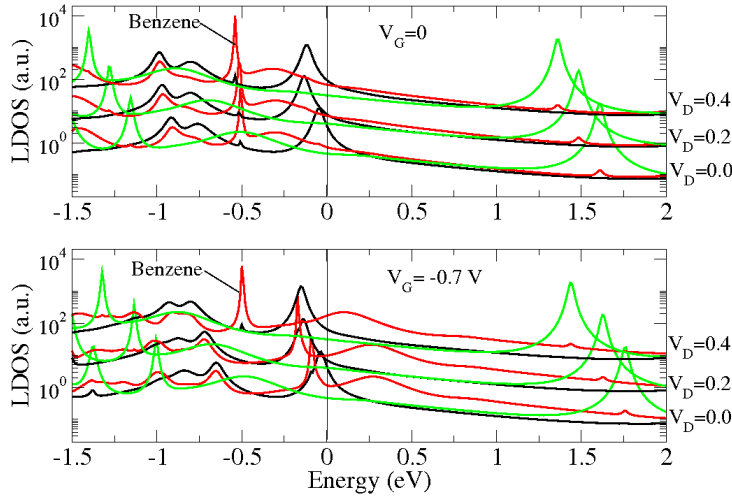


Figure 8.8: Local Dos projected on the TTF (black) BQD (green) and benzene+EDT (red) subunits. Upper panel obtained at $V_G=0$ and lower panel at $V_G=-0.7$ V and varying V_D .

Another draw back of this molecular configuration is the rather high source-gate leakage current which is due to the good degree of conjugation between TTF and EDT that is broken in the TTF-BQD by the alkyl group.

This problems can be overcome for instance by increasing the degree of conjugation of the “channel”, e.g. by substituting the alkyl separation between the central phenyl ring and the BQD with a Sulphur atom, and by placing an alkyl group for improving the isolation of the EDT island from the channel, as shown in Figure 8.9. This molecular structure has been obtained with the same procedure followed for the previous structure. The result of this strategy is plotted in the I-V curves of Figure 8.10, showing a much larger output current with respect to Figure 8.7 due to a larger degree of conjugation and a slightly better gate pinning, particularly at the highest gate voltages. Also the gate leakage is significantly reduced in this molecular configuration thanks to the alkyl group. The reduction of the leakage current is indeed about one order of magnitude.

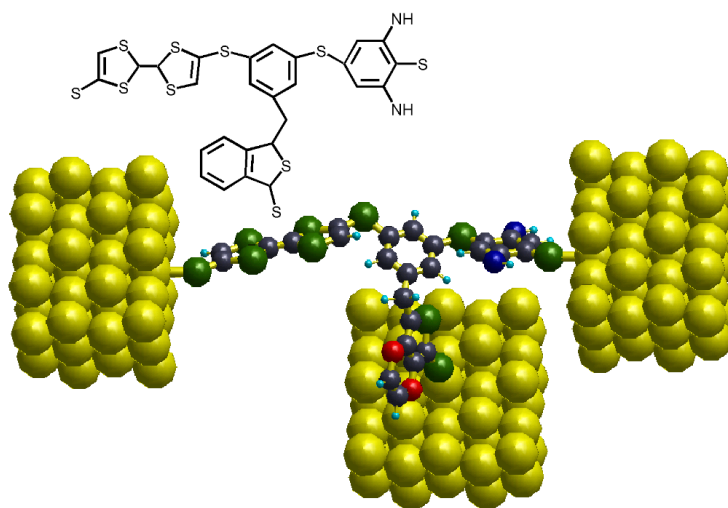


Figure 8.9: molecular structure of the TTF-BQD-BDE three terminal device II. An insulating C_2H_4 bridge is added to better separate the TTF-BQD channel from the gate contact.

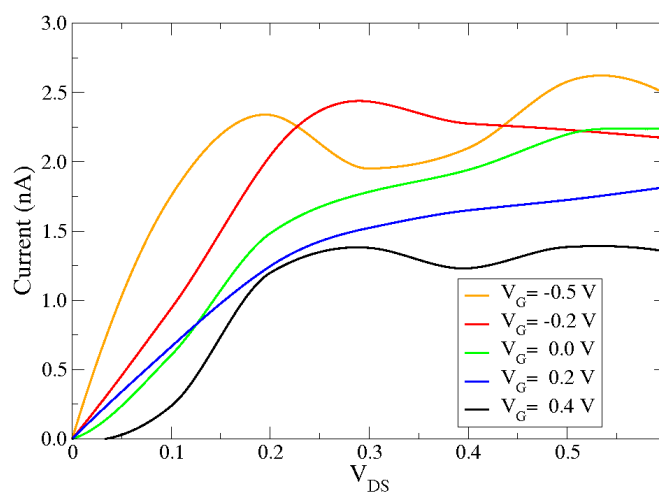


Figure 8.10: I-V characteristics of the TTF-BQD-BDE device II of figure 8.9 at different gate voltages.

8. QUANTUM TRANSPORT: NEGF THEORY AND APPLICATION

Conclusions

In this work the implementation of atomistic models in TIBERCAD, a TCAD code for nanoelectronic devices has been discussed. An environment suitable for mixed atomistic/continuous simulations has been created. Within this environment it's possible to perform different multiscale and multiphysics calculations, having direct comparison between atomistic and continuous in a single framework it's possible. Furthermore, the atomistic description of the device is innerly generated, making the device design easier.

By the atomistic side we dealt with Valence Force Field for calculating strain and structure geometry; with Empirical Tight Binding for calculating electronic and optical properties of semiconductor nanostructures and with Density Functional Tight Binding for calculating geometry and electronic properties of bot semiconductor and molecular devices.

We presented some application including a comparison between Valence Force Field and Continuum Elasticity, a multiscale simulation scheme for calculating optical properties of a quantum dot under bias, and a selfconsistent Schrödinger/Drift-Diffusion scheme.

Finally the development of a NEGF library which take advantage of a novel iterative scheme has been shown. The solution proposed is the only selfconsistent multiterminal NEGF library in literature. As an example the IV characteristic of a three-terminal molecular device has been calculated.

All the works presented have been discussed in journal articles and international conferences during my Ph.D. program.

9. CONCLUSIONS

References

- [1] M. Ameen, *Computational elasticity*, Alpha Science International Ltd., Oxford, U. K., 2008. 11, 13
- [2] M. P. Anantram, M. S. Lundstrom, and D. E. Nikonov, arXiv:cond-mat/0610247v2 (2007). 78
- [3] N. W. Ashcroft and N. D. Mermin, *Solid state physics*, Thomson Learning, 1976. 16
- [4] M. Auf der Maur, , M. Povolotskyi, F. Sacconi, A. Pecchia, G. Penazzi, G. Romano, and A. Di Carlo, *Tibercad: towards multiscale simulation of optoelectronic devices*, Optical and Quantum Electronics **40** (2008), 1077–1083. 8
- [5] M. Auf der Maur, *A multiscale simulation environment for electronic and optoelectronic devices*, Ph.D. thesis, University of Rome Tor Vergata, 2008. 15, 16, 23, 41, 45
- [6] M. Auf der Maur, M. Povolotskyi, F. Sacconi, and A. Di Carlo, *Tibercad: a new multiscale simulator for electronic and optoelectronic devices*, Superlattices and Microstructures **41** (2007), 381–385. 8
- [7] Satish Balay, Kris Buschelman, William D. Gropp, Dinesh Kaushik, Matthew G. Knepley, Lois Curfman McInnes, Barry F. Smith, and Hong Zhang, *PETSc Web page*, 2009, <http://www.mcs.anl.gov/petsc>. 31, 47
- [8] E. B. Becker, F. C. Graham, and J. T. Oden, *Finite elements: an introduction*, vol. 1, Prentice-Hall, 1981. 8
- [9] Steve Benson, Lois Curfman McInnes, Jorge Moré, Todd Munson, and Jason Sarich, *TAO user manual (revision 1.9)*, Tech. Report ANL/MCS-TM-242, Mathematics and Computer Science Division, Argonne National Laboratory, 2007, <http://www.mcs.anl.gov/tao>. 31, 47

REFERENCES

- [10] G. L. Bir and G. E. Pikus, *Symmetry and strain-induced effects in semiconductors*, Wiley, New York, 1974. 21
- [11] T. B. Boykin, *Improved fits of the effective masses at γ in the spin-orbit, second-nearest-neighbour sp^3s^* model: Results from analytic expressions*, Physical Review B **56** (1997), no. 15. 36
- [12] M. G. Burt, *The justification for applying the effective-mass approximation to microstructures*, Journal of Physics: Condensed Matter **4** (1992), no. 32, 6651–6690. 16, 18, 61
- [13] D. Camacho and Y. M. Niquet, *Application of keating’s valence force field model to non-ideal wurtzite materials*, Physica E **42** (2010), 1361–1364. 30
- [14] D. J. Chadi, *Spin-orbit splitting in crystalline and compositionally disordered semiconductors*, Physical Review B **16** (1977), no. 2. 36
- [15] D. J. Chadi and M. L. Cohen, Phys. Stat. Solidi **68** (1975), no. 405. 35
- [16] S. L. Chuang, *Physics of photonic devices*, 2nd ed., Wiley and sons, 2009. 12, 21, 23, 24
- [17] S. L. Chuang and C. S. Chang, *kp method for strained wurtzite semiconductors*, Physical Review B **54** (1996), no. 4. 20
- [18] P. S. Damle, A. W. Ghosh, and S. Datta, *Molecular nanoelectronics*, M. Reed, 2002. 72
- [19] S. Datta, *Electronic transport in mesoscopic systems*, Cambridge University Press, 1995. 70, 71, 73, 74, 75, 76
- [20] A. R. Denton and N. W. Ashcroft, *Vegard’s law*, Physical Review A **43** (1991), 3161–3164. 29, 53
- [21] DFTB+, <http://www.dftb-plus.info>. 41
- [22] A. Di Carlo, *Microscopic theory of nanostructured semiconductor devices: beyond the envelope-function approximation*, Semiconductor Science and Technology **18** (2003), R1–R31. 7, 33, 38, 41
- [23] M. Elnster, D. Porezag, G. Jungnickel, J. Elsner, M. Haugk, Th. Frauenheim, S. Suhai, and G. Seifert, *Self-consistent-charge density-functional tight bindings*

REFERENCES

- method for simulations of complex materials properties*, Physical Review B **58** (1998), no. 11, 7260. 43, 44
- [24] P. Enders, A. Bärwolff, and M. Woerner, *kp theory of energy bands, wave functions, and optical rules in strained tetrahedral semiconductors*, Physical Review B **51** (1995), no. 23. 22, 24
- [25] R. P. Feynman, *There's plenty of room at the bottom*, Engineering and Science (1960), 22–36. 5, 6
- [26] R. Fletcher and C. M. Reeves, *Function minimization by conjugate gradients*, Computer Journal **7** (1964), 149–154. 30
- [27] S. Froyen and W. A. Harrison, *Elementary prediction of linear combination of atomic orbitals matrix elements*, Physical Review B **20** (1979), no. 6. 38
- [28] C. Geuzaine, *Gmsh 3d finite element mesh generator*, <http://www.geuz.org>. 45
- [29] F. Grosse and J. Neugebauer, *Limits and accuracy of valence force field models for $\text{In}_x\text{Ga}_{1-x}\text{N}$ alloys*, Physical Review B **63** (2001), no. 085207. 30
- [30] Optolab group homepage, <http://www.optolab.uniroma2.it>. 45
- [31] S. Hackenbuchner, *Elektronische struktur von hbleiter-nanobauelementen im thermodynamischen nichtgleichgewicht*, Ph.D. thesis, Walter Schottky Institute Technische Universität München, 2002. 20, 21
- [32] F. B. Hildebrand, *Finite-difference equations and simulations*, Prentice-Hall, 1968. 8
- [33] Synopsis Inc., <http://www.synopsis.com>. 45
- [34] J. Jancu, R. Scholz, F. Beltram, and F. Bassani, *Empirical spds* tight-binding calculation for cubic semiconductors: Genral method and material parameters*, Physical Review B **57**, no. 11. 36, 39
- [35] J. M. Jancu, F. Bassani, F. Della Sala, and R. Scholz, *Transferable tight-binding parameters for the group-iii nitrides*, Applied Physics Letters **81** (2002), no. 25. 36
- [36] P. N. Keating, *Effect of invariance requirements on the elastic strain energy of crystal with application to the diamond structure*, Physical Review **145** (1966), no. 2. 26

REFERENCES

- [37] L. V. Keldysh", *Diagram technique for nonequilibrium processes*, Soviet Physics JETP **20** (1964), 1018. 74
- [38] A. Kikuchi, K. Kishino, et al., Japanese Journal of Applied Physics **43** (2004). 58
- [39] B. S. Kirk and J. W. Peterson, *The libmesh library*, <http://libmesh.sourceforge.net>. 47
- [40] C. Kittel, *Introduction to solid state physics*, 7th ed., Wiley and Sons, New York, 1953. 15, 25
- [41] O. L. Lazarenkova, P. Von Allmen, F. Oyafuso, S. Lee, and G. Klimeck, *Effect of anharmonicity of the strain energy on band offsets in semiconductor nanostructures*, Applied Physics Letters **85** (2004), no. 18. 28
- [42] S. Lee, F. Oyafuso, P. von Allmen, and G. Klimeck, *Boundary conditions for the electronic structure of finite-extent embedded semiconductor nanocstructures*, Physical Review B **69** (2004), no. 045316. 40
- [43] P. O. Löwdin, *On the non-orthogonality problem connected with the use of atomic wave functions in the theory of molecules and crystals*, Journal of Chemical Physics **18** (1950), 350. 32
- [44] B. Luan and M. O. Robbins, *The breakdown of continuum models for mechanical contacts*, Nature **435** (2005), 929–932. 7
- [45] P. A. Markovich, C. A. Ringhofer, and C. Schmeiser, *Semiconductor equations*, 1st ed., Springer-Verlag Wien New York, 1990. 15
- [46] P. A. Markowich, *The stationary semiconductor device equations*, 1st ed., Springer-Verlag Wien New York, 1986. 7
- [47] R. M. Martin, *Elastic properties of zns structure semiconductors*, Physical Review B **1** (1970), no. 10. 28
- [48] ———, *Relation between elastic tensor of wurtzite and zinc-blende structure materials*, Physical Review B **6** (1972), no. 12. 30
- [49] R. D. Mattuck, *A guide to feynman diagrams in the many-body problem*, Dover Publications, INC., 1976. 74
- [50] J. L. Mercer and M. Y. Chou, *Tight-binding model with intra-atomic matrix elements*, Physical Review B (1994), 8506–8509. 33

-
- [51] G. E. Moore, *Cramming more components onto integrated circuits*, Electronics **38** (1965), 114–117. 5
- [52] R. S. Mulliken, *Electronic population analysis on lcao-mo molecular wave functions*, Journal of Chemical Physics **23** (1955), no. 1833. 41
- [53] J. F. Nye, *Physical properties of crystals*, Oxford University Press, 1969. 14, 15
- [54] G. C. Osbourn, Physical Review B **27** (1983), 5126. 54
- [55] M. Paulsson, *Non equilibrium green's functions for dummies: Introduction to the one particle negf equations*, arXiv:cond-mat/0210519v2 (2008). 74
- [56] A. Pecchia and A. Di Carlo, *Atomistic theory of transport in organic and inorganic nanostructures*, Reports on Progress in Physics **67** (2004), 1497–1561. 70, 74, 75, 78
- [57] A. Pecchia, G. Penazzi, L. Salvucci, and A. Di Carlo, *Non-equilibrium green's functions in density functional tight binding: method and applications*, New Journal of Physics **10**, 065022. 78, 81, 82, 85
- [58] T. G. Pedersen, K. Pedersen, and T. B. Kriestensen, *Optical matrix elements in tight-binding calculations*, Physical Review B **63** (2001), no. 201101. 41
- [59] Gabriele Penazzi, *Development of a quantum transport simulator*, Master's thesis, University of Rome Tor Vergata, 2006. 70, 71, 77, 78, 81
- [60] J. P. Perdew and A. Zunger, Physical Review B **23** (1981), no. 10, 5048. 42
- [61] J. Pèrez-Conde and A. K. Bhattacharjee, *Exciton states and optical properties of cdse nanocrystals*, Physical Review B **63** (2001), no. 245318. 40
- [62] D. Porezag, Th. Frauenheim, Th. Köhler, G. Seifert, and R. Kaschner, *Construction of tight-binding-like potentials on the basis of density functional theory: Application to carbon*, Physical Review B **51** (1995), no. 19, 12947. 41
- [63] M. Povolotskyi, *Theoretical study of electronic and optical properties of low-dimensional semiconductor nanostructures*, Ph.D. thesis, University of Rome Tor Vergata, 2004. 11, 20, 21, 23
- [64] The TiberCAD project, <http://www.tibercad.org>. 8, 45

REFERENCES

- [65] C. Pryor, L. W. Kim, J. ad Wang, A. J. Wiallamson, and A. Zunger, *Comparison of two methods for describing the strain profiles in quantum dots*, Journal of Applied Physics **83** (1998), 2548. 12, 28, 53, 55
- [66] J. Ristić et al., Phys. Stat. Sol. b **234** (2002), no. 3, 717–721. 58
- [67] R. E. Rudd and J. Q. Broughton, *Concurrent coupling of lenght scales in solid state systems*, Physica Status Solidi b **217** (2000), 251. 7, 9
- [68] H. Saito, K. Nishi, and S. Sugou, *Shape transition of inas quantum dots by growth at high temperature*, Applied Physics Letters **74** (1994), 1224. 54
- [69] J. J. Sakurai, *Modern quantum mechanics*, revisited edition ed., Addison-Wesley, 1994. 17
- [70] G. Sarusi, O. Moshe, S. Khatsevich, and H. D. Rich, Physical Review B **75** (2007). 58
- [71] M. Schulz, *The end of the road for silicon?*, Nature **399** (1999), 729–730. 6
- [72] G. Seifert, D. Porezag, and Th. Frauenheim, *Calculations of molecules, clusters and solids with a simplified lcao-dft-lda scheme*, **58** (1996), no. 2, 185. 41
- [73] S. Selberherr, *Analysis and simulation of semiconductor devices*, 1st ed., Springer-Verlag Wien New York, 1984. 15
- [74] J. C. Slater and G. F. Koster, *Simplified lcao method for the periodic potential problem*, Physical Review **94** (1954), 1498–1524. 32, 33, 35
- [75] O. Stier, M. Grundmann, and D. Bimberg, *Electronic and optical properties of strained quantum dots modeled by 8-band kp theory*, Physical Review B **59** (1999), no. 8. 12, 27, 53, 55
- [76] G. Timp, *The rentless march of the mosfet gate oxide thickness to zero*, Microelectronic Reliability **40** (2000), 557–562. 6
- [77] W. T. Tsang, *Semiconductor and semimetals*, vol. 22, Academic Press, New York, 1985. 12
- [78] P. Vogl, P. Kjalmarson, and J. D. Dow, *Semi-empirical tight-binding theory of the electronic structure of semiconductors*, Journal of Physics and Chemistry of Solids **44**, no. 5, 365–378. 35, 36

REFERENCES

- [79] Z. Xiao Guo, *Multiscale materials modelling: Fundamentals and applications*, Woodhead Publishing, 2007. 7
- [80] P. Y. Yu and M. Cardona, *Fundamentals of semiconductors*, 3rd ed., Springer Berlin Heidelberg New York, 2005. 12, 17, 24, 28
- [81] F. Zahid, M. Paulsson, and S. Datta, *Advanced semiconductors and organic nano-techniques*, 2002. 72